INVESTIGATION ON CARBON FIBRE REINFORCED POLYMER (CFRP) STRENGTHENED, OUT OF PLANE CURVED CONCRETE BEAM SUBJECTED TO COMBINED EFFECTS OF SHEAR AND TORSION

Warnakulasuriya Chinthana Vimukthi Fernando

198096T

Degree of Master of Science

Department of Civil Engineering

University of Moratuwa

Sri Lanka

January 2021

INVESTIGATION ON CARBON FIBRE REINFORCED POLYMER (CFRP) STRENGTHENED, OUT OF PLANE CURVED CONCRETE BEAM SUBJECTED TO COMBINED EFFECTS OF SHEAR AND TORSION

Warnakulasuriya Chinthana Vimukthi Fernando

198096T

A thesis submitted in partial fulfilment of the requirements for the degree Master of Science in Civil Engineering

Department of Civil Engineering

University of Moratuwa

Sri Lanka

January 2021

DECLARATION

I declare that this is my work and this thesis does not incorporate without acknowledgement any material previously submitted for a Degree or Diploma in any other university or institute of higher learning and to the best of my knowledge and belief it does not contain any material previously published or written by another person except where the acknowledgement is made in the text.

Also, I hereby grant to the University of Moratuwa the non-exclusive right to reproduce and distribute the thesis, in whole or in part in print, electronic or other media. I retain the right to use this content in whole or part in future works (such as articles or books).

Signature: ***UOM Verified Signature*** Date: 28/02/2022

The above candidate has carried out research for the Masters under my supervision

Name of the supervisor: Dr. (Mrs.) J.C.P.H. Gamage

Signature of the supervisor: Date:

ACKNOWLEDGEMENT

Under the Research Project, I had the opportunity of gaining very valuable experience of how to apply the theoretical knowledge gathered throughout the four years as an undergraduate to produce important findings for the well-being and development of the community. There are a number of persons whom I must pay my gratitude for their help towards the successful completion of the research project and report.

First, I am very grateful for the valuable guidance and encouragement were given by my research supervisor, **Dr. (Mrs.) J.C.P.H. Gamage**, Senior lecturer in the Department of Civil Engineering, University of Moratuwa. Without her support and guidance none of this would be possible. Further, I am thankful to, **Prof. A.A.D.J. Perera and Prof. C. Jayasinghe**, Senior Professors in the Department of Civil Engineering, University of Moratuwa, for the progress evaluation and for providing valuable instructions to move forward in my research direction.

Next, I would like to express my gratitude to **Mr. D.M.N.L. Dissanayaka**, technical officer and the non-academic staff in the structural Testing, building material, rock mechanics and computer laboratories in the Department of Civil Engineering, University of Moratuwa.

W. C. V. Fernando
Department of Civil Engineering
University of Moratuwa

06.11.2020

ABSTRACT

Carbon Fibre Reinforced Polymer (CFRP) strengthening technique had been shown excellent performance in externally strengthening Reinforced Concrete (RC) elements due to their superior properties compared to the alternatives. A substantial amount of studies had been done to study the behaviour of externally CFRP strengthened RC elements. However, as per the authors' knowledge, while most of the studies have been focused on the external strengthening of straight RC beams using CFRP, none of the studies had been focused on strengthening horizontally curved RC beams. Curved beams innately respond with flexure, shear and especially torsion under out-of-plane loads due to its curvature. Hence, it is important to study the effect of the additional torsional stress on the CFRP external reinforcement.

A detailed experimental program, a theoretical analysis and a numerical analysis were conducted in order to reduce the aforementioned research gap. A series of testing was conducted on beam specimens with 2 m and 4 m radii and externally strengthened with normal modulus CFRP fabrics to enhance the effects; shear, torsion and their combination.

From series one experimental results, it was found that the wrapping CFRP fabrics have enhanced the shear capacity of the curved RC beams by at least 30 % and the enhancement is higher for beams with lower curvatures. It showed that CFRP wrapping is a very effective method to enhance the shear capacity of horizontally curved beams.

The series two experimental results showed that U-socketing of CFRP fabrics for shear has increased the shear strength by 15.61 kN (16.7 %) and 17.41 kN (18.2 %) respectively for 2 m and 4 m radius specimens. The main failure mode was crack induced intermediate debonding of CFRP U-sockets. However, the predicted shear enhancements according to theoretical investigation are 23.64 kN and 24.51 kN for 2 m and 4 m radius beams respectively. It can be observed that for 2 m and 4 m specimens recorded respectively 33.97 % and 28.97 % less than the predicted enhancement by the theoretical study. This can be explained by the additional

torsional stresses contributing to the direct shear stresses which cause to reduce the shear capacities of RC beams.

The results from numerical models showed excellent agreement with experimental results which was used to carry out a parametric study. Subsequently, a capacity reduction factor was defined as the ratio between numerical shear gain and theoretically predicted shear gain to quantify the effect of torsional stresses on the shear enhancement of U-socketed CFRP on RC beams with a 1.4 m support distance which can be used to modify the currently existing analytical model adopted by ACI 440.2R-17 guide to design of FRP as external reinforcement for RC beams.

LIST OF PUBLICATIONS

International Conferences (Published)

1. Fernando, W. C. V., Chandrathilaka, E. R. K. & Gamage, J. C. P. H., (2019). "Experimental Study on Shear Behaviour of CFRP Strengthened Curved RC Beams". 10th International Conference on Structural Engineering and Construction Management (ICSECM2019), Kandy, Sri Lanka.
2. Kulendran. S., Fernando, W. C. V. & Gamage, J. C. P. H., (2020). "Strengthening of Damaged Out of Plane Curved Reinforced Concrete Beam Using Carbon Fiber Reinforced Polymer". 6th Moratuwa Engineering Research Conference (MERcon 2020), Moratuwa, Sri Lanka.

Journal papers (in preparation)

1. Himasha, M. W. C., Fernando, W. C. V. & Gamage, J. C. P. H., 2020. Study on Shear Behaviour of CFRP Strengthened Horizontally Curved RC Beams. *Case Studies in Construction Materials*. (In preparation)
2. Fernando, W. C. V. and Gamage, J. C. P. H., 2020. Bond characteristics of Carbon Fibre Reinforced Polymer Strengthened, Out of Plane Curved Reinforced Concrete Beam Subjected to Combined Effects of Shear and Torsion. (In preparation)
3. Fernando, W. C. V. and Gamage, J. C. P. H., 2020. A theoretical approach to quantify the combined effects of shear and torsion in Carbon Fiber Reinforced Polymer (CFRP) strengthened out of plane curved Reinforced Concrete Beams. (In preparation)

TABLE OF CONTENTS

LIST OF FIGURES

LIST OF TABLES

CHAPTER 1: INTRODUCTION

1.1 Background

Back in the 19th century, concrete was only used in applications where axial forces are dominant such as arches and columns due to its superior compressive performance and weak tensile performance. Later, Engineers discovered that embedding steel in concrete would create a composite material with more compressive strength and most importantly far more superior tensile performance compared to plain concrete. This composite material called Reinforced Concrete (RC) was used throughout the 20th century as the main construction material until a few decades ago when engineers realized the need for alternative reinforcement materials due to weaknesses of steel in specific scenarios. The research community identified that FRP materials are a good alternative to steel due to their superior properties in some regards. Corrosion of steel is a good example of FRP being more superior in that regard since, FRPs are resistant to corrosion by various chemicals especially, against chlorides. Subsequently, research regarding FRP as an internal and external reinforcement material started accelerating and many studies had been conducted so far throughout the last few decades.

Any structural member is designed in such a way that it can safely withstand subsequent responses in the member caused by the applied loads, which are mainly axial, flexural, shear and torsional stresses. Structural design must ensure the designed (carrying) capacities are safely and sufficiently greater than the expected capacities. This condition can be violated either by the reduction of carrying capacities or the increment of expected capacities. Increment in expected capacities can happen when the usage of the structure change, for example, repurposing a building floor for different usage. Decrement of carrying capacities can happen mainly by the degradation or depreciation of steel and concrete that the structural member is made of due to unfavourable environmental conditions (Hollý et al., 2016). Furthermore, errors in the construction process can lead to strength deficient RC elements.

There are mainly two solutions to remedy this issue which are destruction and re-construction of structure with sufficient capacities or renovate it using retrofitting techniques. Usage of the FRP materials for external retrofitting of RC members has been gaining popularity since it was introduced to the industry a few decades ago as a result of its superior properties: extraordinary strength, corrosion resistivity, low weight. FRPs are available in several types: Carbon Fibre Reinforced Polymer (CFRP), Glass Fibre Reinforced Polymer (GFRP) and Glass Fibre Reinforced Polymer (AFRP). It is available as fabrics, plates and fibres which will be applied on structural members using mostly a type of resin epoxy adhesive (Ehsani, M. R., Saadatmanesh, H. & Tao, 1996).

A typical RC beam is generally designed for flexure and shear since under typical load conditions RC beams generally respond with flexure and shear. However, the out-of-plane curved RC beam responds with shear, flexure and additionally torsion. Hence, an out of plane loaded curved beam is structurally more critical than a straight beam due to its torsional stresses contributing to shear stresses of the beam which can lead to a brittle failure mode (Lee, 1956; Wong, 1970). Curved structures always have been very popular in the industry due to their aesthetic quality which leads to the necessity of studying the behaviour of FRP strengthened horizontally curved RC beams (Lee, 1956).

Even though there are numerous studies and guides available for retrofitting straight RC beams using CFRP, according to the author’s knowledge none of the studies had been focused on studying the effect of torsional and shear responses in a horizontally curved beam on external CFRP reinforcement and the overall behaviour. Hence, to minimize this gap of knowledge, an experimental and numerical program has been developed and carried out and compared with theoretically expected results based on currently existing design guidelines and codes.

1.2 Research Objectives

- To conduct an experimental program to determine the behaviour of CFRP strengthened out-of-plane curved RC beam subjected to combined effects of shear and torsion.
- To develop a numerical/computational model by utilizing an advanced Finite Element Analysis (FEA) program to predict the sensitivity geometry on strength enhancements.
- To develop a theoretical model to determine the general responses of an out-of-plane curved beam subjected to vertical loads.
- To propose design recommendations on the application of CFRP to retrofit the out of plane curved reinforced concrete beams.

1.3. Methodology

Conducting a literature review to investigate and recognize on research gaps

↓

Investigation of currently existing theoretical knowledge on application of FRP as an external reinforcement in RC beams

↓

Conducting an experimental study, investigating behaviour of CFRP strengthened horizontally curved concrete beam

↓

Developing a numerical/computational model (validated by experimental results) to predict the sensitivity of bond parameters on strength enhancements

↓

Developing a theoritical relationship to predict the capacity enhancement using experimental, numerical results and data available in literature.

↓

Conclusions & design recomendations

Figure 1: Summary of methodology

1.4. Thesis Arrangement

The thesis is presented as a sum of several chapters and the descriptions are as follows.

Chapter 1: Introduction

An introduction is presented in this chapter including clear objectives of the research and, the flow and steps of the methodology.

Chapter 2: Literature review

A detailed literature survey/review regarding the topic was done and summarization is presented in this chapter. The purpose of this chapter is to recognize the research gaps existing in the relevant research areas which act as the foundation for developing this research.

Chapter 3: Experimental program

This chapter explains the material properties, specimen preparation, instrumentation, testing procedure, observations and results.

Chapter 4: Theoretical analysis

This chapter is devoted to theoretical calculations of general responses of an out-of-plane curved beam with fixed boundary conditions and theoretical/empirical formulas for determining flexural, shear and torsional strengths of an RC beam based on design guidelines and codes that are currently in practice.

Chapter 5: Numerical analysis

This chapter describes in detail the process of developing a numerical model using an advanced finite element analysis program. Relevant theories, assumptions, material models, results and parametric studies are described in the chapter.

Chapter 6: Conclusions and recommendations

This chapter identifies the areas that should be further researched and also provide important aspects to be considered in the design, detailing and construction of CFRP strengthened out of plane curved reinforced concrete beams.

CHAPTER 2: LITERATURE REVIEW

This chapter is devoted to exploring the currently existing research knowledge base regarding the application of FRP composite material as an external reinforcement in RC members. Even though there are numerous studies focused on this research area, there are still gaps in the research knowledge base. The main purpose of the chapter is to recognize such important research gaps and focus this research on diminishing them.

2.1. FRP Composite Materials

Fibre Reinforced Polymer (FRP) is created by impregnating the aforementioned types of fibres to a protective resin (polymer). Fibres behave as reinforcement for FRP composite and it provides the directional stiffness and strength hence, the strength of FRPs material heavily depend on the volume proportion of the fibres. The resin matrix has several contributions for the composite: transfer the stresses to fibres, provide the in-plane & inter-lamina shear strength and compressive strength, hold the fibres together and protect the fibres from environmental attacks. To transfer the stresses properly Young's modulus of the matrix must be significantly less than Young's modulus of the fibres. Combining both material types results in a composite material with important properties of each material (ACI Committee 440, 2017; Karaca and Buyukozturk, 2002; Nanni et al., 2014).

The combining process of the two materials also affects the strength of FRP. The orientation of fibres, manufacturing method and quality control can be recognized as the main factors of the manufacturing process that affect the properties of FRP composites. Furthermore, the length and shape of the fibres affect the properties of FRP. Even though the length of the fibres can be long or short, usually in the construction industry for FRP composites long and continuous fibres are used which are usually in parallel to one direction two perpendicular planar directions. This makes the composite to be highly anisotropic. However, there are less common FRP products with multidirectional fibres or randomly oriented short fibres which tends to be isotropic hence, such composites are suitable for cases where shear strength is necessary (Hull and Clyne, 1996; Nanni et al., 2014).

For other important properties, high corrosion resistance and lack of electromagnetic properties can be taken. High corrosion resistance is one of the main reasons that FRP becomes a substitute for steel but in the alkaline environment, it can be vulnerable to corrosion. The lack of electromagnetic properties can be very useful in some special scenarios (Richardson and Drew, 2011).

Generally concrete has a coefficient of thermal expansion of 14 x 10-6 m/mk and steel has a value of 13 x 10-6 m/mk, which is very close to each other. Hence, steel is a perfect reinforcement material for concrete. The coefficient of thermal expansion for FRP varies from (16 to 22) x 10-6 m/mk which is not near perfect as steel but adequate to retain structural integrity throughout general thermal changes (Allen and Iano, 2009; Nanni et al., 2014).

Table 01 represents the comparison of the physical properties of steel and different FRP materials. When properties presented in Table 01, Table 02 and 03 are given in the below sections, it can be observed that even though the tensile strengths of fibres lie in the range of 1.7 – 4.6 GPa, the tensile strengths of the FRPs are in the range of 480 – 2600 MPa. This is due to the bottlenecking of the strength by relatively lower strengths of resins compared to fibres.

Table 1: Comparison of physical properties between different FRPs and steel (Nanni et al., 2014)

Fibre	*Yield stress*	*Tensile strength (MPa)*	*Elastic modulus (GPa)*	*Yield strain*	*Rupture strain*
Steel	275.9 – 517	483 – 690	200	0.14 – 0.25	6.0 – 12.0
GFRP	-	483 – 1600	35 – 51	N/A	1.2 – 3.1
CFRP	-	600 – 3690	120 – 580	N/A	0.5 – 1.7
AFRP	-	1720 – 2540	41 – 125	N/A	1.9 – 4.4

2.2. Types of fibres

As mentioned before, fibres give the strength and directional stiffness of the FRP composites. In the construction industry mainly three types of fibre are used for FRPs which are carbon, glass and aramid. Basalt fibres have been gaining attention last few years as an alternative for glass fibres however, it is not common as the other three types of fibre. The selection of fibres should be done considering various factors: cost, specific strength requirements and specific environmental conditions (Karaca and Buyukozturk, 2002; Nanni et al., 2014). Table 02 presents a summary of the various properties of different fibres.

2.2.1. Carbon fibre

Carbon fibres are classified into two separate types based on Young's modulus due to the wide variation of strength and stiffness of the material which depends on the manufacturing process. For civil engineering applications, mostly PAN-based carbon fibre is used due to its high strength and relatively higher Young's modulus. As low modulus carbon fibres, rayon-based fibres can be recognized. Several superior chemical properties compared to other alternative materials: resistance to alkali/acid attacks, high electrical conductivity and ability to cause galvanic corrosion on metal can be recognized as a disadvantage or an advantage depending on the application. As for the physical properties, brittleness, relatively low impact resistance and low coefficient of thermal expansion can be recognized in carbon fibres (Karaca and Buyukozturk, 2002; Nanni et al., 2014).

2.2.2. Glass fibre

Even though there are several types of glass fibres available, mainly three types can be recognized as most commonly used in civil engineering applications: Electrical glass fibres (E-glass), High Strength glass fibres (S-glass) and Alkali Resistance glass fibres (AR-glass). E-glass provides superior corrosion resistance and electrical insulation while S-glass provides higher strength and stiffness. However, S-glass is costlier compared to E-glass. AR-glass provides much more superior alkali attacks whereas E-glass and S-glass are weak against alkaline induced corrosion compared to other alternative types of fibre. Hence, a suitable matrix must be used with glass-based fibres for durable applications (Karaca and Buyukozturk, 2002; Nanni et al., 2014).

2.2.3. Aramid fibre

Aramid fibres are organic synthetic materials with superior mechanical properties: high strength, high toughness, high impact resistance and high resistance for creep and rupture. Due to its high strength and low density (low weight), aramid fibres are used in the sports industry and military applications, i.e. Kevlar bulletproof vests, other than civil engineering applications. Furthermore, aramids have higher resistance against electricity, heat fire and various chemical attacks, however, vulnerable to ultraviolet (UV) light (Karaca and Buyukozturk, 2002; Nanni et al., 2014).

2.2.3. Basalt fibre

Basalt fibres are relatively new to the civil engineering industry and research studies are ongoing to improve the properties of the material. It is mainly used as an alternative to glass fibres as a result of its relatively superior strength, stiffness and ease of production and high availability of Basalt material (Nanni et al., 2014).

Table 2: Properties of Fibres (Nanni et al., 2014)

Fibre type	Density (kg/m^3)	Tensile strength (GPa)	Tensile modulus (GPa)	Ultimate tensile strain (%)	Poisson's ratio
E-glass	2501	3.45	72	2.4	0.22
S-glass	2501	4.55	86	3.3	0.22
AR-glass	2254	1.79 – 3.45	70 – 76	2.0 – 3.3	N/A
High modulus carbon	1952	2.48 – 4.00	350 - 650	0.5	0.2
Low modulus carbon	1750	3.50	240	1.1	0.2
Aramid (Kevlar 29)	1440	2.76	62	4.4	0.35
Aramid (Kevlar 29)	1440	3.62	123.5	2.2	0.35
Aramid (Kevlar 29)	1440	3.45	174	1.4	0.35
Basalt	2799	4.82	88.5	3.1	N/A

2.3. Types of Matrix resins

As mentioned above, the main purposes of the matrix are to transfer stresses to fibres. Additionally, it provides protection for fibres and shear & compressive strength of the composite. Two types of matrix materials can be recognized, namely, thermosetting polymers and thermoplastic polymers. Former is usually used in civil engineering applications. Thermoplastic and thermoset polymers usually are liquid or semi-solid and once they are cured it will result in a solid, comparatively strong rigid material. However, thermoplastic polymers can be turned back to the liquid form even after the curing process which makes them highly unsuitable for civil engineering applications whereas, thermoset materials retain their strength and rigidity once curing is done which is highly suitable for structural engineering applications. Mainly three types of thermoset polymers are currently in practice, which are epoxies, polyesters and vinyl ester resins. Furthermore, fillers are usually used to engineer the properties of polymers and reduce the overall cost of the materials(Grumezescu and Grumezescu, 2019; Karaca and Buyukozturk, 2002; Nanni et al., 2014). A tabular comparison between important properties of types of matrices is presented in Table 03.

Table 3: Properties of resins (Nanni et al., 2014)

Resin type	Density (kg/m3)	Tensile strength (MPa)	Longitudinal modulus (GPa)	Poisson's ratio (%)	Glass Transition temperature (C^0)
Vinyl ester	1127 - 1365	3.0 – 8.9	3.00 – 3.45	0.36 – 0.39	70 - 165
Polyester	1187 - 1424	4.2 – 11.3	2.76 – 4.14	0.38 – 0.40	70 - 100
Epoxy	1187 - 1424	5.9 – 6.5	2.07 – 3.45	0.35 – 0.39	95 - 175

2.3.1. Epoxies

Epoxies are dominantly used in civil engineering applications due to their superior mechanical and physical properties and low shrinkage compared to alternatives. Even though, there are disadvantages to epoxies: the cost of epoxies are higher, long curing time and difficulty of application to concrete, it is preferred over other alternative materials due to the aforementioned advantages. Furthermore, Good adhesion to fibres, superior performance against environmental conditions and high compatibility with all four main types of fibres can be recognized as other important properties of epoxies (Karaca and Buyukozturk, 2002; Nanni et al., 2014).

2.3.2. Vinyl Esters

Vinyl esters typically show close superior mechanical properties of epoxies, however, has a higher cost compared to epoxies. Vinyl esters are encouraged to use in GFRP over epoxies even though it has a higher cost, due to its highly impressive resistance for alkaline environmental conditions and good wetting and adhesion with glass fibres (Karaca and Buyukozturk, 2002; Nanni et al., 2014).

2.3.3. Polyesters

Polyesters show the optimum cost to strength characteristics. Two types of polyesters are commonly used: orthophthalic and isophthalic acidic polyesters. Iso polyesters have superior mechanical properties and superior thermal and chemical resistance compared to ortho polyesters, however, costlier. Even though there are advantages for polyesters as mentioned before, it is usually discouraged to use polyesters for FRPs as a result of their low strength and resistance against environmental conditions compared to epoxies and vinyl esters (Karaca and Buyukozturk, 2002; Nanni et al., 2014).

2.4. Failure modes of RC members

Failures in RC members are rare in properly designed RC elements due to several safety factors involved in all design guidelines and codes in practice. However, due to errors in design calculations and assumptions or errors in the construction stage, strength deficient RC members can result. Furthermore, a change of purpose in a structure may increase the service loads resulting in, the capacities of existing RC members resulting in being insufficient. In such cases, the RC members could fail in several failure modes which can be classified into two main categories: brittle and ductile. Brittle failures are very sudden in nature, hence, must be avoided at any cost. However, ductile failure modes are relatively slow and early signs such as cracks and abnormal deformation of RC elements will occur prior to the failure. Hence, due to the early signs, ductile failure modes are preferred in design codes and guides in practice, except for special cases (Arya, 2009).

2.4.1. Failure modes in beams

There are mainly two failure modes in RC beams which are, flexural failure and shear failure. Flexural failure depends on two factors which are the beam is over-reinforced or under-reinforced. When a beam is under flexure, three regions in the beam section can be recognized (Figure 2): compression zone where the material is under compressive stress, tension zone where the material is under tensile stresses and Neutral plane where zero stresses exist.

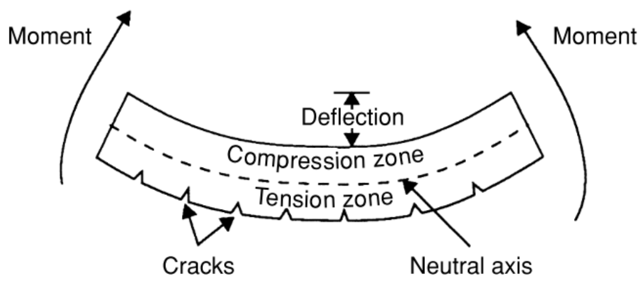

Figure 2: Compression and tension zones in a beam under flexure (Arya, 2009)

When the load/moment increases, since concrete has very low tensile strength, all tensile stress will transfer to reinforcement bars as shown in Figure 3c. In the compression zone, the stress distribution will start as linear variation and further increment of the load will result in a non-linear (assumed to be parabolic) variation in the compressive stress distribution. If the beam is under-reinforced, the steel reinforcement bars will yield while showing the aforementioned signs before ultimately failing by crushing concrete in the compressive region. It means the failure is a ductile failure followed by a brittle failure mode. However, if the beam is over-reinforced, the beam will fail by crushing the concrete at the compressive zone before the yielding of steel, which means the failure is a brittle mode. Hence, in design practices usually, beams are designed as under-reinforced sections to avoid brittle compressive failure under flexure (Arya, 2009).

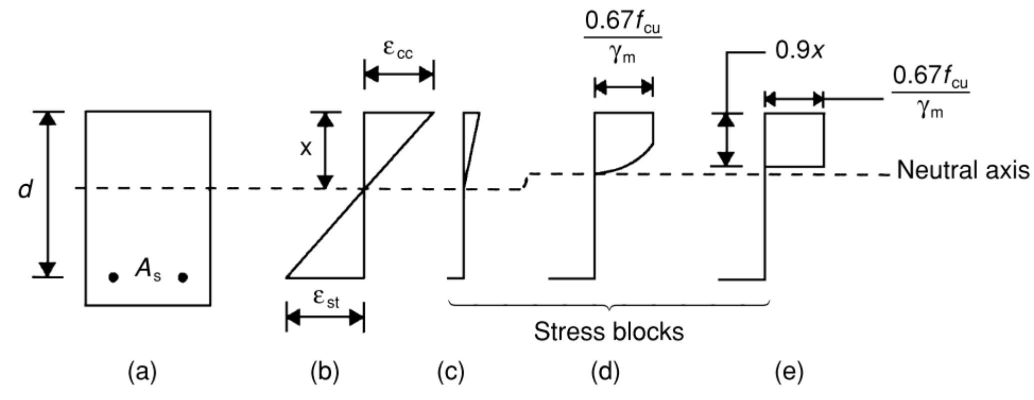

Figure 3: Stress and strain distributions at a beam section under flexural moment: (a) section, (b) strains, (c) triangular (low strain), (d) rectangular parabolic (large strain), (e) equivalent rectangular (Arya, 2009).

Another way that a beam can fail is a shear failure which can occur mainly in two ways: diagonal tensile failure and diagonal compressive failure as shown in Figure 4.

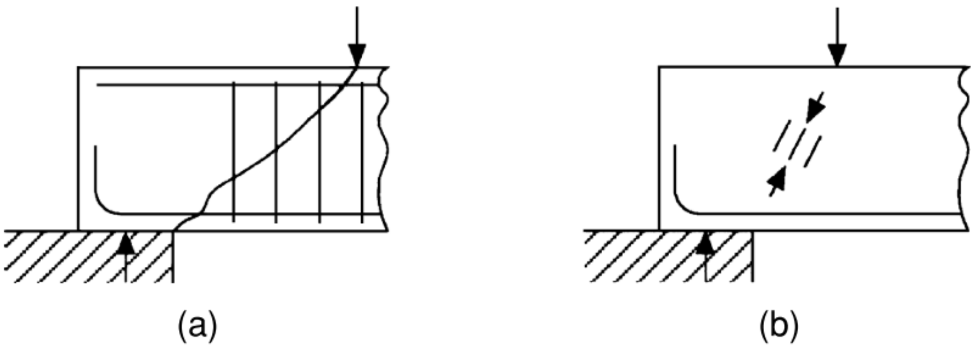

Figure 4: Types of shear failure: (a) diagonal tensile failure (b) diagonal compressive failure (Arya, 2009)

Diagonal tensile failure is highly critical in a concrete beam without shear links, compared to diagonal compressive failure due to the low tensile capacity of concrete. This failure mode is brittle and will rapidly occur leading to a catastrophe. Hence, in most cases, shear links will be provided to avoid such failures. However, there are cases that do not need shear links due to the low service loads which can be resisted by the shear capacity of plain concrete. After shear links are added, the failure mode can be either by yielding shear links or diagonal compressive failure. Hence, if the applied load is more than compressive shear strength, the beam must be redesigned in such a way that the applied load is less than the compressive shear strength of the beam. It will ensure that the failure mode to be yielding of shear links which is a relatively ductile failure mode (Arya, 2009; BS 8110-1:1997, 1997; BS EN 1992-1-1, 2004). Figure 5 presents some experimental results done by (Dinh et al., 2011) regarding different types of shear failures.

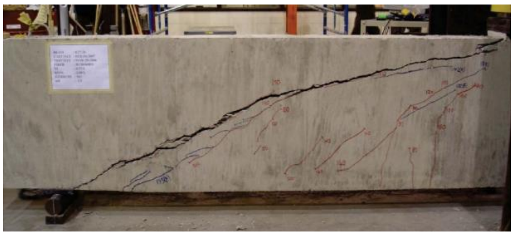

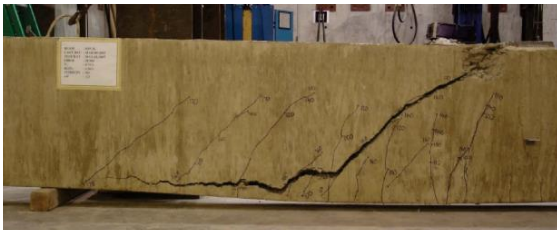

(a) (b)

(c)

Figure 5: Shear failure modes and crack patterns (a) diagonal tensile failure with shear links (b) diagonal compressive failure (c) diagonal tensile failure without shear links (Dinh et al., 2011)

Mainly three factors affect the shear failure modes: the grade of concrete, aggregate interlock across the crack region and dowel action of the tensile reinforcement. The grade or strength of the concrete governs the compressive strength or tensile strength of the concrete which determine load of initial shear crack. When load increases furthermore, the aggregate in the crack zone will lock each other resisting even more shear force. When load increases, even more, the aggregate interlock will be lost transferring the load to the shear links and tensile reinforcement. The shear links and by the dowel action of the tensile reinforcement, the shear force will be resisted until the failure occurs by either yielding of shear links or diagonal compression (Arya, 2009; Cranston et al., 1996; Dinh et al., 2011; Johnoehlers and Rudolf, 2004). The aggregate interlock and dowel action are illustrated well in Figure 6.

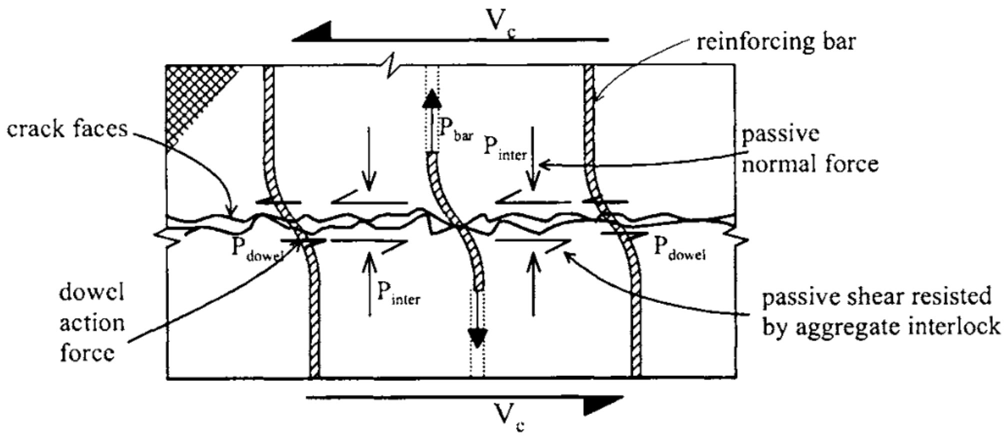

Figure 6: Aggregate interlock and dowel action of tensile rebars (Johnoehlers and Rudolf, 2004).

2.4.2. Failure modes in columns

There are mainly two failure modes in RC columns which are, compressive failure of concrete and steel reinforcement or buckling failure due to axial force or a combination of both failures. Short columns usually fail in compressive failure whereas, slender columns tend to fail in buckling mode. To quantify the slenderness of the column the slenderness ratio is used, and in the design stage usually, the slenderness of columns is avoided by increasing sectional dimensions. Figure 7 illustrates the two types of failures of a column (Arya, 2009).

Under dynamic loads, mainly earthquake loads, the connection between beam and column can fail in a brittle failure. The failure occurs by crushing and spalling the concrete in the joint region. Lateral reinforcement in the joint and anchorage dominantly resist this failure. Figure 8 presents some of the disasters that happened and the effect of earthquake loads on beam-column joints (Cosgun et al., 2020; Hassan et al., 2010).

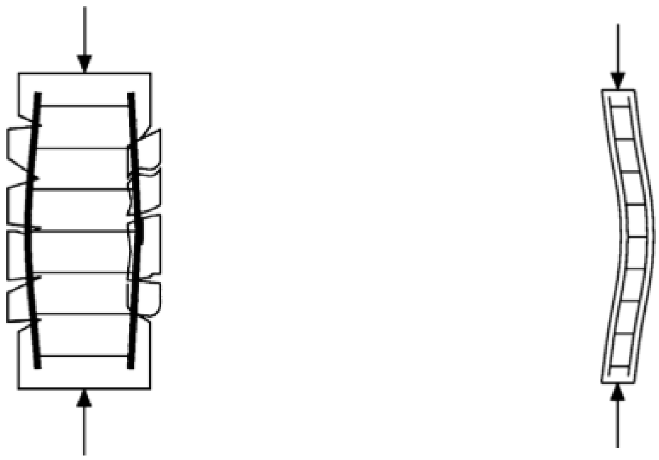

(a) (b)

Figure 7: Failure modes of columns (a) Compressive failure of concrete and steel (b) buckling (Arya, 2009).

(a)

(b)

Figure 8: Column-beam joint failure due to earthquake load (a) Kaiser Permanente Building, Northridge earthquake, 1994 (Hassan et al., 2010) (b) Column-beam failure due to Van Tabanli and Edremit earthquakes (Cosgun et al., 2020).

2.4.3. Failure modes in slab-type elements

Various types of members in an RC structure consists of slab-type elements as shown in Figure 9. A slab can be considered as a series of beams connected together in such a way that stresses are transferred between each adjacent beam element. Hence, all flexural and shear failure mods discussed in 2.4.1 are also valid for slabs-types elements although, flexural failure is far more critical in slabs compared to beams. Most of the times shear links are not necessary at the ends of slab elements.

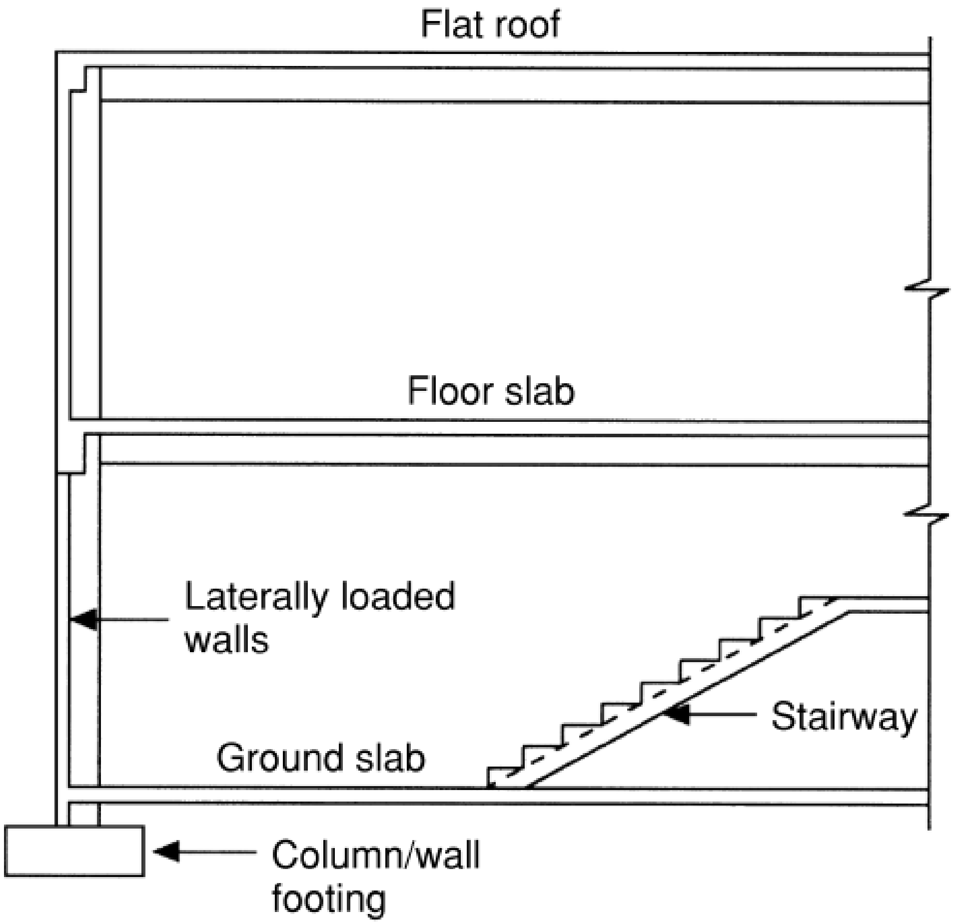

Figure 9: Various types of structural members in an RC structure that consists of slab elements (Arya, 2009).

There are several types of slabs solid slabs (beam-slab system), ribbed slab systems (waffle slabs), precast and flat slabs. The other most common failure of slab-type elements is punching shear which usually occurs in slab-column joint regions that do not have beams over columns, for example, flat slabs, footing, rafts and pile caps.

Punching shear is a brittle failure mode, hence, must be avoided. There are various methods in practice to avoid punching which can be categorized into two methods. The first method is manipulating either column dimensions or the slab thickness around the punching element to achieve a high shear resistance (Figure 10). The other method is to provide shear resisting reinforcement around the punching region (Figure 11) (Arya, 2009; Silva et al., 2021).

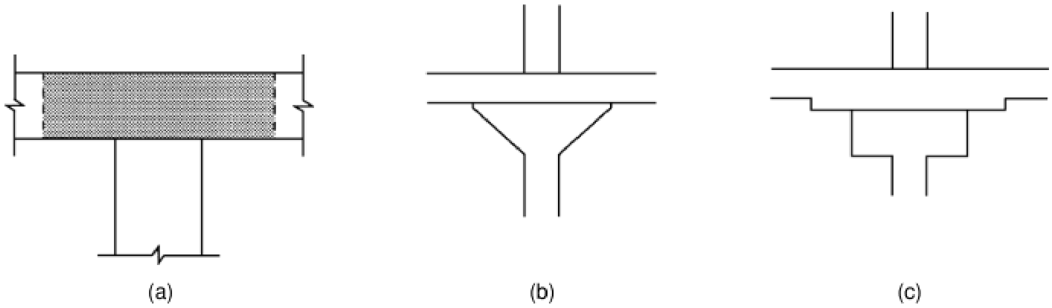

Figure 10: Manipulating element dimensions to resist punching shear (a) deep slab and large column (b) slab with flared column head (c) slab with drop panel and column head (Arya, 2009).

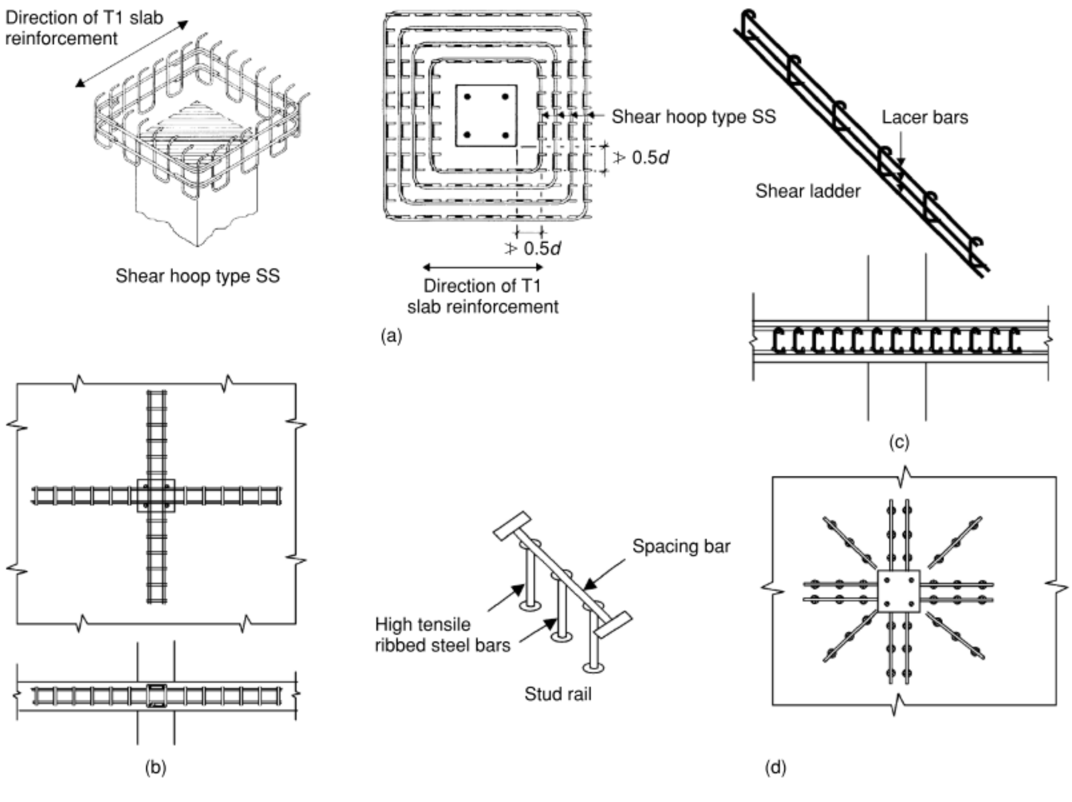

Figure 11: Providing shear reinforcement in various forms (a) shear hoops (b) ACI shear stirrups (c) shear ladders (d) stud rails. Typical arrangements for an internal column (Arya, 2009)

2.5. Curved RC elements

Curved structures are very popular among architects and engineers due to their aesthetic appearance. Beams that are curved before a bending moment or a load is applied, are called curved beams. Two main types of curved beams can be recognized, which are vertically curved beams and horizontally curved beams. There can be variations of these types of beams such as curved beams with varying curvature, angled from the horizontal plane and a combination of vertical and horizontal curvatures.

Figure 12: Curved bridge (Yindeesuk, 2009)

Figure 13: Curved building (Griffiths, 2014)

2.5.1. Vertically curved in-plane loaded beams

Vertically curved beams can be defined as beams that are curved in space and in-plane loaded, such as curved members in arches and bents. Horizontally curved beams can be defined as the beams curved in the plan such as curved girder members in circular buildings & domes, beams in curved sections of bridges and curved elevated highway ramps (Lee, 1956).

The vertically curved beams have much relatively higher structural integrity than the straight beams due to their shape, the loads almost completely transfer axially producing nominal stresses on cross-sections and minor bending moments. Hence, the ultimate capacity of vertically curved beams depends on the ultimate compressive strength of the concrete rather than the ultimate tensile capacity of concrete and since the compressive capacity of concrete is much greater compared to the tensile capacity, vertically curved beams have much higher structural integrity compared to horizontally curved and straight beams.

2.5.2. Horizontally curved, out-of-plane loaded beams

When a horizontally curved beam is subjected to out-of-plane loads, additional torsional stresses (Figure 14) will be produced along with flexural and shear stresses. However, in a straight beam, there will be only flexural and shear stresses. This additional torsional stress in curved beams will cause to reduce the beams' shear capacity by adding a component from torsional stresses to shear stresses subsequently causing the beam to fail in shear at a lower load. Hence, horizontally curved beams are more critical and vulnerable to shear failure compared to straight and vertically curved beams (Wong, 1970).

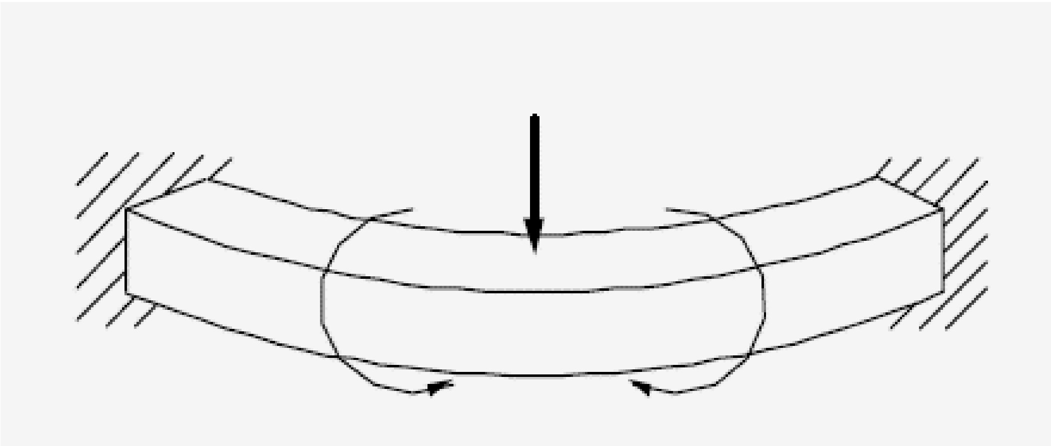

Figure 14: Out of plane loaded horizontally curved beam (Tamura and Murata, 2010)

2.6. Application of FRPs on RC elements

FRP materials have been gaining attention as a solution to avoid such failures discussed in section 2.4 due to their superior properties which are explained in sections 2.1 to 2.3. As explained before, structural failures can occur in RC members as a result of errors in the design and construction stage, change of purpose of structure and degradation of internal reinforcement and concrete due to environmental attacks. However, if the application methodology is not done properly the maximum strength enhancements cannot be achieved due to premature delamination of FRPs (Ehsani,

M. R., Saadatmanesh, H. & Tao, 1996). Hence, the proper form of FRP, proper type of FRP and the proper arrangement of FRPs depending on the specific conditions of the structure and the specific strength enhancement that has to be achieved, and proper constituent materials must be selected prior to the application of FRPs.

2.6.1. Application methods that are currently in practice

FRPs are available in several forms: bars, plates, weaved fibre fabrics and separate fibres which can be classified mainly into two categories, wet layup and precured systems. The wet layup method is done in-site in two main methodologies: installation of uni-directional or multi-directional fibre fabrics by using a saturating resin which also acts as the adhesive between fibres and the concrete surface and to apply fibre tows by wounding or mechanical means while impregnating with a resin. Prepreg systems another method that instead of impregnating fibre with resin in the site, is available as partially cured pre-impregnated fibre composite by the manufacturer. Usually, an adhesive is used to install in this system and further curing should be done until FRP get fully cured. Precured systems are the same as prepreg systems instead, it comes as a fully cured system hence, no further curing is needed. Near Surface Mounting (NSM) is the other main method used for installing FRP to concrete (ACI Committee 440, 2017).

2.6.2. Constituent materials

There are several kinds of constituent material available commercially for different purposes. Primer is used to achieve an improved bond by penetrating the concrete surface. Existence of voids in the concrete substrate will reduce the surface area that FRP and concrete use to bond. And it can cause entrapment of air bubbles between FRP and concrete which must be avoided. It can be costly too since expensive adhesive or saturating resin will be used to fill those voids. Putty fillers are the solution for this in the industry which is a low-cost material that can be used to the voids. Finally, protective coating materials are used to improve the resistance of FRP systems against environmental conditions, fire, heat and chemical attacks (ACI Committee 440, 2017).

2.6.3. FRP installation procedure

FRP installation procedures vary with manufacturer, type of installation and the condition of the structure. However, there are general procedures that have to be done properly which will be discussed in this section.

The enhancement, failure patterns and FRP material utilization of RC structures largely depended on the bonding performance between FRP and concrete. Hence, the bond should be able to produce a continuous load transfer between the FRP composite and concrete substrate in the form of shear stresses to develop a full composite. The main considerations for a good bond include surface preparation, substrate repair, proper mixing of resins, application of FRPs, alignment of FRPs and curing. (ACI Committee 440, 2017; Sayed-Ahmed et al., 2009; Yao et al., 2005).

2.6.3.1. Surface preparation

There are mainly three application methods: bond-critical, contact-critical and NSM systems. Hence, surface preparation for each method differs from each others. Contact-critical applications don't need a good bond hence, a properly levelled surface without out of plane variations and a void-repaired surface is enough for contact-critical applications. For bond-critical applications, this is not the case since stress transfer to FRP heavily rely on the bond between FRP and the concrete surface. Hence, proper surface preparation should be done before applying the FRP system. For good surface preparation, mechanical grinding, sandblasting and grit blasting, must be done to remove weak layers and a proper cleaning method should be utilized to remove the detritus. Good surface preparation will expose the aggregates in concrete resulting in proper load transfer between two materials. Before adhering the plates to the concrete, they must be cleaned with weak acid and protected. If the fibres are wrapping around corners, the corners must be rounded to at least a 13 mm radius. All voids must be repaired using putty and all obstructions, inferences and embedded objects should be removed from the surface before application. NSM systems are usually installed by cutting grooves on the concrete substrate where FRP laminate strips or bars will be inserted with an adhesive. The groves must be free of any debris from the cutting process, any compound or moisture and must be properly cleaned before installation of FRP to ensure a proper bond (ACI Committee 440, 2017; Sayed-Ahmed et al., 2009).

2.6.3.2. Substrate repair

Substrate repair is needed when corrosion-induced deterioration and cracks are wider than 0.3 mm in a structural element. FRP should not be applied for RC elements with corroded steel internal reinforcement. First, the corrosion must be addressed and repairing must be done before the application. For cracks must be filled with a suitable repairing material using a pressure-injecting technique prior to FRP application if the crack widths are wider than 0.3 mm (ACI Committee 440, 2017).

2.6.3.2. Installation of FRP systems

Firstly, mixing of resins should be done being considerable for the fumes of resins since it can be volatile and toxic. The proper batch sizes, mixing ratios, mixing methods and mixing time must be done according to the manufacturer's specifications. Resins usually come as two-part with different colours hence, when mixing it should be done until colour streaks disappear and it takes a uniform colour. The mixing can be done either means of machinery or by hand. Then a primer and putty should be applied as explained above in Section 2.6.3.1 in this thesis. In the wet-layup method, firstly, the saturating resin should be applied at the concrete surface where FRP is supposed to apply. Dry fibres can be impregnated via a separate process before gently placing them over the saturating resin applied at the FRP applying area. The pre-impregnated fibres should be carefully pressed while placing and should be rolled out before resins sets to remove entrapped air between two materials. Another method to apply FRP is usages of machines where it can be used to automatically apply prepreg fibres to concrete elements, especially wrapping of concrete columns. In pre-cured systems, the first adhesive should be applied to the FRP applying area. Soon after FRP laminates should be placed and rolled out any entrapped air bubbles. For NSM systems as explained above grove should be cut on the correct location with correct depth and width. Then adhesive should be inserted and soon after FRP laminates should be inserted (ACI Committee 440, 2017).

2.6.4. Anchoring FRP to the concrete substrate

To avoid premature failure of FRP by debonding, there are several anchoring techniques used as illustrated in Figure 15. According to studies done by several researchers, (ACI Committee 440, 2017; Ebead, 2010; Ferreira et al., 2020; Grelle and Sneed, 2013; Kahandawaarachchi et al., 2019; Kalfat et al., 2013; Lee et al., 2010; Orton et al., 2008) with anchoring techniques either the premature failure of FRP sheet or plate can be delayed or completely avoided allowing to FRP-beam system fail in other common failure modes. Figure 15 illustrates various anchoring techniques that are used in the industry.

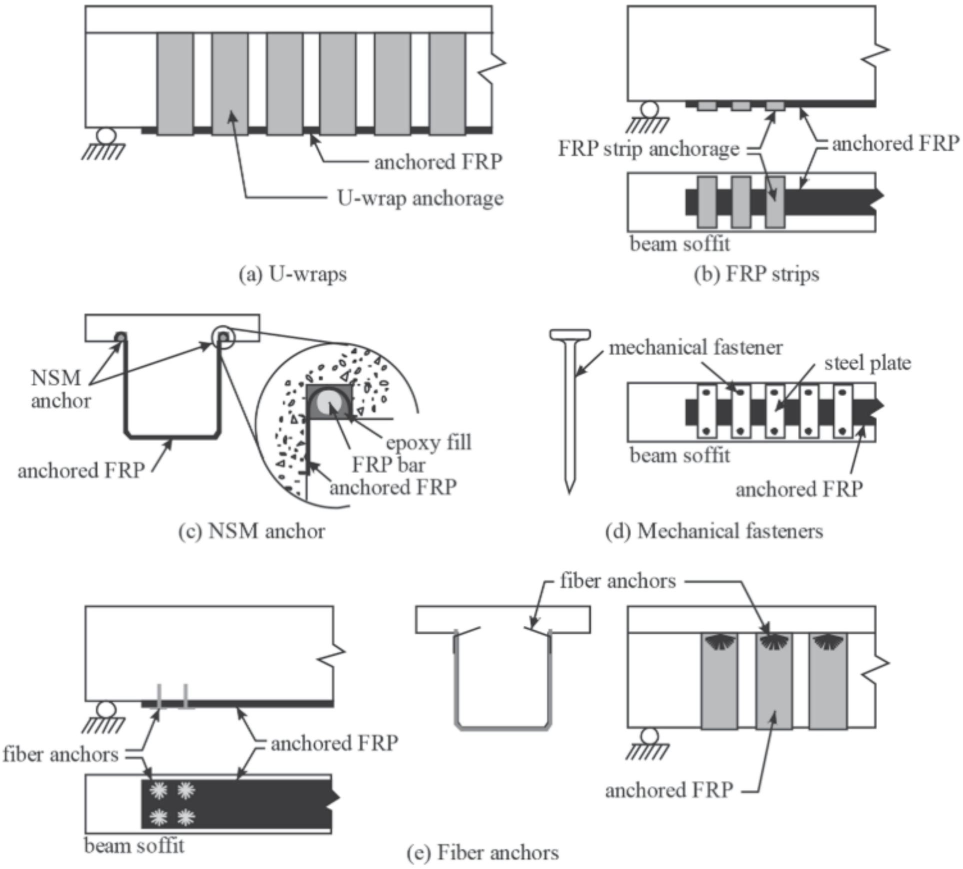

Figure 15: Various FRP anchoring techniques (ACI Committee 440, 2017)

2.7. Past research studies on strength enhancement of RC elements by FRP external reinforcement

As explained in section 2.4, RC members can fail in several failure modes and some of them can be avoided by the proper application of FRP as external reinforcement. This chapter is focused on research studies done regarding the strength enhancement of RC members for different types of scenarios. However, rehabilitation of earthquake damaged and seismically deficient RC members by the application of FRP and prestressed members or prestressed FRP external reinforcement, are not considered in this chapter, since the literature survey is focused on rehabilitation of RC members under quasi-permanent loading since aforementioned research areas are not included in the scope of this study.

2.7.1. FRP strengthening of RC beams

The ultimate strength of an RC beam depends on several factors: compressive strength of concrete, yield/tensile strength of internal steel reinforcement and shear strength of the beam. FRP can be applied to enhance said factors except for the strength of the concrete and there are numerous experimental studies done to quantify the enhancement and study the overall behaviour of the FRP applied RC beams.

2.7.1.1. Enhancement of flexural strength of RC beams

According to the experimental studies done by, (Diab et al., 2020; Ebead, 2010; Guo et al., 2021; Lorenzis and Nanni, 2002; Meier, 1995; Paul and Datta, 2018; Ritchie et al., 1991; Sharif et al., 1994) suggest that flexural strength enhancement by FRP external reinforcement can vary between 10 to 160 percent. However, when ductility and serviceability limits are defined in (ACI Committee 440, 2017) considered, a 40 percent flexural enhancement is reasonable for achieving a safe structure. The reason for this wide variation of the results is that the enhancement for flexure depends on a few factors which are, the condition of the bond between concrete and FRP, FRP type and form and mainly the failure mode of the system. There are mainly several failure modes that can be recognized in FRP strengthened RC beams under flexure, according to studies done by, (Hota V. S. GangaRao, 1998; Teng et al., 2001; Zhang et al., 2016). The failure modes are as follows.

a) Crushing of the concrete in compression before yielding the reinforcing steel.
b) Yielding of the steel in tension followed by rupture of the FRP laminate.
c) Yielding of the steel in tension followed by concrete crushing.
d) Shear/tension delamination of the concrete cover (cover delamination).
e) Plate end interfacial debonding failure.
f) Intermediate crack induced interfacial debonding failure

If the ends of the plate are properly anchored and the bond is adequate, then failure occurs when the ultimate flexural capacity of the beam-FRP system is reached, by either tensile rupture of the FRP plate or crushing of concrete. When the summation of the tensile capacity of steel and FRP is more than the compressive capacity of the top region of the beam, the classic failure mode of RC beams, crushing of concrete at the top region of the beam can occur.

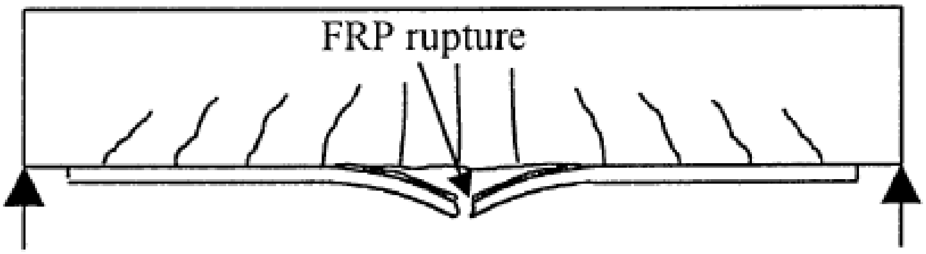

Figure 16: Failure by FRP rupture

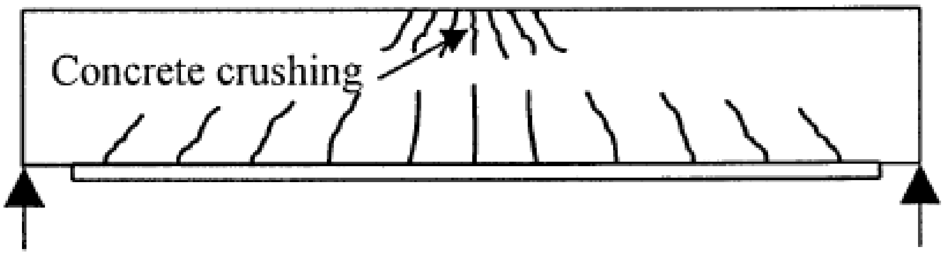

Figure 17: Failure by concrete crushing

If the compressive capacity of the top region of the beam reinforcement is greater than both the tensile capacity of steel and the tensile capacity of the FRP external reinforcement, yielding of steel followed by rupture of FRP can occur. If the compressive capacity of the top region of the beam reinforcement is greater than the tensile capacity of steel but less than the tensile capacity of the FRP external reinforcement, the yielding of steel followed by concrete crushing can occur.

However, the above failure modes are preferable to classic concrete crushing failure since when steel yielding it will be a ductile failure and warning signs will be available whereas, concrete crushing failure is very sudden and brittle.

In cover delamination failure, debonding is initiated at or near the plate end and propagates away from the plate end along with the level of the steel tension reinforcement. The bonded plate remains attached to the concrete cover in such a failure as shown in Figure 18. This failure occurs when the bond between the FRP plate and concrete is stronger than the tensile strength of the concrete. The high tensile stresses build up at the ends of the plates cause concrete at the cover area to fail. By using anchors at the end of the plates, this failure mode can be avoided.

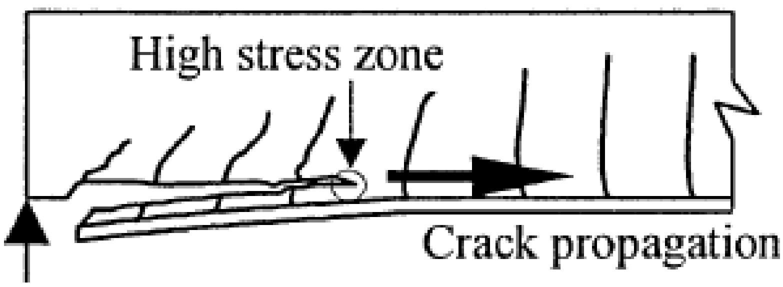

Figure 18: Cover separation failure (Teng et al., 2001)

The plate end interfacial debonding is the failure of the bond between the materials due to a weak or improper bond between the concrete and the FRP plate as illustrated in Figure 19.

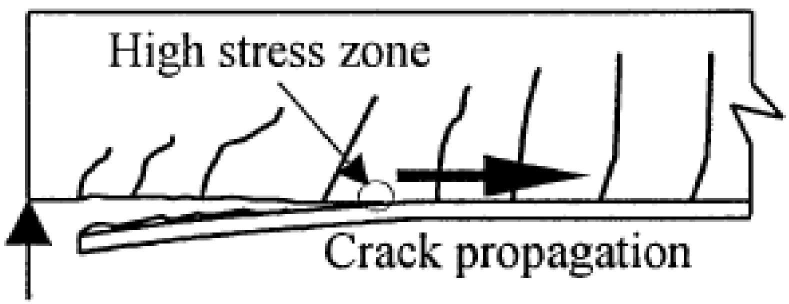

Figure 19: Plate end interfacial debonding failure (Teng et al., 2001)

The failure initiates at or near the plate end and then propagates away from the plate end in the concrete adjacent to the adhesive-to-concrete interface. Using strong adhesives and anchors this failure can be avoided.

The other main debonding failure mode is Intermediate crack induced interfacial debonding failure which is induced by a flexural or flexural-shear crack (intermediate crack) away from the plate ends as shown in Figure 20.

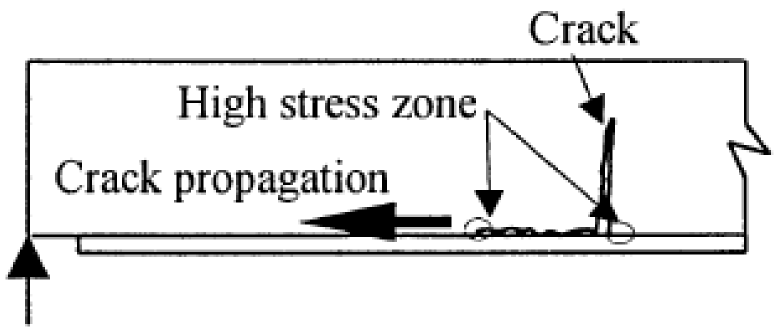

Figure 20: Intermediate crack induced interfacial debonding failure (Teng et al., 2001)

The plated RC beam can fail in shear if the flexural capacity of the plated beam exceeds the shear capacity of the RC beam after strengthening of RC beam for flexure by using FRP. In such cases, shear strengthening of the RC beam is required to ensure that the desired strength enhancement is achieved, and that flexural failure precedes shear failure because shear failure is more brittle than flexural failure which is not desirable in any case.

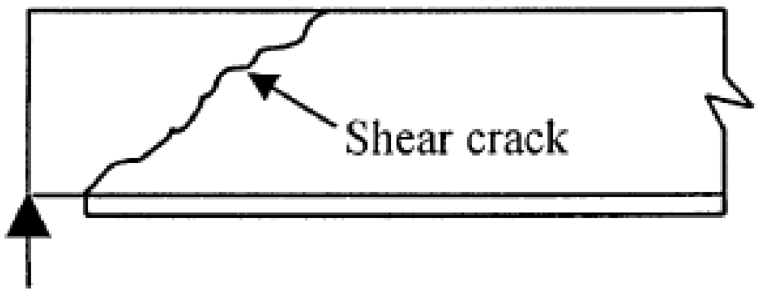

Figure 21: Shear failure of a typical RC beam (Teng, 2001)

2.7.1.2. Enhancement of shear strength of RC beams

Existing experimental studies suggest that the application of FRP external reinforcement increases the shear resistance of RC beams. The application of FRP can be done in three ways: fully wrapping, U-socketing and side bonding as shown in Figure 22.

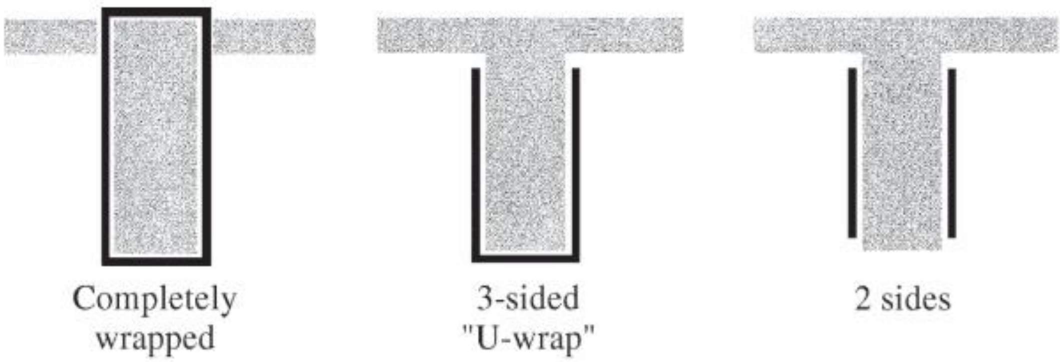

Figure 22: Different FRP application methods for the shear enhancement (ACI Committee 440, 2017)

(Chajes et al., 1995) reported that the application of FRP fabrics externally for shear has increased the shear ultimate capacity of the beam by from 60 to 150 percent. (Damian I. Kachlakev and David D. McCurry, 2000) reported a 50 percent of shear strength enhancement and 30 percent increments of the rigidity of bridge crossbeams with GFRP external shear reinforcement. (Saribiyik et al., 2020) reported 43 to 100 percent shear enhancement with Basalt FRP on RC beams. Furthermore, additionally to the above studies, several more studies (Adhikary and Mutsuyoshi, 2004; Koutas and Triantafillou, 2012; Li et al., 2020; Mofidi and Chaallal, 2011; Norris et al., 1997; Pellegrino and Modena, 2002; Sundarraja and Rajamohan, 2009; Triantafillou, 1998; Zhang and Hsu, 2005) confirmed that with externally bonded FRP, RC beams are showing very good shear enhancement performance.

The reasons for the high variation of results are mainly, the application method, fibre orientation and anchorage technique which have been adopted for the strengthening process. These factors affect the failure mode of the system which will change the shear capacity. Researchers (Adhikary and Mutsuyoshi, 2004; Saribiyik et al., 2020; Sundarraja and Rajamohan, 2009; Triantafillou, 1998) recognized that the shear enhancement performance of the fully wrapping method is far better than U-wrapping or side bonding methods. However, fully wrapping is utilized very rarely since the beam-slab system is very common in the construction industry whereas, U-socketing and side bonding is much more realistic for a beam-slab system. Fully wrapping can be adopted for beams and precast slab structures or bridge girders. (Adhikary and Mutsuyoshi, 2004; Norris et al., 1997; Saribiyik et al., 2020; Sundarraja and

Rajamohan, 2009; Triantafillou, 1998) showed that, when fibres are oriented perpendicular to potential shear cracks, the RC beam's shear capacity is more than the vertically oriented fibre system.

Existing experimental studies on RC beams shear strengthened with FRP composites have identified two main failure modes which are FRP rupture and FRP debonding failure. FRP rupture is the dominant failure mode for fully wrapped systems, due to its top and bottom regions acting as anchors for side bonded regions. The rupture failure seems to occur at the corner and mid-height of the beam sections as shown in Figures 23 and 24 (Cao et al., 2005).

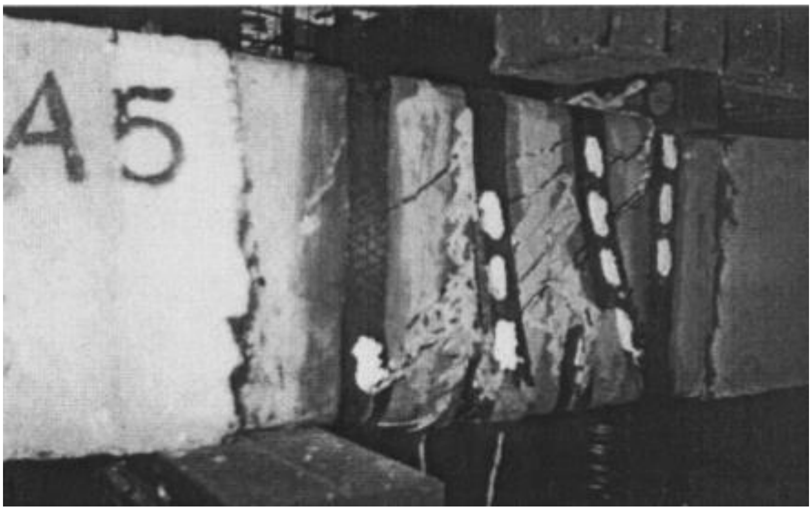

Figure 23: FRP rupture at beam corner on the fully wrapped system (Cao et al., 2005)

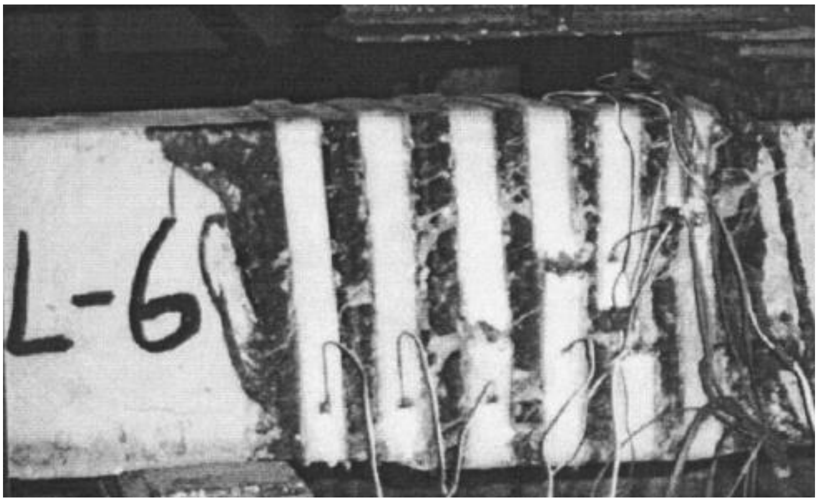

Figure 24: FRP rupture near mid-height of the beam on a fully wrapped system (Cao et al., 2005)

Researchers, (Chen, 2010; Chen and Teng, 2003; Teng, 2001; Teng et al., 2004, 2003, 2002, 2001) showed that FRP debonding is dominant in U-socketed and sided bonded systems, and recognized that bond failure can occur as peeling off of FRP due to adhesive failure or cover separation (Figure 25) and shear crack induced debonding (Figure 26). FRP rupture was also observed as crack induced FRP rupture (Figure 27) or due to the implementation of an anchoring system. Shear failure without FRP rupture, local compressive failure and anchorage failure were also observed in experimental studies however, they are not as common as debonding failure.

Figure 25: FRP debonding failure of a U jacketed RC beam (Teng et al., 2001)

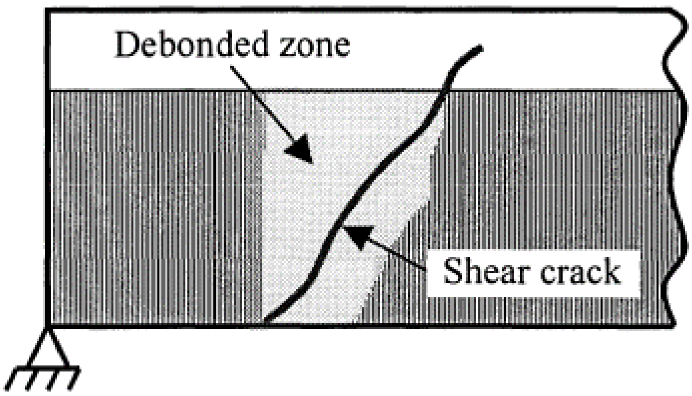

Figure 26: Shear crack induced debond failure (Teng, 2001)

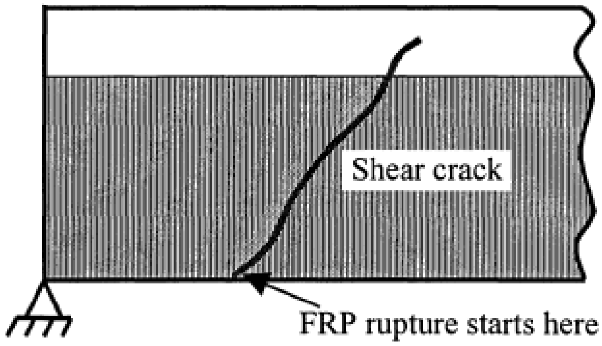

Figure 27: Shear crack induced FRP rupture (Teng, 2001)

2.7.1.2. Enhancement of torsional strength of RC beams

According to experimental studies done by (Ghobarah et al., 2002), under pure torsion, the fully wrapping of FRP was observed to be increasing the torsional capacity and significantly delaying the failure. However, with the increment of the torque, it was observed that the beam ultimately fails in crushing between FRP wraps (Figure 28). The FRP strips wrapped around the beam prevents the spalling of the concrete cover as shown in Figure 28 where concrete spalling occurs only between the FRP strips and was prevented at the FRP strips under torsion.

Figure 28: Spawling of concrete due to torsional failure (Ghobarah et al., 2002)

The FRP will provide additional tension reinforcement to the concrete increasing its ability to resist diagonal tension resulting from the applied torsion. Also, observed that the application of FRP with 45^0 fibre orientation is more effective than the vertical orientation of fibres for resisting torsional stresses.

2.7.2. FRP strengthening of RC columns

Several studies (Bousias et al., 2004; Chaallal and Shahawy, 2000; Iacobucci et al., 2003; Memon and Sheikh, 2005; Ozbakkaloglu and Fanggi, 2014; Sheikh and Yau, 2002; Triantafillou et al., 2016; Zeng et al., 2018) done on FRP strengthened columns under axial load and flexure has observed that wrapping of columns with FRP is to be highly effective for strength enhancement of RC columns. Under an axial load, the concrete column wrapped with FRP responds with tri-axial stresses which will be transferred to FRP as hoop stress.

Hence, the rupture of FRP was observed to be the dominant failure mode of columns wrapped with FRP as shown in Figures 29(a). Furthermore, debonding of FRP is also observed as shown in Figure 29(b). Since hoop stress is dominant in FRP, the implementation of rounding of corners must be done to avoid premature rupture due to stress concentration at corners. Usually, for RC columns, the application is done with the wet-layup method or prefabricated FRP jackets with an adhesive.

(a) (b)

Figure 29: Failure modes FRP strengthened RC columns (a) Rupture of FRP (Zeng et al., 2018) (b) Debonding of FRP (Ozbakkaloglu and Fanggi, 2014)

2.7.2. FRP strengthening of RC slab-type elements

A substantial amount of research done regarding strengthening one-way slabs for flexure where it was observed that it behaves the same as FRP strengthened RC beams since a slab can be considered to be a laterally connected series of beams (Karbhari and Seible, 2000; Ross et al., 1997; Shahawy et al., 1996; Teng et al., 2002). However, a very limited number of studies done regarding two-way slabs and (Teng et al., 2002) have shown that the application of FRP in two-way slab enhances the flexural capacity of the slab. Same failure modes as in FRP strengthened RC beam were observed in the above studies.

Figure 30: FRP strenghtneing of slab elements for flexure (Karbhari and Seible, 2000)

The main and most critical failure mode of slab-type elements is punching shear due to its sudden and brittle nature. (Silva et al., 2021) observed a punching shear enhancement of 20 to 90 percent with FRP external reinforcement. Several more studies observed an increment in punching shear capacity by a considerable amount with an FRP fan configuration (Meisami et al., 2014; Polak and Lawler, 2011). However, the studies done regarding punching shear of slab-type elements are very limited hence, further studies should be done to increase the reliability of said results.

2.8. Summary of the literature review

The main goal of the literature survey was to investigate on research gap existing in the current research knowledge base regarding the application of FRP as external reinforcement to enhance the strengths of RC curved concrete beams. However, only a few research studies have been focused on the retrofitted inplane curved beams while no research studies have been done on FRP strengthened out of plane curved RC beams. Hence, the first quarter of the survey was dedicated to investigating the background of FRP composite materials including, FRP types and forms, type of fibres and type of matrices. The second quarter was focused on failure modes of several types of RC members under typical loading conditions. Then the focus was on the application of FRP composite materials as external reinforcement to avoid or delay failure modes that were investigated in the second quarter of the survey. It was found that the application of FRP as external reinforcement was observed to effectively enhance the shear and flexural capacity of RC beams, bi-axial bending and axial compression capacity of RC columns and flexural and punching shear capacity of RC slab-type elements. Finally, it was focused on several installation processes and techniques of FRP to RC elements as external reinforcement and constituent materials involved in the installation process including the FRP strengthened out of plane and in-plane curved RC beams.

2.9. Future research needs

As a result of the literature review, several research gaps were identified. The main identification was that none of the studies has been focused on the behaviour of CFRP strengthened out-of-plane curved RC beam even though, many studies have been focused on the effect of flexural, shear, torsion and their combinations acting on FRP strengthened straight RC beams. Hence, it was decided to focus this study to contribute to filling the latter cited gap of research knowledge. Furthermore, it was identified that a very low number of studies has been done regarding bonding failure modes of FRP strengthened RC beam for shear, flexural strengthening of two-way slabs and strengthening for punching shear in slab-type elements. The lack of experimental results for the aforementioned research needs was also highlighted and the lack of analytical models or unreliability of existing analytical models due to it being developed on inadequate experimental data, also identified as a significant problem existing in the relevant research areas.

CHAPTER 3: EXPERIMENTAL PROGRAM

The experimental study contains two series. The first part contains a series of horizontally curved RC beams strengthened for shear by fully wrapping CFRP whereas, the second part contains a series of horizontally curved RC beams strengthened for shear by U-socketing of CFRP.

A total of eight medium-scale beams were tested for series one as summarized in Table 4. The series of specimens consists of a 2 m radius, 4 m radius and straight beams to investigate the effect of the curvature on the shear enhancement due to CFRP application. Figure 31 illustrates the schematics of the specimens in series one. Shear links in the regions which are subjected to direct shear are removed to allow the specimens to fail in shear without fully wrapped CFRP.

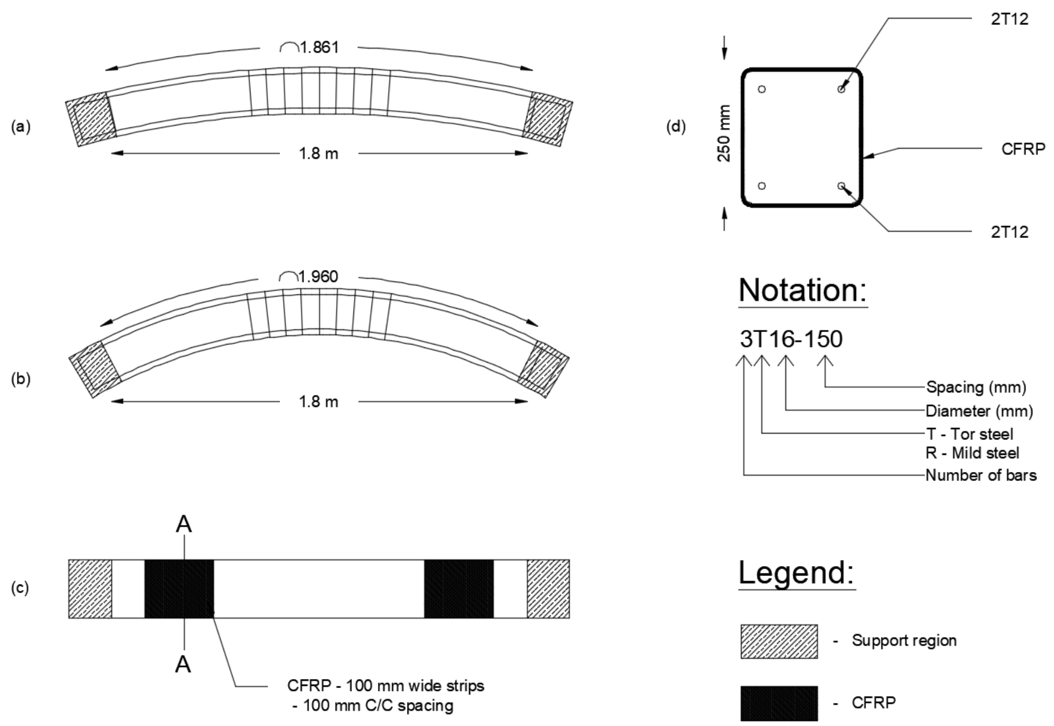

Figure 31: Schematics diagrams of specimens in series 1 (a) Plan view of a curved beam with 4 m radius (b) Plan view of a curved beam with 2 m radius (c) Side view of a CFRP strengthened beam (d) Sectional view of A-A.

The second series also contains twelve medium-scale RC curved beams and details are as shown in Table 4. It was divided into three sub-series with every four beams having a 4 m radius, 2 m radius and straight beams. The two radii were selected in order to investigate the effect of torsional stresses since the magnitude of the torsion heavily depends on the curvature of the beam, by comparing with the results of straight beams and results of each other. The torsion in the 2 m radius beam is expected to be higher than the torsion in the 4 m radius beam which results in 2 m beams being more vulnerable for shear failure. These three sub-series consists of two nen-strengthened control beams and two externally CFRP strengthened beams. For the external strengthening, the U-socketing application method was adopted since fully wrapping is impractical for the beam-slab systems, especially for internal beams. Hence, U-socketing is done leaving 100 mm from the top of the beam assuming an imaginary slab with a thickness of 100 mm.

Table 4: Details of specimens

Series	**Designation**	**Number of specimens**	**Type**	**Section dimensions (mm x mm)**	**Radius (mm)**	**Distance between support faces (mm)**
1	1-2-CO-EX	2	Control	200 x 200	2000	1800
	1-2-FW-EX	2	Fully wrapped	200 x 200	2000	1800
	2-4-US-EX	2	Fully wrapped	200 x 200	4000	1800
2	2-2-CO-EX	2	Control	200 x 250	2000	1400
	2-2-US-EX	2	U-socketed	200 x 250	2000	1400
	2-4-CO-EX	2	Control	200 x 250	4000	1400
	2-4-US-EX	2	U-socketed	200 x 250	4000	1400
	2-S-CO-EX	2	Control	200 x 250	∞	1400
	2-S-US-EX	2	U-socketed	200 x 250	∞	1400

Uni-directional CFRP fabric was used for strengthening due to its flexibility which is very important when U-socketing since CFRP has to be wrapped around the bottom corners of the beam section. The height of the beams was selected considering the allowance for slab thickness and the height of side sections of U-socketed CFRP to get a considerable increase in shear strength. The spacing and width of CFRP strips too were selected for achieving a considerable gain in shear strength. The distance between supports for all beams is kept as a constant of 1.4 m. The selection of 1.4 m distance and all internal reinforcement were done in order to reduce the possibility of a flexural failure and increase the possibility of a shear failure. An additional 300 mm length was added at the ends of the beam to support properly and clamp the beam to achieve fixed end conditions for all specimens. The arrangement of all specimens is illustrated in Figure 32.

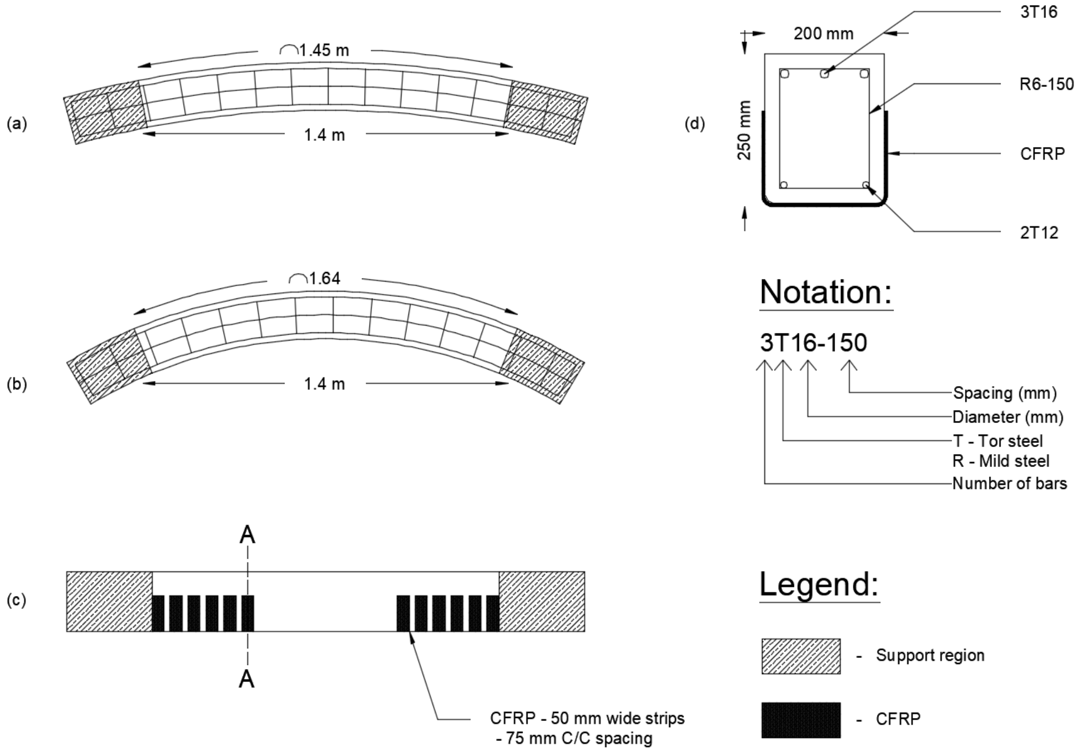

Figure 32: Schematics of specimens of series 2 (a) Plan view of a curved beam with 4 m radius (b) Plan view of a curved beam with 2 m radius (c) Side view of a CFRP strengthened beam (d) Sectional view of A-A.

3.1. Material and specimen preparation

The average 14-day compressive strength of the specimens was measured according to (BS EN 12390-3, 2019) and it was recorded as 28.3 N/mm2 with a standard deviation of 2.8 N/mm2. The measured average tensile strength of deformed steel bars and plain bars are 522 N/mm2 and 267.5 N/mm2 respectively which was measured according to BS EN 12390. Coupon tests were conducted according to American Standard Testing Methods (ASTM) to obtain the required material properties for CFRP (ASTM, 2014) and the obtained results are given in Table 5. The properties of the primer are also included in Table 5 which was obtained from the manufacturer (X-Calibur Construction Chemistry, 2017).

Table 5: Properties of carbon fibre fabric

Properties of carbon fibre fabric		**Properties of adhesive for fabrics**		**Properties of primer**	
Thickness (mm)	0.166	Tensile Strength (MPa)	23	Volume solids (%)	100
Yield Strength (MPa)	1575	Flexural Strength (MPa)	50	Specific gravity	1.05 ± 0.05
Elongation at rupture (%)	2	Shear Strength (MPa)	18	Pot life (mins)	60
Modulus of elasticity (GPa)	1.67	Young's modulus (GPa)	0.58	Recoat time (hours)	6 to 24

To achieve accurate radii of the specimens, customized steel shuttering systems were made. Steel reinforcement bars were prepared and put into the steel formwork. 25 mm thick cover blocks were used in order to maintain the design cover throughout the beam. The concrete was mixed using a mechanical mixer and subsequently, specimens were cast and properly compacted using a mechanical poker vibrator. Proper curing of beams was carried out using wetted gunny bags. All of the above steps are presented in Figure 33. Additionally, for each mix of concrete, three test cubes were cast and cured for 7 days under similar conditions as in test specimens.

Figure 33: Specimen preparation (a) Custom made steel shuttering for formwork (b) Steel reinforcement cages placed in steel shuttering and cover maintained with cover blocks (c) Concreting and compacting (d) Curing of cast specimens using sand and gunny bags.

3.2. Strengthening of specimens using CFRP

As per the guidelines (ACI Committee 440, 2017), the weak concrete layer in the bonding area of CFRP was ground off using an angle grinder and corners were rounded to at least 13 mm radius. A thin layer of primer was applied and kept to cure for 30 Minutes. Then the two-part epoxy adhesive was mixed, and the first coating was applied over the ground area of the specimen. Subsequently, the CFRP fabric strips were carefully placed into the proper location and spacing. Finally, the second coating was applied over carbon fibre strips until adhesive saturate the fabric and left the CFRP to be cured over 7 days. All of the above steps are presented in Figure 34.

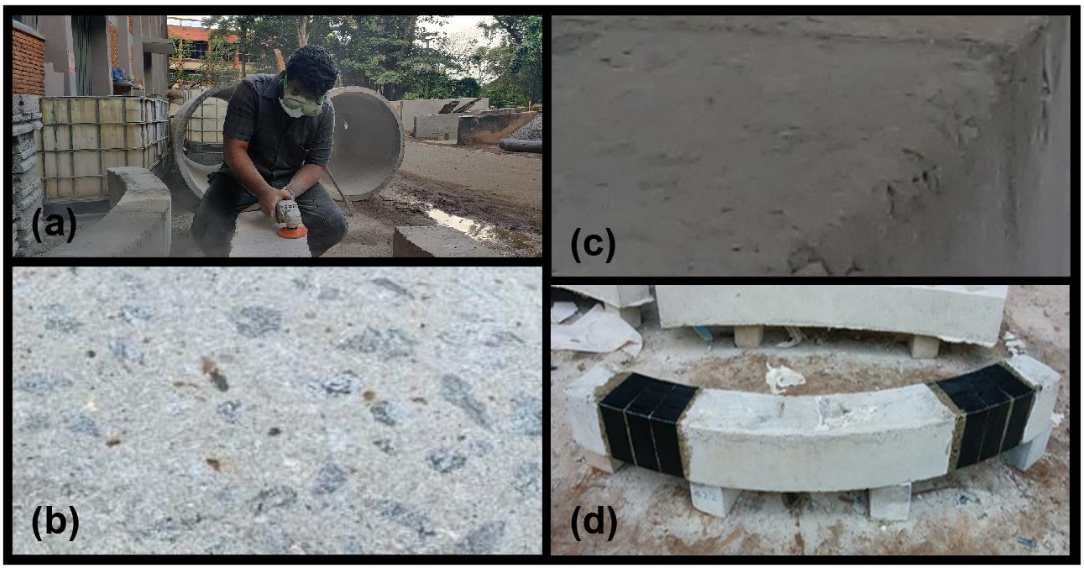

Figure 34: Strengthening procedure (a) Grinding off the weak layer of concrete (b) Rounded off corners of the beam (c) Appearance of ground concrete surface (d) Application of adhesive and carbon fibre fabric.

3.3. The test setup, instrumentation, and procedure

The specimens were fixed at supports to emulate typical beam to column connections in RC structures. Even though a uniform load along the beams should be applied to emulate typical loading conditions of an RC beam, due to the difficulties in applying, managing, and monitoring such a load, the four-point bending method was adopted. Furthermore, a four-point bending setup is more favourable for a shear failure whereas, a three-point bending setup would be more favourable for a flexural failure at the mid-span. The testing setup and instrumentation is illustrated in Figure 35.

The first step of the testing procedure is to place a specimen on the supports and clamp it down to strongly grip all four sides of the support section of the specimen to achieve a fixed boundary condition as much as possible. The next step was to place two rollers at one-third of the effective curved distance from both supports. An I-beam was placed over the two rollers and the loading cell was placed over the I-beam in slightly touching condition to avoid premature loading on the specimen. Before initiating the load application, digital dial gauges were placed to measure vertical deformation at the mid-span of the beam. Strain gauges were placed to measure the compressive strain at the top surface of the beam at the mid-span. A data logger was used to record all readings from applied gauges. The loading was applied gradually and continuously until the ultimate failure occurs. The load at the initial crack, crack propagation and failure modes were reported while the application of transient loading till failure.

Figure 35: Test setup (a) Clamp and support system (b) Loading setup (c) Test setup and instrumentation

3.4. Results and observations of series one

Load–deflection behaviour, crack propagation and ultimate strength of tested samples were monitored during the testing process of the specimens.

3.4.1. Control beams with 2 m radius

As expected, when the applied load increases the flexural cracks at mid-span appeared and small shear cracks appeared at the ends with a further widening of flexural cracks (Figure 36). When the applied load is 41 kN, the beam failed in the shear mode as shown in Figure 37.

Figure 36: Cracks in a failed control beam

Figure 37: Shear failure of a control beam

The major cracks observed were the shear cracks and flexural cracks were also formed with increased load. A component from torsion also could have contributed to the shear cracks, which arises due to the curvature of the beam.

3.4.2. CFRP applied RC beams with 4 m radius

When the applied load increased the flexural cracks at mid-span appeared as shown in Figure 38. Around 30 kN load, shear cracks have appeared at the edges of the CFRP wraps as shown in Figure 39.

Figure 38: Initial flexural cracks

Figure 39: Shear cracks near CFRP wrappings

The effect of shear and torsional stresses was observable at higher loads as cracks started propagating with an inclination as shown in Figure 40.

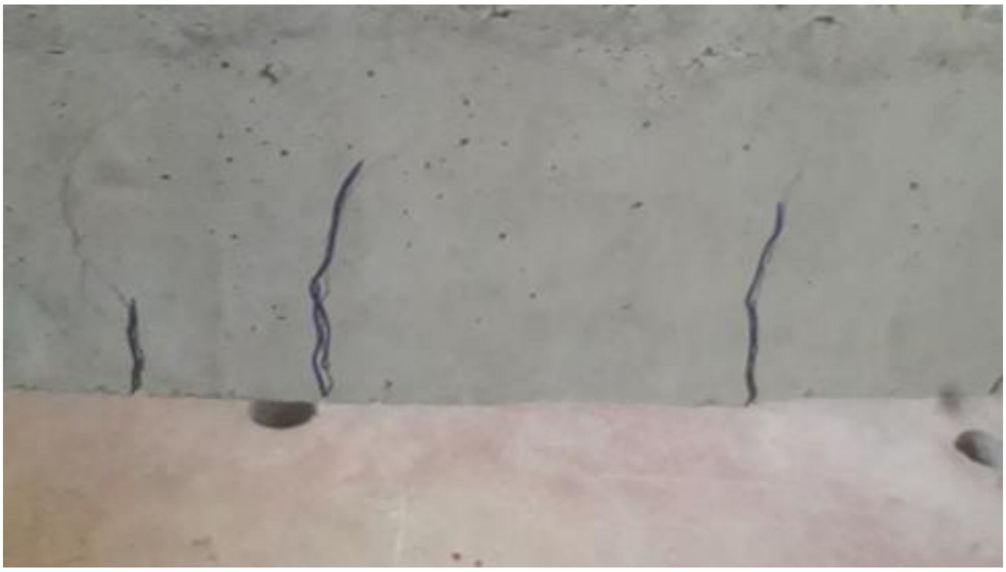

Figure 40: Cracks propagating with an inclination at loads beyond ultimate strength

The beam failed in flexure at around an average 64 kN load level. Since the flexural failure is the dominant failure mode, the evidence is provided for the successful shear capacity enhancement of the CFRP strengthened beam compared to the control beams.

3.4.3. CFRP applied RC beams with 2 m radius

Similar to the 4 m radius beam, flexural cracks appeared at the mid-span when the load was increasing as shown in Figure 41. In addition to that, minor shear cracks appeared at the edges of the CFRP wrappings.

Figure 41: Flexural cracks at mid-span

When the load is reaching higher values the effect of torsional and shear stresses was much more obvious and observable than the 4 m radius beam as shown in Figure 42.

Figure 42: Cracks propagating with an inclination

The beam failed in flexure at around a load of 53 kN. This provides further evidence on the successful application of CFRP to enhance the shear capacity.

Table 6 presents a summary of the failure loads of tested specimens.

Table 6: Summary of the results

Specimen NO.	Radius (m)	Type	Failure load (kN)	Failure mode
1-2-CO-EX	2	Control	43.36	Shear
2-2-CO-EX	2	Control	39.20	Shear
1-2-FW-EX	2	Fully wrapped	54.40	Flexural
2-2-FW-EX	2	Fully wrapped	52.32	Flexural
1-4-FW-EX	4	Fully wrapped	57.76	Flexural
1-4-FW-EX	4	Fully wrapped	69.76	Flexural

Compared to the control beams with a 2 m radius, CFRP strengthened beams shows a shear capacity increment of 30 %. Compared to CFRP strengthened beam with a 2 m radius, CFRP strengthen beam with a 4 m radius shows a shear capacity increment of 20 %. Since the flexural failure was dominant in strengthen beams, the possible shear capacity enhancement should be more than observed.

3.4.4. Comparison of deflections of specimens

The load vs. Deflection relationship of tested specimens are shown in Figure 43.

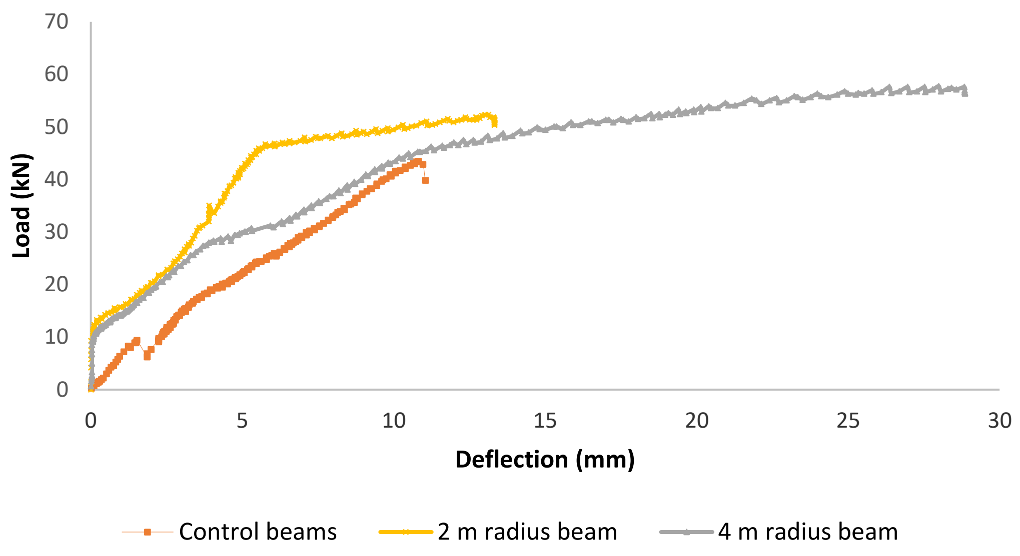

Figure 43: Load vs. deflection

It can be observed that the slope of the graphs for CFRP strengthened beams are greater than that of non-strengthened beams, which indicate an increase in the stiffness due to the application of CFRP fabrics.

3.5. Results and observations of series two

Load–deflection behaviour, crack propagation, compressive strain at mid-span and ultimate failure load of tested samples were monitored during the testing process of the specimens.

3.5.1. Control beams with 2 m radius

When the applied load increases, around 41 kN, the flexural cracks at mid-span appeared and propagated with the increasing load as presented in Figure 44. When the applied load is 93 kN, the beam failed in the shear mode as shown in Figure 45.

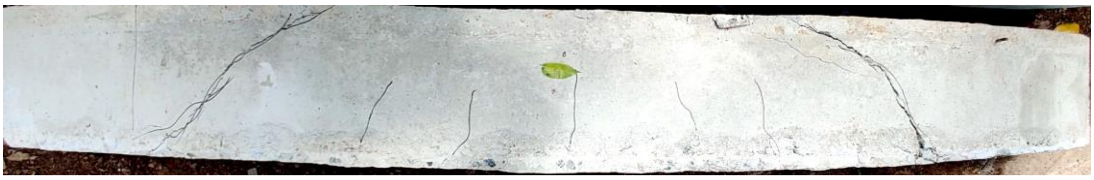

Figure 44: Cracks in a failed control beam

Figure 45: Shear failure of a control beam

The major cracks observed were the shear cracks and flexural cracks were also formed with increasing load. The crack pattern of the shear crack is wrapping around the beam indicate the effect of torsional stresses.

3.5.2. Control beams with 4 m radius

When the applied load increases, around 42 kN, the flexural cracks at mid-span appeared and propagated with the increasing load as presented in Figure 46. When the applied load is 95.44 kN, the beam failed in the shear mode as shown in Figure 47.

Figure 46: Cracks in a failed control beam

Figure 47: Shear failure of a control beam

The cracking behaviour was similar to 2 m radius specimens, however, the lower effect of torsion was observable from the shape of the cracks.

3.5.3. CFRP applied RC beams with 2 m radius

When the applied load increased the flexural cracks at mid-span appeared around 45 kN, as shown in Figure 48. Around 90 kN load, shear cracks have appeared at the edges of the CFRP sheets as shown in Figure 49 and ultimately failed in shear by debonding of CFRP fabrics at 108 kN load as shown in Figure 50.

Figure 48: Initial flexural cracks

Figure 49: Shear cracks near CFRP wrappings

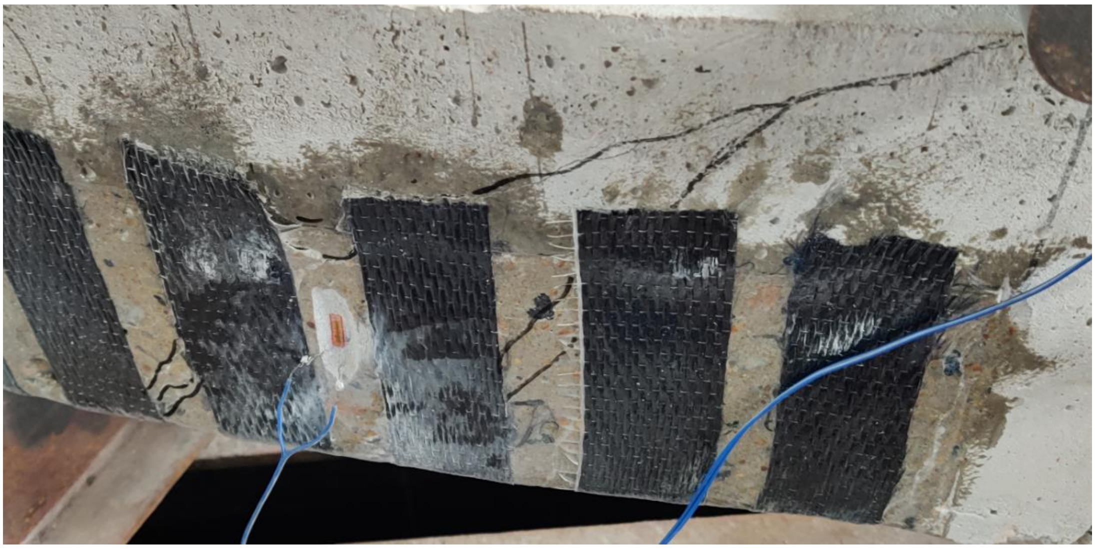

Figure 50: Cracks propagating with an inclination at loads beyond ultimate strength

3.5.4. CFRP applied RC beams with 4 m radius

The flexural cracks at the mid-span appeared around 45 kN, as shown in Figure 51. Around 92 kN load, shear cracks have appeared at the edges of the CFRP sheets as shown in Figure 52 and ultimately failed in shear by debonding of CFRP fabrics at 112.85 kN load as shown in Figure 53.

Figure 51: Flexural cracks at mid-span

Figure 52: Cracks propagating with an inclination

Figure 53: Shear crack induced intermediate debonding

The summary of series two experimental results is presented in Table 7.

Table 7: Summary of the results

Specimen NO.	**Failure load (kN)**	**Failure mode**
1-2-CO-EX	93.69	Combined shear and torsional
2-2-CO-EX	92.85	Combined shear and torsional
1-2-US-EX	108.88	Intermediate debonding
2-2-US-EX	-	-
1-4-CO-EX	95.19	Combined shear and torsional
2-4-CO-EX	95.69	Combined shear and torsional
1-4-US-EX	112.73	Intermediate debonding
2-4-US-EX	112.97	Intermediate debonding
1-S-CO-EX	99.9	Combined shear and torsional
1-S-US-EX	127.1	Intermediate debonding

The results for the ultimate failure load of 2-2-2-US was neglected due to an unexpected failure of the test setup, however, the load vs. deflection behaviour indicate a similar behaviour to its identical beam 2-1-2-US.

Compared to the control beams with a 2 m radius, CFRP strengthened beams shows a shear capacity increment of 16.74 %. Compared to CFRP strengthened beam with a 2 m radius, CFRP strengthen beam with a 4 m radius shows a shear capacity increment of 18.24 %. It can be observed that the reduction of radius from 4 m to 2 m has reduced the shear capacity by 8.2 % which shows the negative effect of torsional stresses on the shear capacity of specimens.

3.5.5. Comparison of deflections and strains of specimens

The load vs. Deflection relationship of tested specimens are shown in Figures 54 and 55 for 2 m radius specimens and 4 m radius specimens, respectively. Load vs. compressive strain at mid-span, plots were presented in Figures 56 and 57.

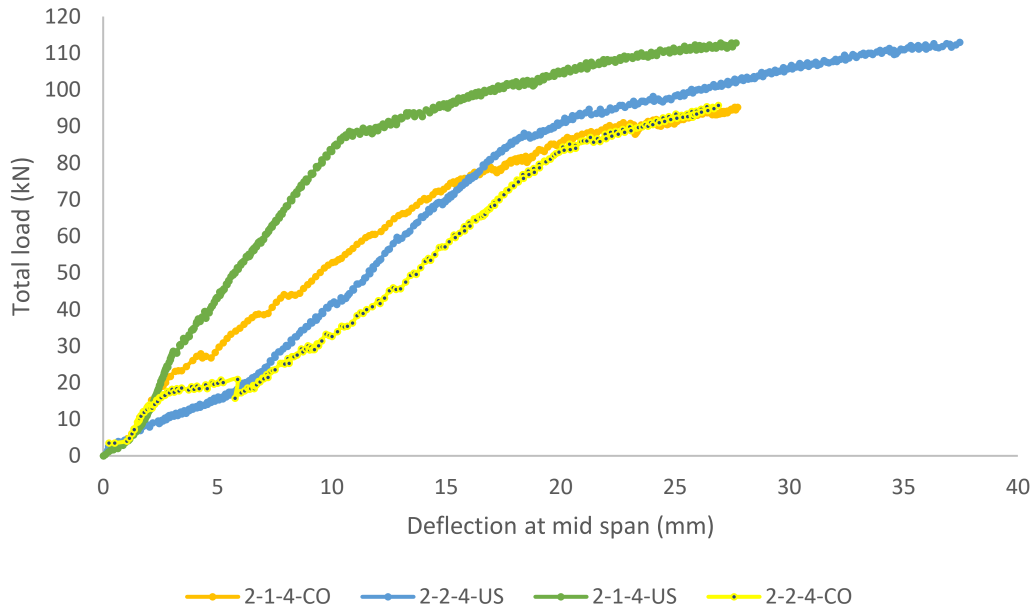

Figure 54: Load vs. deflection for 4 m radius specimens

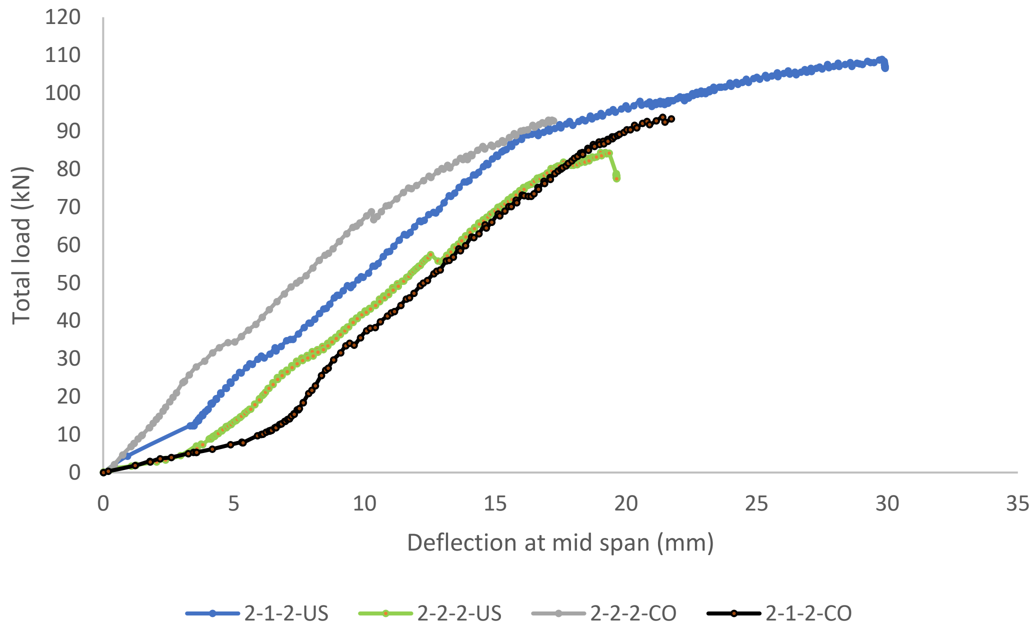

Figure 55: Load vs. deflection for 2 m radius specimens

It can be observed that the slope of the graphs for CFRP strengthened beams are greater than that of non-strengthened beams, which indicate an increase in the stiffness due to the application of CFRP fabrics.

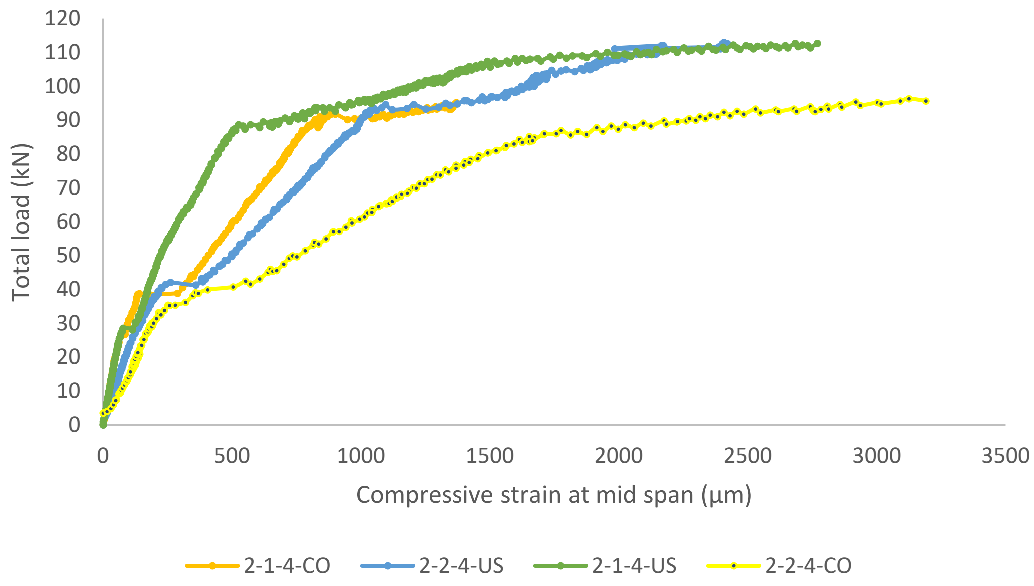

Figure 56: Load vs. compressive strain at mid-span for 4 m radius specimens

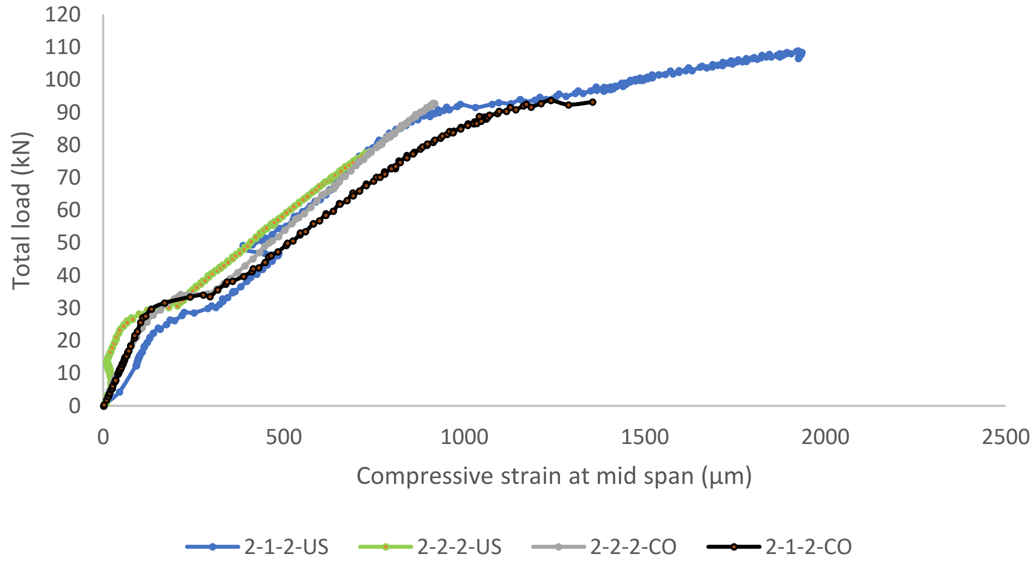

Figure 57: Load vs. compressive strain at mid-span for 2 m radius specimens

It can be observed that the strain behaviour is similar for all the specimens which indicate that the application of U-socketed CFRP has not affected the flexural behaviour of the specimens.

CHAPTER 4: THEORETICAL ANALYSIS

The theoretical analysis consists of two steps. The initial step is to determine the general responses of the horizontally curved beam element under an out-of-plane, four-point bending load. The next step is to determine the flexural and shear capacities by referring to existing studies and guidelines. This will help to design the experimental program with clear expectations and verification of experimental and numerical analyses.

4.1. General response expressions of a horizontally curved beam under out-of-plane loads

(Pilkey, 2005) summarizes the expressions for various loading scenarios which will be used in this chapter to calculate the general responses. The results from the expressions were verified by comparing the results obtained using Castigliano's theorem (Wong, 1970).

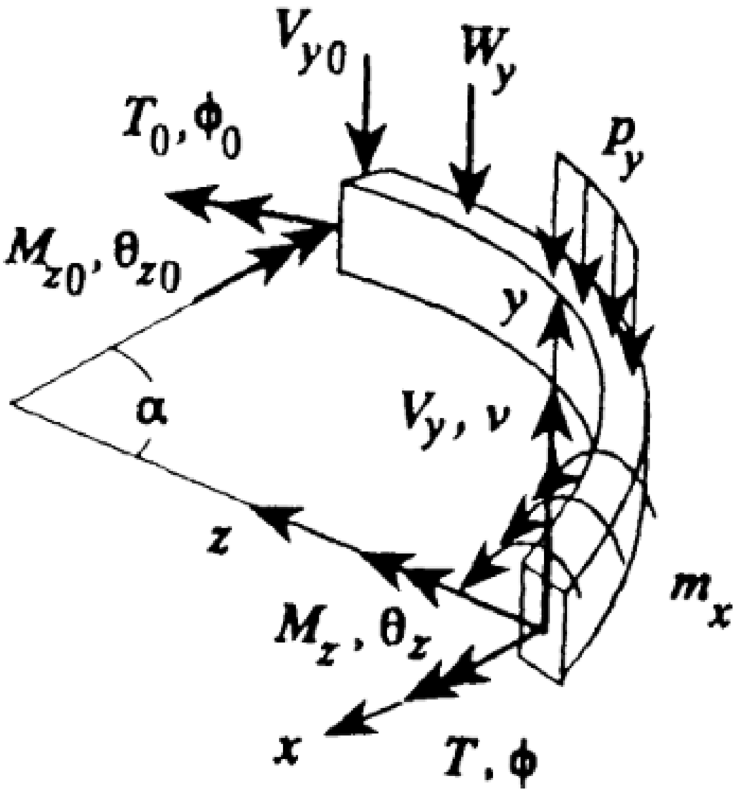

Figure 58: Horizontally curved beam under out-of-plane loads (Pilkey, 2005)

The below notations are valid for all the expressions in this 3.1 section.

E	=	Modulus of elasticity
G	=	Shear modulus of elasticity
R	=	Radius of arch
J	=	Torsional constant
I_z	=	Moment of inertia about the z-axis
λ_1	=	$\frac{1}{GJ} + \frac{1}{EI_z}$
λ_2	=	$\frac{1}{2}(\sin\alpha - \alpha\cos\alpha)$
λ_3	=	$\frac{1}{2}(2 - 2\cos\alpha - \alpha\sin\alpha)$
λ_4	=	$\frac{1}{2}(2\alpha + \alpha\cos\alpha - 3\sin\alpha)$
λ_5	=	$\frac{1}{2}(\alpha\cos\alpha + \sin\alpha)$
$< \alpha - \alpha_1 >^0$	=	$\begin{cases} 0 & \alpha < \alpha_1 \\ 1 & \alpha \geq \alpha_1 \end{cases}$
$< \alpha - \alpha_1 >$	=	$\begin{cases} 0 & \alpha < \alpha_1 \\ (\alpha - \alpha_1) & \alpha \geq \alpha_1 \end{cases}$

There are six general response expressions for each three deformation parameters and the internal forces depend on the initial loading and boundary conditions of the system. The expressions can only be used for one single loading scenario, for example, one concentrated load on the beam or one concentrated torsion on the beam. It cannot be used for two loads in the same beam. Therefore, to obtain the results for a four-point bending scenario, the general responses for each load should be calculated using the below expressions and the principal of superposition must be used. The expressions are shown below.

Angle of twist:

$$\emptyset = \emptyset_0\cos\alpha + \theta_{z0}\sin\alpha - V_{y0}\lambda_1 R^2 + \frac{1}{2}M_{z0}\lambda_1 R\alpha\sin\alpha + T_0\left(\frac{R}{GJ}\lambda_5 - \frac{R}{EI_z}\lambda_2\right) + F_{\emptyset} \quad 1$$

Deflection:	$\upsilon = -\phi_0 R(\cos\alpha - 1) + \upsilon_0 + \Theta_{z0} R\sin\alpha + V_{y0}\left(\frac{R^3}{GJ}\lambda_4 - \frac{R^3}{EI_z}\lambda_2\right) + M_{z0}\left(\frac{R^2\alpha}{2EI_z}\sin\alpha - \frac{R^2}{GJ}\lambda_3\right) - T_0\lambda_1 R^2\lambda_2 + F_\upsilon$	2
Slope:	$\Theta_z = -\phi_0\sin\alpha + \Theta_{z0}\cos\alpha + V_{z0}\left(\frac{R^2}{GJ}\lambda_3 - \frac{R^2\alpha}{2EI_z}\sin\alpha\right) + M_{z0}\left(\frac{R}{EI_z}\lambda_5 - \frac{R}{GJ}\lambda_2\right) - \frac{1}{2}T_0\lambda_1 R\alpha\sin\alpha + F_{\Theta z}$	3
Shear force:	$V_y = V_{y0} + F_{\upsilon y}$	4
Bending moment:	$M_z = -V_{y0}R\sin\alpha + M_{z0}\cos\alpha - T_0\sin\alpha + F_{Mz}$	5
Torque:	$T = V_{y0}(\cos\alpha - 1) + M_{z0}\sin\alpha + T_0\cos\alpha + F_T$	6

Loading functions $F_\emptyset, F_\upsilon, F_{\Theta z}, F_{\upsilon y}, F_{Mz}$ and F_T are defined for an applied concentrated load and concentrated torque scenarios in the below sections.

Loading functions for a concentrated vertical load are as below.

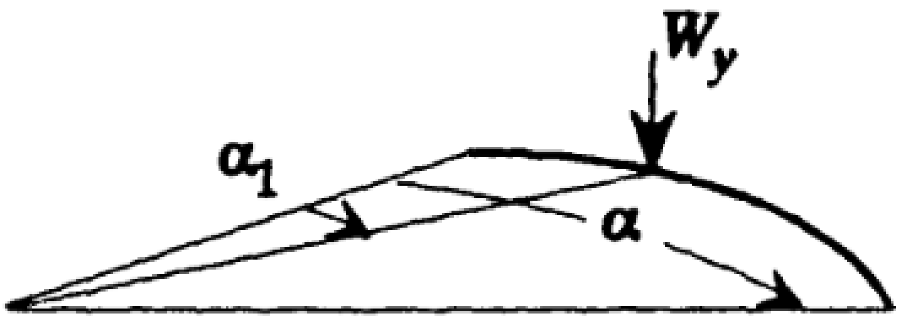

Figure 59: Concentrated vertical load on a horizontally curved beam (Pilkey, 2005)

$$F_{\phi} = \frac{W_y \lambda_1 R^2}{2}[\sin < \alpha - \alpha_1 > - < \alpha - \alpha_1 > \cos(\alpha - \alpha_1)] \quad 7$$

$$F_{v} = -\frac{W_y R^3}{2}\left\{\frac{1}{GJ}[2 < \alpha - \alpha_1 > + < \alpha - \alpha_1 > \cos(\alpha - \alpha_1) - 3\sin < \alpha - \alpha_1 >] - \frac{1}{EI_z}[\sin < \alpha - \alpha_1 > - < \alpha - \alpha_1 > \cos(\alpha - \alpha_1)]\right\} \quad 8$$

$$F_{\theta z} = \frac{W_y R^2}{2}\left\{\frac{1}{EI_z}[< \alpha - \alpha_1 > \sin(\alpha - \alpha_1)] - \frac{1}{GJ}[2 < \alpha - \alpha_1 >^0 - 2 < \alpha - \alpha_1 >^0 \cos(\alpha - \alpha_1) - < \alpha - \alpha_1 > \sin(\alpha - \alpha_1)]\right\} \quad 9$$

$$F_{vy} = -W_y \quad 10$$

$$F_{Mz} = W_y R \sin < \alpha - \alpha_1 > \quad 11$$

$$F_{T} = W_y R(< \alpha - \alpha_1 >^0 \cos(\alpha - \alpha_1) - < \alpha - \alpha_1 >^0) \quad 12$$

Loading functions for a concentrated torque are as below.

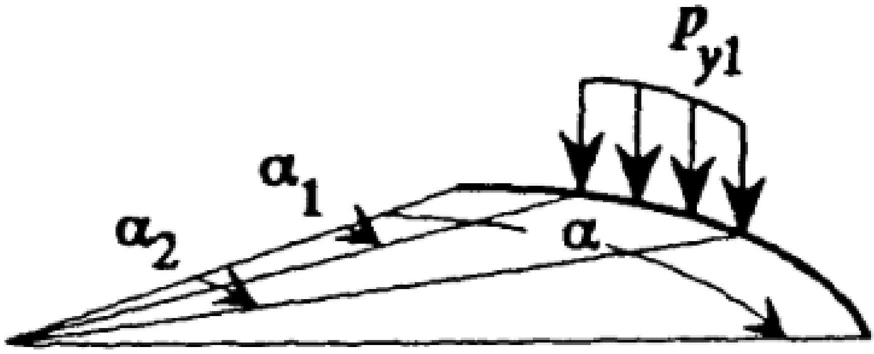

Figure 60: Concentrated torque on a horizontally curved beam (Pilkey, 2005)

$$F_{\phi} = -\frac{P_{y1} R^3}{2}\lambda_1(< \alpha - \alpha_1 >^0 - 2 < \cos\alpha > - < \alpha \sin\alpha >) \quad 13$$

$$F_v = \frac{P_{y1}R^4}{2}\left[\lambda_1(< \alpha \sin\alpha > + < \cos\alpha > - < \alpha - \alpha_1 >^0) - \left(\frac{1}{EI_z} + \frac{3}{GJ}\right) < \cos\alpha > - \frac{2}{GJ} < \alpha^2 >\right] \tag{14}$$

$$F_{\theta z} = -\frac{P_{y1}R^3}{2}\left[\lambda_1(< \sin\alpha > - < \alpha\cos\alpha >) - \frac{2}{GJ}(< \alpha > - < \sin\alpha >)\right] \tag{15}$$

$$F_{vy} = -P_{y1}R < \alpha > \tag{16}$$

$$F_{Mz} = P_{y1}R^2 < \cos\alpha > \tag{17}$$

$$F_T = P_{y1}R^2(< \alpha > - < \sin\alpha >) \tag{18}$$

4.2. Determination of deflection (Rigorous method)

Even though the deflection of a homogeneous and isotropic curved beam under general loads can be obtained by the aforementioned expression for deflection, for an RC beam when the applied moment for a cross-section is more than the cracking moment, the second moment of the area considerably reduces due to cracking resulting high deformations. Both (BS EN 1992-1-1, 2004) and (ACI Committee 318, 2014) presents a rigorous method for determining the deflection of RC elements and International Federation for Structural Concrete (fib) (International Federation for Structural Concrete (fib), 1999) presents a well-described procedure to carry out the aforementioned rigorous method for RC beam as shown below.

The first step is to divide the considered beam into at least 10 equal sections. If it was divided into more than 10 sections the accuracy of the results will get increased, however, the difference with 20 sections results with 10 sections results is only just 1.2 %. Then the depths of the neutral axis and second moment of areas for the uncracked and cracked states and cracking moments should be determined at each node along the beam using the expressions given below (Bond et al., 2006).

Notations and definitions are used in section 3.2.

A_s	=	Area of tensile reinforcement
A_{s2}	=	Shear modulus of elasticity
b	=	Breadth of section
d	=	Effective depth to tension reinforcement
d_2	=	Depth to compression reinforcement
α_e	=	Modular ratio
E_c	=	Elastic modulus
f_{ctm}	=	Mean tensile strength
E_s	=	Elastic modulus of steel

Depth to the neutral axis for the uncracked condition:

$$x_u = \frac{\frac{bh^2}{2} + (\alpha_e - 1)(A_s d + A_{s2} d_2)}{bh + (\alpha_e - 1)(A_s + A_{s2})} \qquad 19$$

The second moment of area for the uncracked condition:

$$I_u = \frac{bh^3}{12} + bh\left(\frac{h}{2} - x_u\right)^2 + (\alpha_e - 1)[A_s(d - x_u)^2 + A_{s2}(x_u - d_2)^2] \qquad 20$$

Depth to the neutral axis for the cracked condition:

$$x_c = \frac{1}{b}\left\{\left[\left(A_s\alpha_e + A_{s2}(\alpha_e - 1)\right)^2 + 2b\left(A_s d\alpha_e + A_{s2}d_2(\alpha_e - 1)\right)\right]^{0.5} - \left(A_s\alpha_e + A_{s2}(\alpha_e - 1)\right)\right\} \qquad 21$$

The second moment of area for the cracked condition:

$$I_c = \frac{bx_c^3}{3} + \alpha_e A_s(d - x_c)^2 + (\alpha_e - 1)A_{s2}(d_2 - x_c)^2 \qquad 22$$

Cracking moment:

$$M_{cr} = \frac{f_{ctm} I_u}{(h - x_u)} \qquad 23$$

Where,

Modulus ratio:

$$\alpha_e = \frac{E_s}{E_c} \qquad 24$$

The curvature (κ) of the deformed beam is given by Equation 25.

$$\kappa = \frac{1}{r} = \frac{\frac{d^2y}{dx^2}}{\left[1 + \left(\frac{dy}{dx}\right)^2\right]^{3/2}} \qquad 25$$

However, compared to unity the $\left(\frac{dy}{dx}\right)^2$ term is negligible. Therefore, the relationship can be simplified as shown in Equation 26.

$$\kappa = \frac{1}{r} = \frac{d^2y}{dx^2} \qquad 26$$

According to (Bond et al., 2006) the curvature of the deformed beam is given by Equation 27.

$$\frac{1}{r} = \xi \frac{M}{EI_c} + (1 - \xi) \frac{M}{EI_u} \qquad 27$$

Where,

$$\xi = 1 - \gamma \left(\frac{M_{cr}}{M}\right)^2 \qquad 28$$

Here, γ is a parameter that depends on the loading condition. According to (ACI Committee 318, 2014) for instantaneous loading, it can be taken as 0.8. M is the moment response at each node due to applied loads and it can be determined by the expressions given in section 3.1. Here, x is the curve distance from one end to the considered node of the beam.

It also should be noted that in the aforementioned codes and guidelines there are procedures to calculate the deformation curvature from shrinkage and creep. However, in this study the only curvature due to instantaneous loading is considered since in both numerical and experimental studies only the deflection due to mechanically applied loads will be obtained. Hence, the curvature due to self-weight was also not considered in the theoretical calculations.

By combining the above expressions for the curvature of the deformed beam Equation 29 can be obtained.

$$\frac{d^2y}{dx^2} = \xi \frac{M}{EI_c} + (1 - \xi)\frac{M}{EI_u} \qquad 29$$

Furthermore, it also can be written in a radial form as Equation 30 below since x is equal to Rθ in a curve beam.

$$\frac{d^2y}{R^2 d\theta^2} = \xi \frac{M}{EI_c} + (1 - \xi)\frac{M}{EI_u} \qquad 30$$

This equation can be solved by numerical integration for all nodes that the beam was divided into. It is recommended to carry this out using a computer program, such as a simple spreadsheet or a sophisticated program such as Matlab, since carrying it out manually will be a very tedious process. The integration should be corrected based on the boundary conditions for the slope of the curve and the deflections at ends by a linear transformation. Subsequently, the deflection diagram can be obtained for the curved beam.

4.3. The shear force due to torsion

The shear force response of the fixed curved beam under a point load is given by Equations 4 or 16. However, there is a torsional shear flow acting about the centroid of the beam with a distribution as shown in Figure 61 due to the torsion arising from the eccentricity of the load relative to supports.

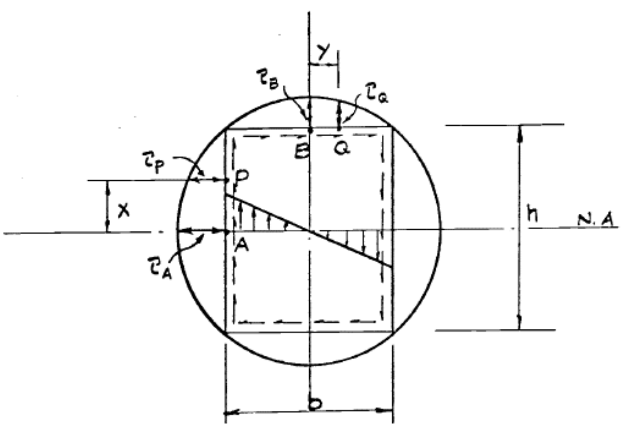

Figure 61: Shear flow due to torsion in a rectangular beam section (Wong, 1970)

This component of torsional stress contributes to the main shear stress at one side of the beam while reducing the direct shear stress on the other side of the beam. However, a failure will occur at the side in which torsional stress is contributing to the shear stress when the load increases. The Euro standard (BS EN 1992-1-1, 2004) presents an expression to obtain shear force due to torsion as shown in Equation 31.

$$V_{Ed,i} = \frac{T_{Ed}}{2A_k} z_i \tag{31}$$

Where,

T_{Ed} is the applied torsion (see Figure 62)

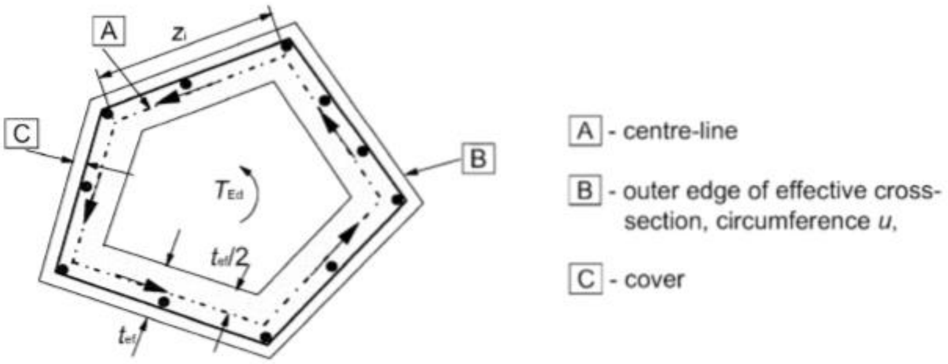

Figure 62: Notations and definitions used in chapter 3.3 (BS EN 1992-1-1, 2004)

A_k is the area enclosed by the centerlines of the connecting walls, including inner hollow areas. z_i is the side length of a wall "i" defined by the distance between the intersection points with the adjacent walls. By superimposing the shear stress due to vertical load and torsion, the effective shear force can be obtained.

4.4. Determination of flexural and shear capacities of the beam.

In this section, the flexural and shear load carrying capacities are presented based on the design codes and guidelines which are currently used in the industry.

4.4.1. Flexural capacities of RC beams without CFRP external reinforcement

According to the Euro standard (BS EN 1992-1-1, 2004), the ultimate moment of resistance (M_1) is given by Equation 32.

$$M_1 = 0.25092 f_{ck} b d^2 \quad 32$$

The following expressions are based on expressions from the Euro standard (BS EN 1992-1-1, 2004) which were modified by removing all the safety factors considered in the code considering the nature of experimental results and the reliability of material properties and quality control. The relationship between the applied moment and the tensile reinforcement area is as follows:

$$M = A_s f_{yk} z \quad 33$$

Where,

$$z = \frac{d}{2}\left[1 + \sqrt{1 - \frac{2.353M}{f_{ck} b d^2}}\right] \quad 34$$

Substituting z to the expression of M above and subsequently simplifying Equation 35 for the ultimate moment that tensile reinforcement can resist, can be obtained.

$$M_2 = A_s f_{yk} d - 0.58825 \frac{A_s^2 f_{yk}^2}{b f_{ck}} \quad 35$$

Then, the ultimate flexural capacity is the minimum of M_1 and M_2.

4.4.2. Shear capacities of RC beams without CFRP external reinforcement

4.4.2.1. Shear capacity without shear links.

The shear capacity of an RC beam without shear link (BS EN 1992-1-1, 2004) is given by,

$$V_{Rd,c} = C_{Rd,c} k (100 \rho_1 f_{ck})^{1/3} b_w d \geq v_{min} b_w d \quad 36$$

Where,

$k = 1 + \sqrt{\frac{200}{d}}$ with d in mm

$\rho_1 = \frac{A_s}{b_w d} \leq 0.02$

A_s is the area of the tensile reinforcement

b_w is the breadth of the section

$C_{Rd,c} = 0.18$

$v_{min} = 0.035k^{3/2}f_{ck}^{1/2}$

4.4.2.2. Shear capacity with shear links

With the provision of shear links, the failure can occur by either compressive failure of an imagined diagonal concrete strut or tensile failure of the member. For tensile failure, the shear force is given by (BS EN 1992-1-1, 2004),

$$V_{Rd,s} = \frac{A_s}{s} z f_y \cot\theta \qquad 37$$

Where,

The $\cot\theta$ term can vary between 1 and 2.5 depending on the magnitude of the shear force. Hence, for the maximum resistance of shear links, it can be taken as 2.5.

A_s is the area of the tensile reinforcement

s is the spacing of stirrups

$z = d - d'$

f_y is the tensile strength of stirrups

For compressive failure, the shear force is given by,

$$V_{Rd,max} = \alpha_{cw} b_w z v_1 f_{ck} / (\cot\theta + \tan\theta) \qquad 38$$

Where,

$\alpha_{cw} = 1$

$v_1 = 0.6\left[1 - \frac{f_{ck}}{250}\right]$

4.4.3. Shear capacity from FRP strips

There are several standard guides (ACI Committee 440, 2017; International Federation for Structural Concrete (fib), 2001) focused on strengthening RC beams for shear using improved theoretical and analytical models developed by researchers (Chen and Teng, 2003; Khalifa et al., 1998; Triantafillou, 1998). The guidance provided by different institutions or committees (ACI Committee 440, 2017; International Federation for Structural Concrete (fib), 2001) were selected to compare with experimental results due to its reputation and popularity in the industry.

4.4.3.1. Analytical model in ACI440.2R- 17

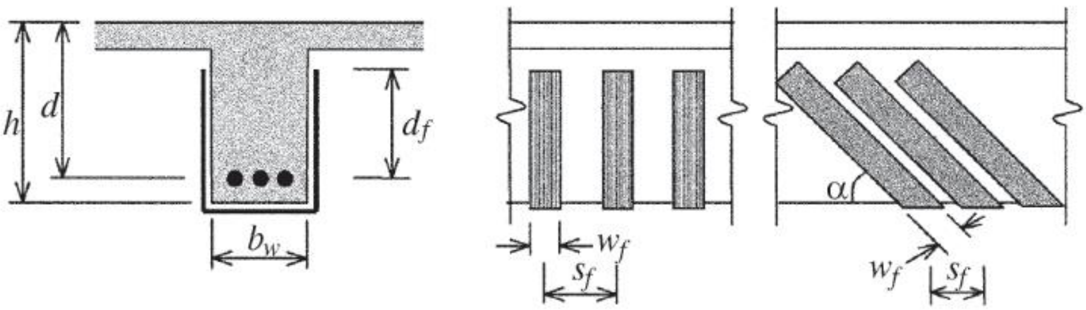

Figure 63: Notations for chapter 3.4.2.3 (ACI Committee 440, 2017)

ACI guide (ACI Committee 440, 2017) presents an expression for the shear capacity enhancement due to external FRP reinforcement is given in Equation 39.

$$V_f = \frac{A_{fv} f_{fe} (\sin\alpha + \cos\alpha) d_f}{s_f} \qquad 39$$

For a rectangular section,

$$A_{fv} = 2nt_f w_f \qquad 40$$

Where,

t_f is the thickness of FRP sheets

By Hook’s law

$$f_{fe} = E_f \varepsilon_{fe} \qquad 41$$

For completely wrapped members

$$\varepsilon_{fe} = 0.004 \leq 0.75\varepsilon_{fu} \quad 42$$

Where,

ε_{fu} is the rupture strain of the FRP and E_f is Young's modulus of FRP.

For U-wraps and side bonding

$$\varepsilon_{fe} = \kappa_v \varepsilon_{fu} \leq 0.004 \quad 43$$

κ_v is a bond-reduction reduction factor which is a function of the active bond length, the strength of concrete and used wrapping scheme and is determined by Equations 44, 45 and 46.

$$\kappa_v = \frac{k_1 k_2 L_e}{11900\varepsilon_{fu}} \leq 0.75 \quad 44$$

$$k_1 = \left(\frac{f_c'}{27}\right)^{2/3} \quad 45$$

$$k_2 = \begin{cases} \dfrac{d_{fv} - L_e}{d_{fv}}, & for\ U-wraps \\ \dfrac{d_{fv} - 2L_e}{d_{fv}}, & for\ side\ bonding \end{cases} \quad 46$$

4.4.3.2. Analytical model in FIB-TG 9.3

International Federation for Structural Concrete (International Federation for Structural Concrete (fib), 2001) presents an expression in Eurocode 2 format as Equation 47.

$$V_f = 0.9\varepsilon_{fd,e} E_{fu} \rho_f b_w d(\cot\theta + \cot\alpha)\sin\alpha \quad 47$$

Where,

$\varepsilon_{fd,e}$ = Design value of effective FRP strain

b_w = Minimum width of cross-section over the effective depth

d = Effective depth of the cross-section

ρ_f = FRP reinforcement ratio equal to $2t_f \sin\alpha / b_w$ for continuously bonded shear reinforcement of thickness t_f (b_w = minimum width of the concrete cross-section over the effective depth), or $(2t_f/b_w)(w_f/s_f)$ for FRP reinforcement in the form of strips or sheets of width bf at a spacing s_f

E_{fu} = Elastic modulus of FRP in the principal fibre orientation

θ = Angle of diagonal crack with respect to the member axis assumed equal to 45^0

α = Angle between principal fibre orientation and the longitudinal axis of the member

Based on experimental studies done by researchers (Khalifa et al., 1998; Priestley and Seible, 1995; Triantafillou and Antonopoulos, 2000), FIB-TG 9.3 presents the following expressions to determine the effective rupture strain for all three wrapping schemes.

For a fully wrapped scheme

$$\varepsilon_{fe} = 0.17\left(\frac{f_{cm}^{2/3}}{E_{fu}\rho_f}\right)^{0.3} \varepsilon_u \qquad 48$$

For U-wrapping and side bonding schemes

$$\varepsilon_{fe} = min\left[0.65\left(\frac{f_{cm}^{2/3}}{E_{fu}\rho_f}\right)^{0.56} \times 10^{-3}, \qquad 0.17\left(\frac{f_{cm}^{2/3}}{E_{fu}\rho_f}\right)^{0.3} \varepsilon_u\right] \qquad 49$$

4.5. Comparison of experimental results with currently existing design codes and guidelines

Table 8 summarizes the comparison between experimental results with theoretical/analytical results obtained from Eurocode 2, ACI 440.2R-17 and FIB-TG 9.3.

Table 8: Comparison of experimental results and theoretical/analytical results

Specimen type	**Actual shear capacity of RC beam (kN)**	**Predicted shear capacity (kN)**	**Actual shear gain from CFRP (kN)**	**Predicted shear gain from CFRP (kN)**		**Percentage difference (%)**	
				ACI 440.2R-17	**FIB-TG 9.3**	**ACI 440.2R-17**	**FIB-TG 9.3**
Control beam with 2 m radius	93.27	90.79	-	-	-	-	-
Control beam with 4 m radius	95.44	94.16	-	-	-	-	-
CFRP U-socketed beam with 2 m radius	108.88	114.43	15.61	23.64	24.5	33.97	36.0
CFRP U-socketed beam with 4 m radius	112.85	118.67	17.41	24.51	24.5	28.97	28.9

It can be observed that due to the curvature and subsequent torsional stresses, the actual shear gain from CFRP is 33.97 % and 28.97 % less than predicted shear gain by ACI 440.2R-17, respectively for 2 m and 4 m radius beams. For FIB-TG 9.3, it is 36 % and 28.9 %.

CHAPTER 5: NUMERICAL MODELLING

Numerical models were developed to predict the bond characteristics of CFRP strengthened and non-strengthened reinforced concrete beams subjected to out of plane, loads using a commercially available Finite Element Modelling (FEM) computer program (Dassault Systèmes, 2014). The main purpose of developing a numerical model is to predict the effects of different parameters on the performance of the composite due to the limitations and time-consuming nature of conducting experiments to identify such behaviour.

Reinforced concrete composite is a very complex material to model due to its combination of different behaviour and responses under general loading. Hence, a proper material model must be adopted to simulate reality. The developed material model must be capable of simulating elastic and plastic behaviour in both compression and tension, different degradation of the elastic stiffness in tension and compression and the damage behaviour. Furthermore, the compression behaviour should include the strain-softening and tension behaviour which consider the effects of tension softening, stiffening and bond behaviour between reinforcement and concrete.

There are three concrete damage models available in the ABAQUS program: (1) Smeared crack concrete model, (2) Brittle crack concrete model, and (3) Concrete damaged plasticity model. Out of the three concrete damage models, the concrete damage plasticity model was selected due to its ability to simulate all aforementioned requirements as it was primarily intended to provide the capability for the analysis of concrete structures under dynamic loading (Dassault Systèmes, 2014).

5.1. Concrete damage plasticity (CDP) model

CDP model simulates mainly two failure mechanisms: compressive failure end tensile failure. To simulate it, the program needs the stress-strain relationship data based on the experimental results or literature for the relevant grade of concrete which will be described briefly in the following sections.

5.1.1. Defining tension stiffening

To develop the model for tensile behaviour, the user should input Young's modulus concrete (E_0), stress (σ_t) values, cracking strain ($\tilde{\varepsilon}_t^{ck}$) values and damage parameter (d_t) values for cracking which are calculated from the source stress-strain curve. It can be calculated as follows (Dassault Systèmes, 2014).

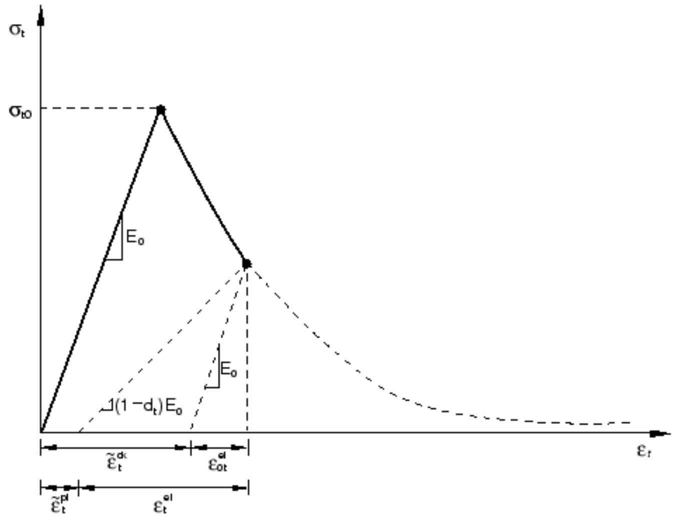

Figure 64: Terms for Tension Stiffening Model (Dassault Systèmes, 2014)

The cracking strain can be calculated by,

$$\tilde{\varepsilon}_t^{ck} = \varepsilon_t - \varepsilon_{ot}^{el} \qquad 50$$

Where,

$\varepsilon_{ot}^{el} = \frac{\sigma_t}{E_0}$, The elastic strain corresponding to undamaged behaviour

ε_t = Total tensile strain

The damage parameter can be calculated as,

$$d_t = \frac{\tilde{\varepsilon}_t^{ck}}{\varepsilon_t} \qquad 51$$

Before inputting calculated data, the plastic strain values must be checked using Equation 52, if the values are negative or/and reducing with increasing cracking strain.

If it is negative or/and reducing with increasing cracking strain, the Abaqus program will terminate the analysis indicating the incorrect damage curve.

$$\tilde{\varepsilon}_t^{pl} = \tilde{\varepsilon}_t^{ck} - \frac{d_t}{(1-d_t)}\frac{\sigma_t}{E_0} \qquad 52$$

5.1.2. Defining compressive behaviour

For compressive behaviour, the user should input stress (σ_c) values, inelastic strain ($\tilde{\varepsilon}_c^{in}$) values and damage parameter values (d_c) for crushing which should be calculated from source stress-strain response curve as described below (Dassault Systèmes, 2014).

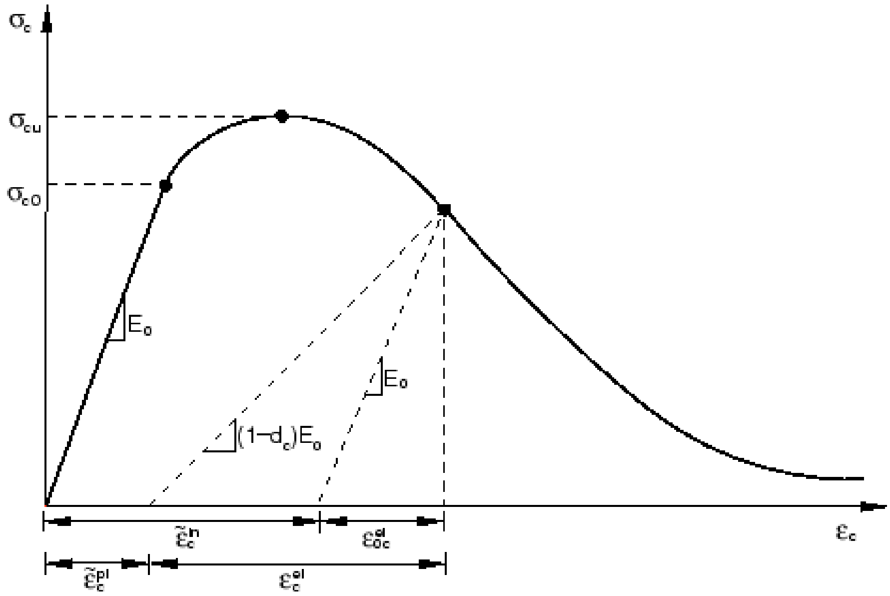

Figure 65: Terms for Compressive Stress-Strain Relationship (Dassault Systèmes, 2014)

The inelastic strain can be calculated by,

$$\tilde{\varepsilon}_c^{in} = \varepsilon_c - \varepsilon_{0c}^{el} \qquad 53$$

Where,

$\varepsilon_{0c}^{el} = \frac{\sigma_c}{E_0}$, The elastic strain corresponding to undamaged behaviour

ε_c = Total compressive strain

The damage parameter can be calculated as,

$$d_c = \frac{\tilde{\varepsilon}_c^{in}}{\varepsilon_c} \tag{54}$$

The same as before for the tension model, before inputting calculated data, using Equation 55, the plastic strain should be checked if the values are negative or/and reducing with increasing cracking strain. If it is negative or/and reducing with increasing cracking strain Abaqus will terminate the analysis indicating the incorrect damage curve.

$$\tilde{\varepsilon}_c^{pl} = \tilde{\varepsilon}_c^{in} - \frac{d_c}{(1-d_c)}\frac{\sigma_c}{E_0} \tag{55}$$

5.1.3. Other parameters for the CDP model

Default stiffness recovery factors were used; hence the compressive stiffness recovery factor was taken as 1 assuming full recovery of compressive stiffness when load changes from tension to compression and the tension recovery factor was taken as 0 assuming no recovery of tensile stiffness when loading changes from compression to tension.

Other plasticity parameters: dilation angle, eccentricity and fb_0/fc_0 were obtained from the study conducted by (Hafezolghorani et al., 2017). A tabular and graphical comparison between (Hafezolghorani et al., 2017)'s model and a model developed from cube testing is presented in Tables 9, 10 and Figure 66.

Table 9: The CDP model for grade 30 concrete from literature (Hafezolghorani et al., 2017)

Material's parameters	B30	Plasticity parameters	
		Dilation angle	31
Concrete elasticity		Eccentricity	0.1
E (Gpa)	26.6	fb0/fc0	1.16
Poisson ratio	0.2	K	0.67
		Viscosity parameter	0
Concrete compressive behaviour		Concrete compression damage	
Yield stress (Mpa)	Inelastic strain	Damage parameter C	Inelastic strain
15.3	0	0	0

19.2	0.000048249	0	0.000048249
22.5	0.000119844	0	0.000119844
25.2	0.000214786	0	0.000214786
27.3	0.000333074	0	0.000333074
28.8	0.000474708	0	0.000474708
29.7	0.000639689	0	0.000639689
30	0.000828016	0	0.000828016
29.7	0.001039689	0.01	0.001039689
28.8	0.001274708	0.04	0.001274708
27.3	0.001533074	0.09	0.001533074
25.2	0.001814786	0.16	0.001814786
22.5	0.002119844	0.25	0.002119844
19.2	0.002448249	0.36	0.002448249
15.3	0.0028	0.49	0.0028
10.8	0.003175097	0.64	0.003175097
5.7	0.003573541	0.81	0.003573541
Concrete tensile behaviour		Concrete tension damage	
Yield stress (Mpa)	Cracking strain	Damage parameter T	Cracking strain
3	0	0	0
0.03	0.001167315	0.99	0.001167315

Table 10: A CDP model developed from experimental data

Material's parameters	B30	Plasticity parameters	
		Dilation angle	31
Concrete elasticity		Eccentricity	0.1
E (Gpa)	17.444	fb0/fc0	1.16
Poisson ratio	0.2	K	0.67
		Viscosity parameter	0
Concrete compressive behaviour		Concrete compression damage	
Yield stress (Mpa)	Inelastic strain	Damage parameter C	Inelastic strain
14.49	0	0	0
18.27	0.0001057	0.004229	0.0001057
21.41	0.0001866	0.007463	0.0001866
29.01	0.0008975	0.0359	0.0008975
29.19	0.001891	0.07563	0.001891
27.14	0.002969	0.1187	0.002969
24.72	0.00406	0.1624	0.00406
22.48	0.005146	0.2058	0.005146
20.52	0.00622	0.2488	0.00622
18.85	0.007284	0.2914	0.007284
17.41	0.008338	0.3335	0.008338
16.18	0.009385	0.3754	0.009385
15.11	0.010425879	0.417	0.010425879
14.18	0.011461317	0.458452698	0.011461317

Concrete tensile behaviour		Concrete tension damage	
Yield stress (Mpa)	Cracking strain	Damage parameter T	Cracking strain
2.44	0	0	0
1.88	0.0000635	0.0639	0.0000635
1.10	0.00039	0.41	0.00039
0.24	0.00093	0.99	0.00093

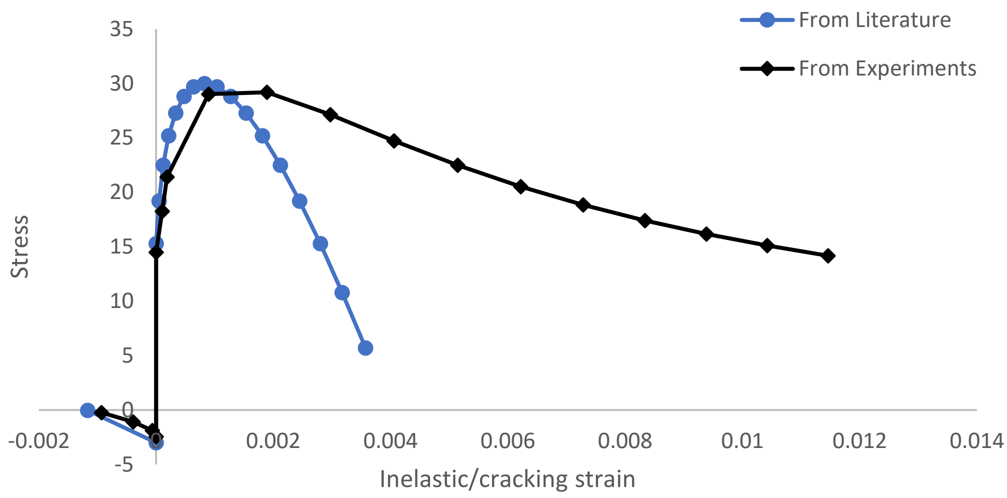

Figure 66: Graphical presentation of the above two CDP models

5.2. Properties of steel reinforcement bars

The elastic behaviour was defined as inputting Young's modulus of steel as 200 Gpa and Poisson's ratio as 0.3. Tensile tests on rebar were done to determine the yield strengths of the main rebar and stirrups. The yield strength was 520 N/mm^2 and 281.5 N/mm^2 for main rebar and stirrups, respectively. The plastic behaviour was defined only for zero plastic strain since the behaviour after the steel failure is not required.

5.3. Properties of FRP fabric

As for the FRP, CFRP was selected for the present study considering its availability in fabric form which is necessary for wrapping the beam. Its elastic properties were entered as engineering constants elastic type as presented in Table 11.

Table 11: Elastic properties of CFRP-adhesive composite

E1	E2	E3	Nu12	Nu13	Nu23	G12	G13	G23
230 GPa	10 GPa	10 GPa	0.3	0.28	0.28	2 GPa	0 GPa	1.5 Gpa

For the damage model, the Hashin damage model was adopted since it is specifically designed to predict the failure of Fibre-reinforced composites (Dassault Systèmes, 2014). The Hashin model considers four different damage initiation mechanisms: fibre tension, fibre compression, matrix tension, and matrix compression. Before the application of CFRP fabric is not a composite since it only consisted of Carbon fibres. However, after the application of the CFRP fabrics adopting the wet-layup method, the CFRP fabric will be submerged in the adhesive epoxy resin layer. It can be modelled as a CFRP fabric and adhesive composite layer sandwiched by two adhesive layers. The required parameters for Hashin damage are shown in Table 12.

Table 12: Hashin damage parameters for CFRP-adhesive composite

Longitudinal tensile strength	Longitudinal compressive strength	Transverse tensile strength	Transverse tensile strength	Longitudinal shear strength	Transverse shear strength
2760 N/mm2	552 N/mm2	1 N/mm2	1 N/mm2	50 N/mm2	1 N/mm2

Energy type damage evolution with linear softening was selected with fracture energy values given in Table 13. Viscosity coefficients for damage stabilization were entered as 0.0002 for all directions.

Table 13: Energy evolution data

Longitudinal tensile fracture energy	Longitudinal compressive fracture energy	Transverse tensile fracture energy	Transverse compressive fracture energy
91600 J	79900 J	1 J	1 J

5.4. Properties of Epoxy Resin Adhesive

As for the adhesive, the manufacturer recommended material properties were used. The traction type elastic model was chosen since the adhesive will be modelled as cohesive elements. Required elastic properties were entered into the program as in Table 14.

Table 14: Traction elastic properties for adhesive

E/Enn	G1/Ess	G2/Ett
4.5 x 109	3.8 x 109	3.8 x 109

Quads damage initiation criteria was used to predict the damage initiation in adhesive layers since it was modelled as cohesive elements defined with traction separation. The following information was entered for the Quads damage model as presented in Table 15.

Table 15: Nominal stresses for Quads damage model

Nominal stress Normal-only mode	Nominal stress first direction	Nominal stress second direction
46 Mpa	46 Mpa	46 Mpa

Energy type damage evolution with linear softening was selected with 400 J for fracture energy values in all modes and directions. Viscosity coefficients for damage stabilization were entered as 0.0002.

5.5. Modelling of the beam

The beam was modelled as a 3D deformable solid part and steel reinforcement as wire parts. CFRP was modelled as deformable shell parts and adhesive as a deformable 3D solid part with cohesive element type. Furthermore, the actual support system and loading roller were modelled as 3D deformable solid parts to simulate as possible as close boundary and loading conditions in the experimental program. Afterwards, the relevant properties which are defined in Sections 5.1 to 5.4 were assigned to each part and followed by assembling the parts consistent with the experimental setup as shown in Figure 68. Each part was partitioned properly to achieve an effective and proper mesh as shown in Figure 68.

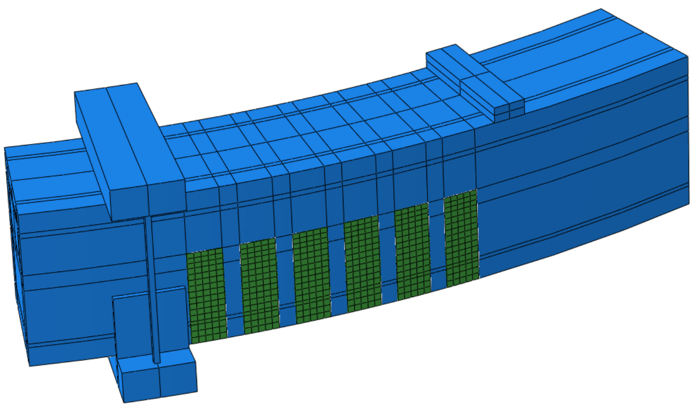

Figure 67: The assembled model

After the assembly of the parts, a Dynamic/Explicit step was defined with required field outputs and history outputs. It was decided to use Dynamic/Explicit analysis instead of General statics due to the existence of interaction definitions in the model which tends to be unstable in General statics analysis. Then interactions were defined for regions where the roller and support part contacted the beam surface, assuming a rough interaction between surfaces. Afterwards, constraints were defined for internal steel reinforcement and the CFRP system. Embedded constrain was used for internal reinforcement since the rebars are embedded in the concrete beam. The adhesion between the concrete substrate and CFRP was simulated by modelling 1 mm thick cohesive elements between the concrete and CFRP layer and tie constraints were used to constrain the adhesive to the concrete and the carbon fibre layer to the adhesive.

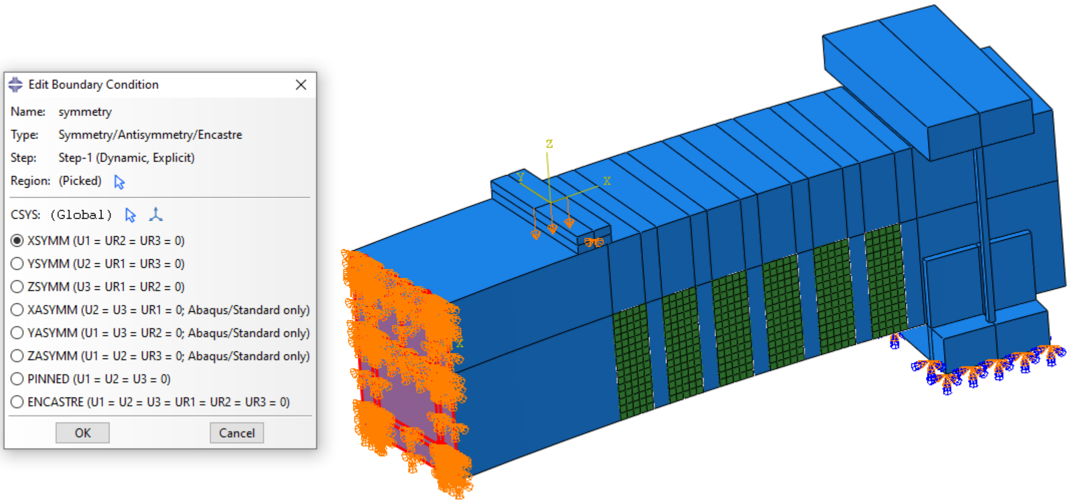

Figure 68: Symmetry boundary condition

Subsequently, loads and boundary conditions were defined. Since the specimen and testing setup is symmetrical about the YZ plane (Figure 69) only half the specimen was modelled, and symmetrical boundary conditions were defined as shown in Figure 69.

Since in the test setup, only the bottom part was fixed to the platform below, the bottom surface of the modelled clamp was fixed in all translations and rotations as shown in Figure 70.

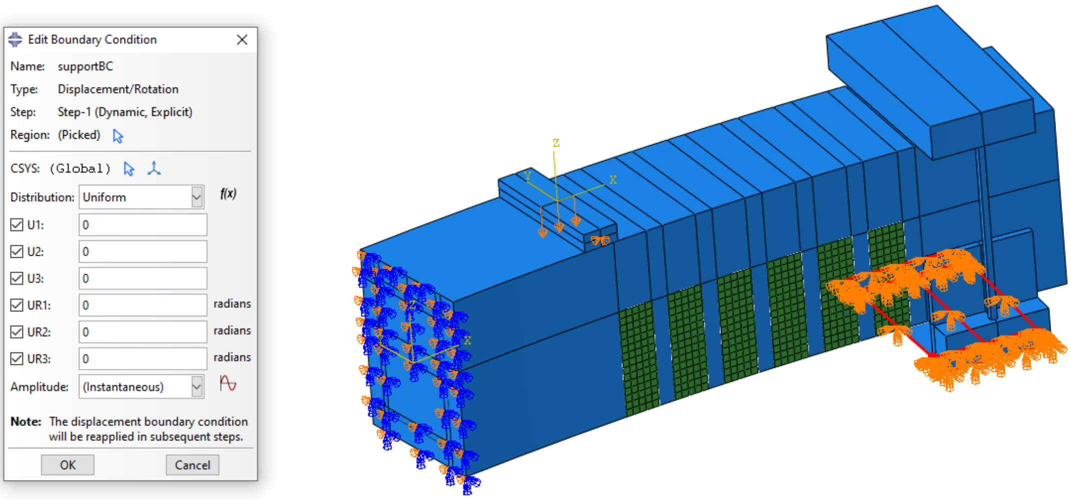

Figure 69: Fully fixed boundary condition on the clamp bottom part.

The roller was modelled to transfer the load without applying the displacement load on the beam itself because if the load is applied on the beam itself it can disturb the rotational displacement of the beam. Hence, a roller part was modelled, and the load was applied to the roller at the mid-top surface on a perpendicular line to the longer axis of the roller as shown in Figure 70. The displacement was defined only in the vertical direction to the beam curved plane and was released in all other translations and rotations to allow the roller to rotate freely around the load line with the rotating beam to keep the contact without getting disconnected.

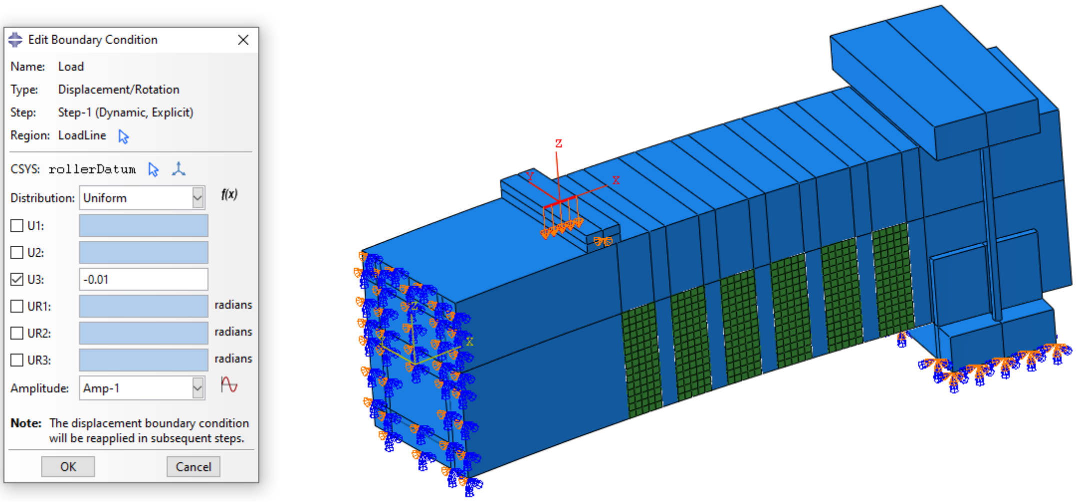

Figure 70: Displacement controlled load on the beam

To stabilize the roller so as not to slip away from the concrete surface, a node at the side of the roller was restrained for translations in the plane perpendicular to the load as shown in Figure 72.

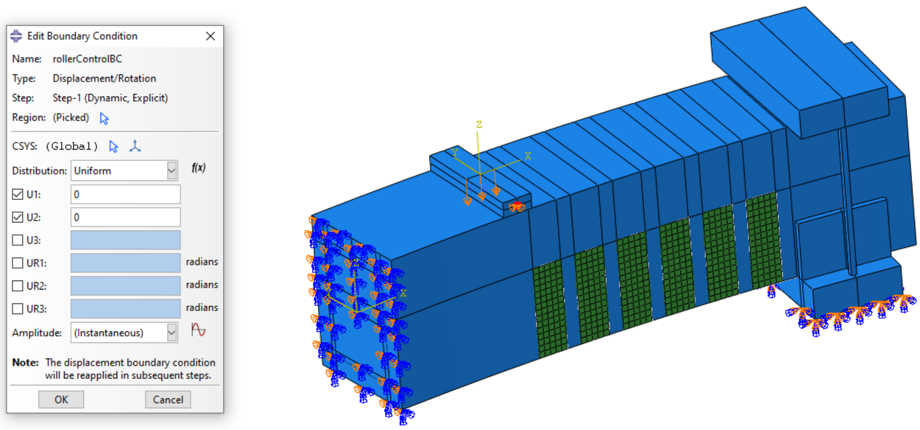

Figure 71: Restrains on the roller to stabilize the model

Finally, the meshing of the assembled parts was done. All 3D deformable solid parts have meshed with 8 – node linear brick also known as C3D8R finite elements. All rebar wire parts have meshed with 2 - node linear beam also known as B31 finite elements. After the meshing of the concrete beam, using the mesh offset function in the program the adhesive and CFRP layer was modelled. The adhesive was modelled as a 3D deformable solid with C3D8R finite element mesh and the CFRP layer was modelled as deformable shell elements with 4-node doubly curved shell S4R finite element mesh. Figure 72 presents a close up look at the adhesive and CFRP layers.

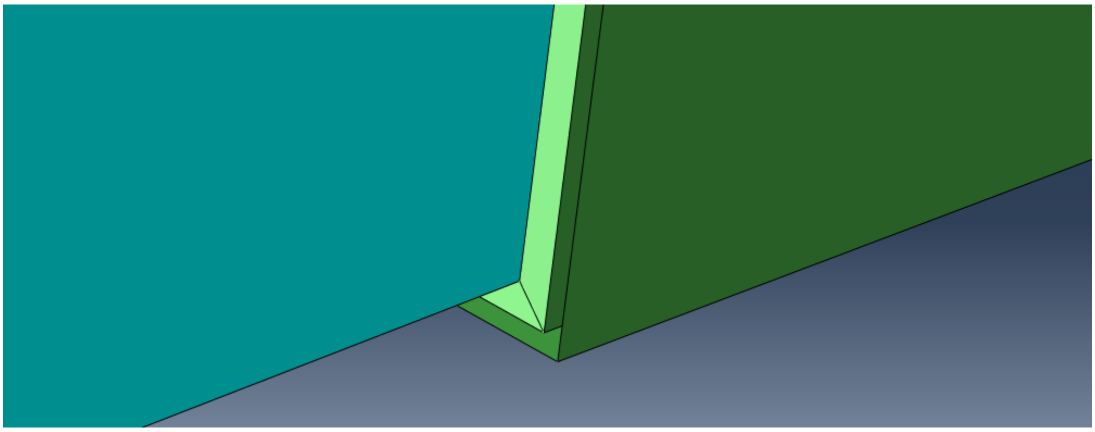

Figure 72: Adhesive and CFRP layers

5.4. Comparison of numerical results with experimental results

In this subchapter, the experimental results and numerical results such as crack patterns, failure loads and load vs. displacement were compared for both series 1 and series 2 separately.

5.4.1. Comparison of numerical results with experimental results for series 1

5.4.1.1. Comparison of failure modes

As shown in Figure 73, in the numerical model similar cracks were observed as in the control specimen of the experimental program. The CFRP strengthened models also showed similar cracks as the experimental specimens as shown in Figures 74 and 75.

The numerical models also showed experimental failure loads where the control beams failed in brittle shear failure mode and CFRP strengthened beams failed in flexure.

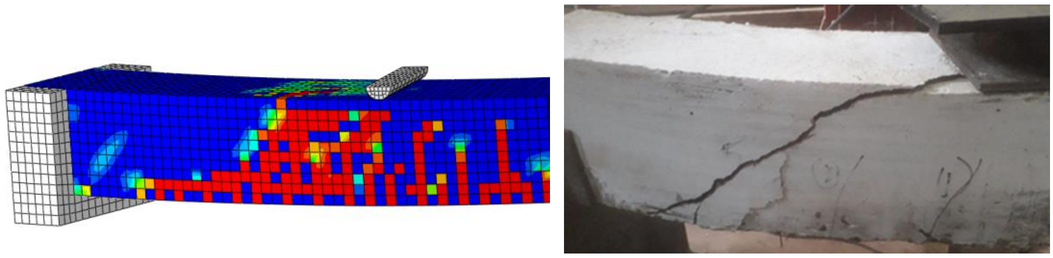

(a) (b)

Figure 73: Comparison of crack patterns in 2 m radius control beams (a) Cracks in numerical model (b) Cracks in the experimental specimen

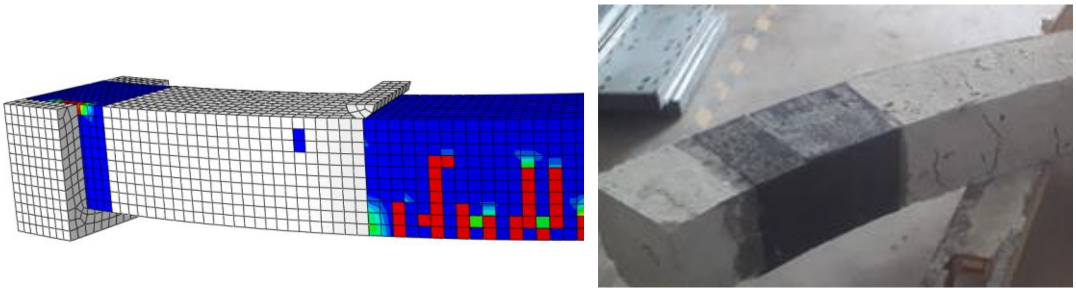

(a) (b)

Figure 74: Comparison of crack patterns in 2 m radius CFRP strengthened beams (a) Cracks in numerical model (b) Cracks in the experimental specimen

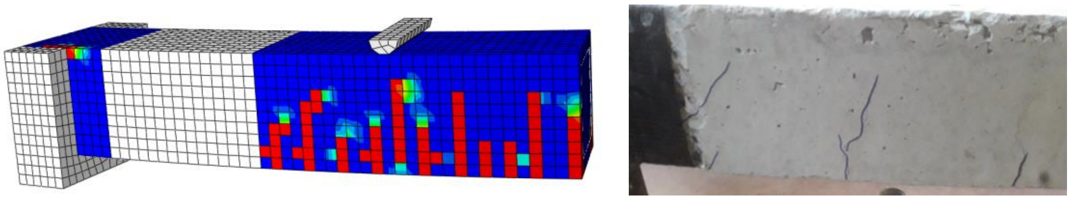

(a) (b)

Figure 75: Comparison of crack patterns in 2 m radius CFRP strengthened beams (a) Cracks in numerical model (b) Cracks in the experimental specimen

5.4.1.2. Comparison of Deflection vs. Load graphs

Figure 83 presents the comparison deflection vs. Load graphs between experimental and numerical results in series 1.

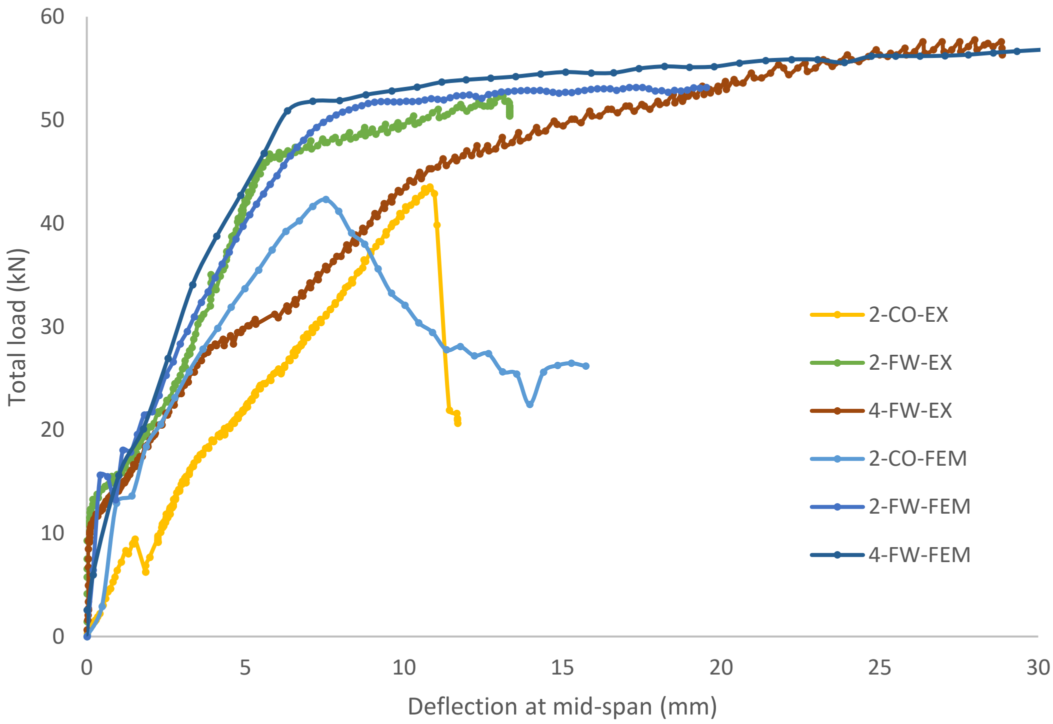

Figure 76: Experimental vs. Numerical results for specimens in series 1

According to Figure 76, it is clear that the numerical models are to be very accurate for the failure loads. However, in some regions, the deflection has deviated considerably which can be explained by the imperfection of the boundary conditions in the experimental setup.

5.4.2. Comparison of numerical results with experimental results for series 2

5.4.2.1. Comparison of failure modes

Following Figures 77 to 80 presents the comparison of crack patterns in numerical models and experimental specimens in series 2 specimens and excellent agreement between the two results can be observed.

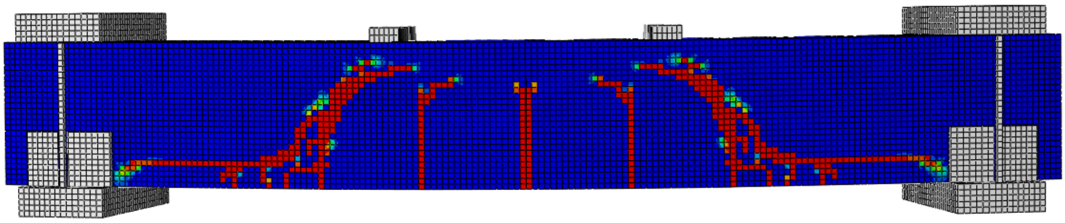

(a)

(b)

Figure 77: Comparison of crack patterns in 4 m radius control beams (a) Cracks in the numerical model (b) Cracks in the experimental specimen

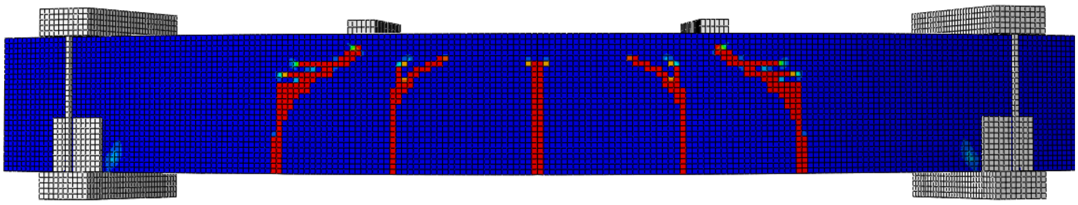

(a)

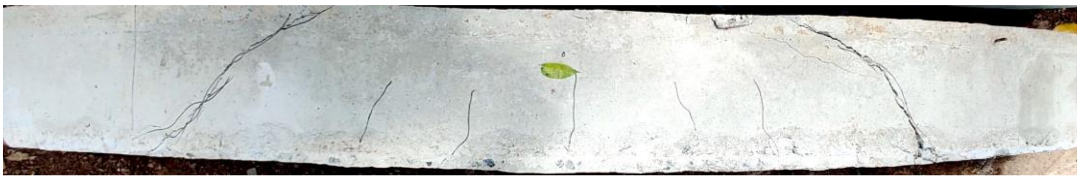

(b)

Figure 78: Comparison of crack patterns in 2 m radius control beams (a) Cracks in the numerical model (b) Cracks in the experimental specimen

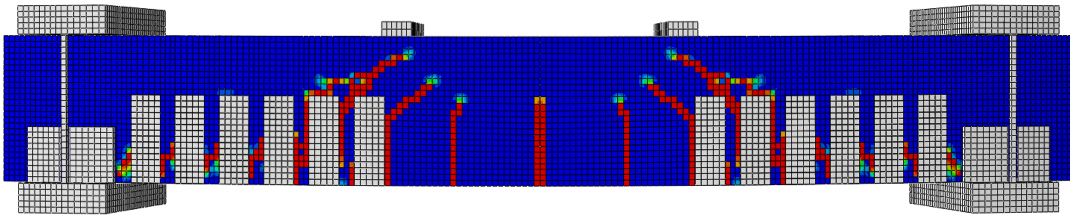

(a)

(b)

Figure 79: Comparison of crack patterns in 4 m radius CFRP strengthened beams (a) Cracks in the numerical model (b) Cracks in the experimental specimen

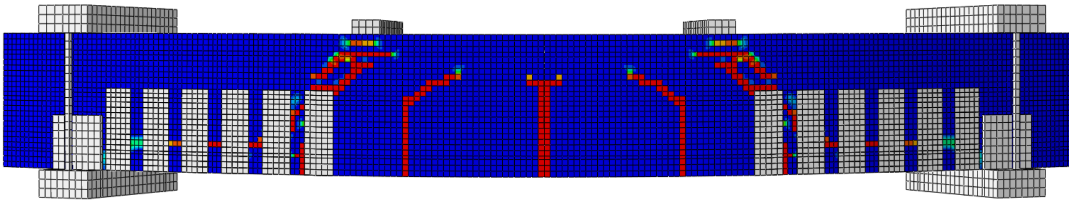

(a)

(b)

Figure 80: Comparison of crack patterns in 2 m radius CFRP strengthened beams (a) Cracks in the numerical model (b) Cracks in the experimental specimen

5.4.2.2. Comparison of Deflection vs. Load graphs

Figure 81 presents the comparison deflection vs. Load graphs between experimental and numerical results in series 2.

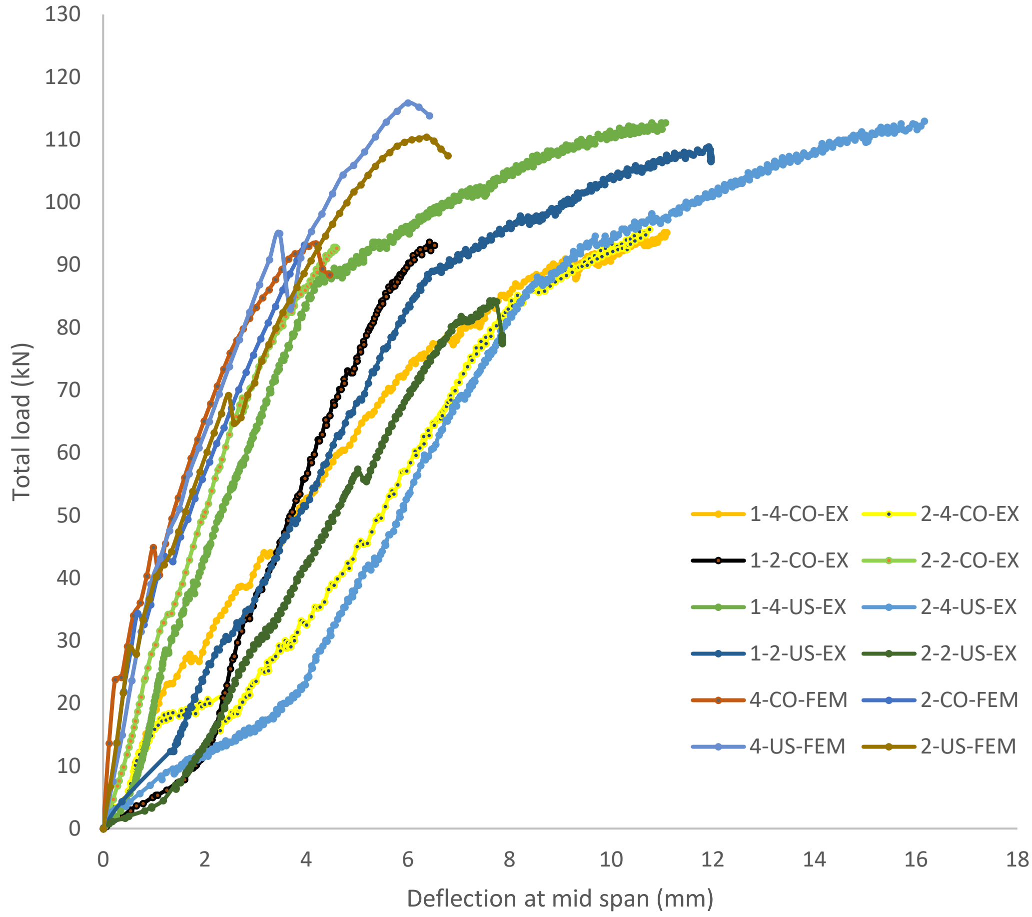

Figure 81: Deflection vs. Load graphs of experimental and numerical results in series 2

The failure loads agree very well between experimental and numerical results. However, the deformation is considerably higher in the experimental results which may have been due to several reasons. The main reason is imperfections in the fixed support in the experimental test setup. Because slipping and settlements were observed while testing which is the main reason for the low slope at the initial region of the deflection vs. load plots of some specimens. Other reasons may be considering the concrete material as an isotropic homogenous material and perfect boundary conditions in the numerical program.

5.4.3. Parametric study

Since the experimental study was done for only two radii of beams and conducting more experimental testing for more radii is time and resource consuming, a parametric study was done using the numerical model described above. In the parametric study, all parameters were kept as constants except for the radius of beams. Using the developed numerical model following results (Figure 82) were obtained for additional beam radii and straight beams for both control and CFRP strengthened (U – socketed) conditions.

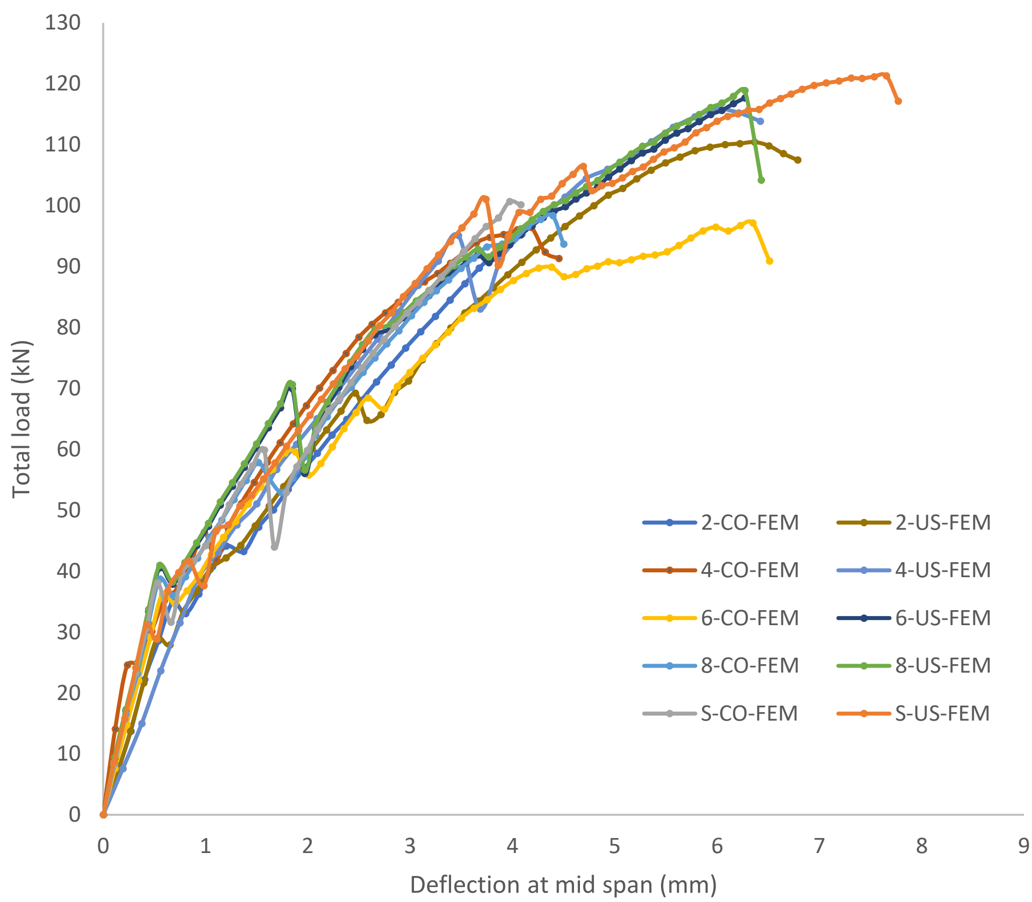

Figure 82: Deflection vs. Load graphs of parametric study

Tabularized summary of experimental, theoretical, and numerical studies is presented in Table 16.

Table 16: Comparison of experimental, theoretical/analytical, and numerical results

Specimen radius (m)	Experimental shear capacity (kN)		Theoretical shear capacity (kN)		Numerical (FEM) shear capacity (kN)		Experimental shear gain (kN)	Theoretical shear gain (kN)	Numerical shear gain (kN)	Percentage error of experimental shear gain	Percentage error of numerical shear gain (%)
	control	U- socketed	control	U- socketed	control	U- socketed					
2	93.27	108.88	90.79	114.43	94.45	110.42	15.61	23.64	15.97	-33.97	-32.45
4	95.44.	112.85	94.16	118.67	96.41	114.47	17.41	24.51	18.06	-28.97	-26.32
6	-	-	95.42	120.25	97.13	117.66	-	24.83	20.53	-	-17.32
8	-	-	96.07	121.07	98.35	120.88	-	25.00	22.53	-	-9.88
∞	-	-	98.09	123.62	100.66	125.30	-	25.52	24 .64	-	-3.45

The percentage errors of experimental and numerical shear gains were calculated compared to theoretically expected shear gain. These error percentages were converted into a capacity reduction factor (C_{tor}) for the analytical models used for determining the theoretical results and plotted as shown in Figure 83.

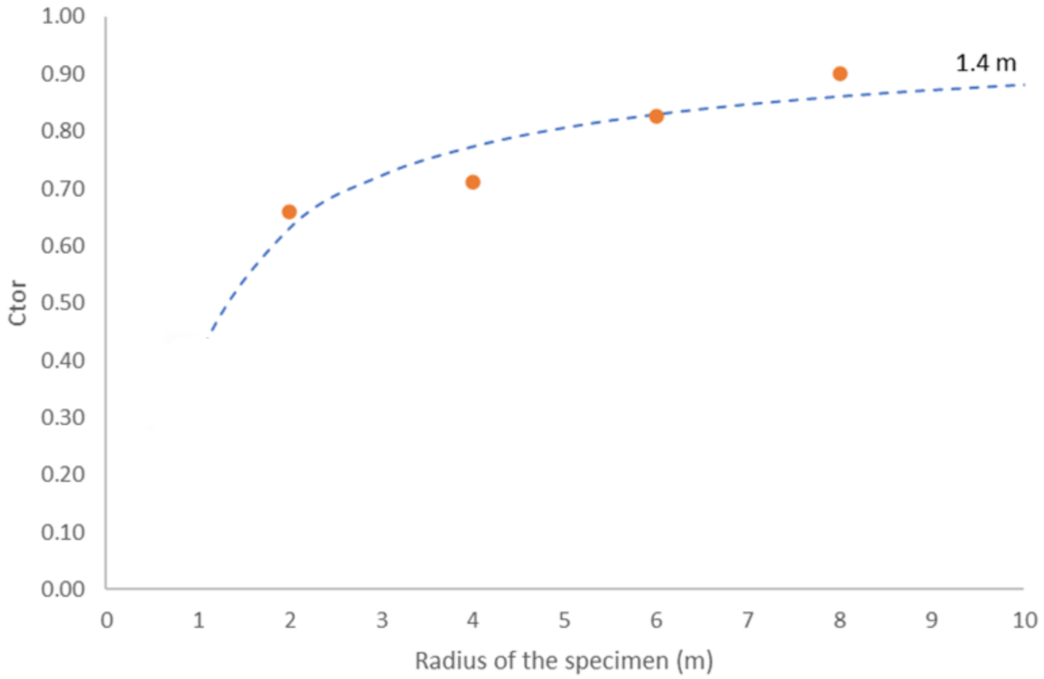

Figure 83: Capacity reduction factor vs. Radius of specimens

Since the deviation between experimental and numerical results is negligible, the reduction factor was calculated as the ratio between numerical shear gain and theoretically predicted shear gain.

The radius of the straight beam is considered as infinity hence, the plot was drawn such that it converges into the reduction factor of straight beam value when the radius goes to infinity. Such that way the approximated relationship between the reduction factor (C_{tor}) and the radius of specimens is presented in Equation 56.

$$C_{tor,1.4\,m} = 0.97 - 0.6R^{-0.8} \qquad 56$$

The parametric study was not extended below 0.7 m since that range of radii is impossible for a 1.4 m support distance. Above 10 m range of radii was also neglected since beams with radii higher than 10 m yield negligible reduction factors according to the numerical parametric study. Therefore, the 0.7 m to 10 m range of radii were only considered for the graph.

Furthermore, it should be noted that these results are only valid for the beam support distance of 1.4 m. Conducting more experimental and numerical parametric studies for various support distances will allow plotting more parallel curves in the Reduction factor vs Radius graph which can be interpolated to obtain the reduction factors for any support distance and radius.

The reduction factor (C_{tor}) can be used to modify Equation 39 to Equation 57. The reduction factor is noted as C_{tor}, since the reduction of shear enhancement is caused by the torsion of the beam due to curvature.

$$V_f = C_{tor}\frac{A_{fv}f_{fe}(\sin\alpha + \cos\alpha)d_f}{s_f} \qquad 57$$

CHAPTER 7: CONCLUSIONS AND RECOMMENDATIONS

From series one experimental results, it was found that the wrapping CFRP fabrics have enhanced the shear capacity of the curved RC beams by at least 30 % and the enhancement is higher for beams with lower curvatures. The deformation of beams had also reduced with the usage of the CFRP fabrics. However, obtaining a definite shear enhancement was not possible since the wrapping of CFRP fabrics as external shear reinforcement had caused for enhancing of the shear capacity of the beam to a point where the shear capacity is more than the flexural capacity in shear deficient beams. However, this shows that CFRP wrapping is a very effective method to enhance the shear capacity of horizontally curved beams.

The effects resulting from the torsional moment also was minor when the applied load is relatively low. With relatively higher loads the effect of torsion became more apparent. It was observed that the capacity enhancement of the 2 m radius beams is less than the 4 m radius beams, which may be due to the component adding from higher torsional stresses in 2 m radius beams causing flexural cracks to propagate more easily. The CFRP wrapping seems to have increased the stiffness of the beams also since the deflections of CFRP wrapped beams are less than the non-strengthened control beam.

The series two experimental results showed that U-socketing of CFRP fabrics for shear has increased the shear strength by 15.61 kN (16.7 %) and 17.41 kN (18.2 %) respectively for 2 m and 4 m radius specimens. The main failure mode was crack induced intermediate debonding of CFRP U-sockets and it could be further improved by providing an anchorage system for the U-sockets. However, the predicted shear enhancements according to theoretical investigation are 23.64 kN and 24.51 kN for 2 m and 4 m radius beams respectively. It can be observed that for 2 m and 4 m specimens recorded respectively 33.97 % and 28.97 % less than the predicted enhancement by the theoretical study. This can be explained by the additional torsional stresses contributing to the direct shear stresses which cause to reduce the shear capacities of RC beams.

Hence, to quantify the said effect of the torsional stresses on the shear capacity of the beam, a numerical (FEA) parametric study was done for different radii by using a developed numerical model which was validated using experimental results. The results from numerical models showed excellent agreement with experimental results which was used to conduct the parametric study. Subsequently, a capacity reduction factor was defined as the ratio between numerical shear gain and theoretically predicted shear gain to quantify the effect of torsional stresses on the shear enhancement of U-socketed CFRP on RC beams with a 1.4 m support distance and it was used to modify the currently existing analytical model which is used to design of FRP as external reinforcement for RC beams.

It is recommended to increase the flexural capacities in the series one specimen and carry out the same experimental procedure to obtain a more definite shear enhancement of RC beams by wrapping of CFRP.

Series two only consisted of specimens with a 1.4 m support distance, hence further experimental studies and numerical parametric studies should be done to quantify the effect of torsion on the shear enhancement of horizontally curved RC beams by CFRP U-socketing for different support distances. Furthermore, the effect of the arrangement of the U-socketed CFRP was kept as a constant which is a parameter that can affect the said shear capacity reduction factor due to torsion. Hence, it is recommended to investigate the effects of the arrangement of CFRP on the C_{tor}.

REFERENCES

ACI Committee 318, 2014. Building Code Requirements for Structural Concrete, American Concrete Institute.

ACI Committee 440, 2017. ACI 440.2R-17 Guide for the Design and Construction of Externally Bonded FRP Systems for Strengthening Concrete Structures, Guide for the Design and Construction of Externally Bonded FRP Systems for Strengthening Concrete Structures.

Adhikary, B.B., Mutsuyoshi, H., 2004. Behavior of Concrete Beams Strengthened in Shear with Carbon-Fiber Sheets. Journal of Composites for Construction 8, 258–264.

Allen, E., Iano, J., 2009. Fundamentals of Building Construction: Materials and Methods, Fifth. ed. John Wiley & Sons, Inc., Hoboken,.

Arya, C., 2009. Design of structural elements: Concreate, steelwork, masonry and timber designs to british standards and eurocodes, Taylor & Francis.

Bond, a J., Brooker, O., Harris, a J., Harrison, T., Moss, R.M., Narayanan, R.S., Webster, R., 2006. How to design concrete structures using Eurocode 2, The Concrete Centre. The Concrete Centre.

Bousias, S.N., Triantafillou, T.C., Fardis, M.N., Spathis, L., O'Regan, B.A., 2004. Fiber-Reinforced Polymer Retrofitting of Rectangular Reinforced Concrete Columns with or without Corrosion. ACI structural Journal 101, 512–520.

BS 8110-1:1997, 1997. BS 8110: Structural Use of Concrete - Part 1: Code of practice for design and construction. British Standard (BS).

BS EN 1992-1-1, 2004. Eurocode 2: Design of concrete structures - Part 1-1 : General rules and rules for buildings. British Standards Institution.

Cao, S.Y., Chen, J.F., Teng, J.G., Hao, Z., Chen, J., 2005. Debonding in RC Beams Shear Strengthened with Complete FRP Wraps. Journal of Composites for Construction 9, 417–428.

Chaallal, O., Shahawy, M., 2000. Performance of Fiber-Reinforced Polymer-Wrapped Reinforced Concrete Column under Combined Axial-Flexural Loading. ACI structural Journal 97, 659–668.

Chajes, M.J., Januszka, T.F., Mertz, D.R., Theodore A. Thomson, Jr., William W. Finch, Jr., 1995. Shear Strengthening of Reinforced Concrete Beams Using Externally Applied Composite Fabrics. ACI Structural Journal 92, 295–303.

Chen, G.-M., 2010. Behaviour and Strength of RC Beams Shear-Strengthened with Externally Bonded FRP Reinforcement.

Chen, J.F., Teng, J.G., 2003. Shear capacity of FRP-strengthened RC beams: FRP debonding. Construction and Building Materials 17, 27–41.

Cosgun, C., Turk, A.M., Mangir, A., Cosgun, T., Kiymaz, G., 2020. Experimental behaviour and failure of beam-column joints with plain bars, low-strength concrete and different anchorage details. Engineering Failure Analysis 109, 104247.

Cranston, W.B., Kamiński, M., Wróblewski, R., 1996. Aggregate interlock in cracked concrete with excessive crack width. Archives of Civil Engineering 42, 176–193.

Damian I. Kachlakev, David D. McCurry, Jr., 2000. Testing of Full-Size Reinforced Concrete Beams Strengthened with FRP Composites: Experimental Results and Design Methods Verification.

Dassault Systèmes, 2014. Abaqus 6.14 Online documentation [WWW Document]. Abaqus Theory Guide. URL https://abaqus-docs.mit.edu/2017/English/SIMACAEMATRefMap/simamat-c-concretedamaged.htm (accessed 5.22.20).

Diab, H.M.A., Abdelaleem, T., Rashwan, M.M.M., 2020. Moment redistribution and flexural performance of RC continuous T-beams strengthened with NSM FRP or steel bars. Structures 28, 1516–1538.

Dinh, H.H., Parra-Montesinos, G.J., Wight, J.K., 2011. Shear Strength Model for Steel Fiber Reinforced Concrete Beams without Stirrup Reinforcement. Journal of Structural Engineering 137, 1039–1051.

Ebead, U., 2010. Mechanically Fastened Frp Flexural Strengthening of RC Beams. In: 13th Structural Faults & Repair.

Ehsani, M. R., Saadatmanesh, H. & Tao, S., 1996. Design Recommendations for bond of GFRP reabars to concrete. Journal of Structural Engineering 122, 247–254.

Ferreira, M., Oliveira, M.H. de, Tapajos, L., Freire, M., 2020. Influence of anchorage on flexural strength of beams strengthened with CFRP sheets. Alconpat 9, 30–47.

Ghobarah, A., Ghorbel, M.N., Chidiac, S.E., 2002. Upgrading torsional resistance of reinforced concrete beams using fiber-reinforced polymer. Journal of Composites for Construction 6, 257–263.

Grelle, S. v., Sneed, L.H., 2013. Review of Anchorage Systems for Externally Bonded FRP Laminates. International Journal of Concrete Structures and Materials 7, 17–33.

Griffiths, A., 2014. Ecological university building by BDG Architects features a circular plan [WWW Document]. dezeen.com. URL https://www.dezeen.com/2014/02/24/stoas-vilentum-university-bdg-architects-circular-plan/ (accessed 5.18.20).

Grumezescu, V., Grumezescu, A.M., 2019. Materials for Biomedical Engineering, Thermoset and Thermoplastic Polymers. Elsevier, Bucharest.

Guo, R., Ren, Y., Li, M., Hu, P., Du, M., Zhang, R., 2021. Experimental study on flexural shear strengthening effect on low-strength RC beams by using FRP grid and ECC. Engineering Structures 227, 111434.

Hafezolghorani, M., Hejazi, F., Vaghei, R., Jaafar, M.S. bin, Karimzade, K., 2017. Simplified damage plasticity model for concrete. Structural Engineering International 27, 68–78.

Hassan, W.M., Park, S., Lopez, R.R., Mosalam, K.M., Moehle, J.P., 2010. Seismic response of older-type reinforced concrete corner joints. 9th US National and 10th Canadian Conference on Earthquake Engineering 2010, Including Papers from the 4th International Tsunami Symposium 7, 5288–5297.

Hollý, I., Bilčík, J., Keseli, O., Gažovičová, N., 2016. Bond of GFRP reinforcement with concrete. Key Engineering Materials 691, 356–365.

Hota V. S. GangaRao, and P.V.Vijay., 1998. Bending Behavior of Concrete Beams. Journal of Structural Engineering 6, 3–10.

Hull, D., Clyne, T.W., 1996. An Introduction to Composite Materials (Cambridge Solid State Science Series), 2nd ed. Cambridge University Press, Cambridge.

Iacobucci, R.D., Sheikh, S.A., Bayrak, O., 2003. Retrofit of Square Concrete Columns with Carbon Fiber-Reinforced Polymer for Seismic Resistance. ACI Structural Journal 100, 785–794.

International Federation for Structural Concrete (fib), 1999. Structural Concrete - Textbook on Behaviour, Design and performance - Updated knowledge of the CEB/FIP Model Code 1990, 2nd ed. International Federation for Structural Concrete (fib), Lausanne.

International Federation for Structural Concrete (fib), 2001. Externally bonded FRP reinforcement for RC structures, International Federation for Structural Concrete (fib).

Johnoehlers, D., Rudolf, S., 2004. Chapter 4 - CDC Debonding of Tension Face Plates. In: Design of FRP and Steel Plated RC Structures - Retrofitting Beams and Slabs for Strength, Stiffness and Ductility. Elsevier, pp. 100–136.

Kahandawaarachchi, K., Gamage, J, C, P, H., Chandrathilaka, E.R.K., 2019. Bond Performance of Carbon Fiber Reinforced Polymer (CFRP) Strengthened Reinforced Concrete Curved Beams. International Conference on Civil Engineering and Applications 6.

Kalfat, R., Al-Mahaidi, R., Smith, S.T., 2013. Anchorage Devices Used to Improve the Performance of Reinforced Concrete Beams Retrofitted with FRP Composites: State-of-the-Art Review. Journal of Composites for Construction 17, 14–33.

Karaca, E., Buyukozturk, O., 2002. FRP strengthening of RC beams in flexure and shear : FRP strengthening of RC beam in flexure and shear : failure modes and design.

Karbhari, V.M., Seible, F., 2000. Fiber reinforced composites - advanced materials for the renewal of civil infrastructure. Applied Composite Materials 7, 95–124.

Khalifa, A., Gold, W.J., Nanni, A., Abdel Aziz, M.I., 1998. Contribution of externally bonded FRP to shear capacity of RC flexural members. Journal of Composites for Construction 2, 195–202.

Koutas, L., Triantafillou, T.C., 2012. Use of anchors in shear strengthening of reinforced concrete T-beams with FRP. Proceedings of the 6th International Conference on FRP Composites in Civil Engineering, CICE 2012.

Lee, J.H., Chacko, R.M., Lopez, M.M., 2010. Use of Mixed-Mode Fracture Interfaces for the Modeling of Large-Scale FRP-Strengthened Beams. Journal of Composites for Construction 14, 845–855.

Lee, S.Y., 1956. Design of curved beams in reinforced concrete.

Li, W., Tang, S., Huang, Z., Yang, X., Shi, T., Xing, F., 2020. Shear behavior of concrete beam reinforced in shear with carbon fiber-reinforced polymer mesh fabric (CFRP-MF) configuration. Engineering Structures 218, 110828.

Lorenzis, L. de, Nanni, A., 2002. Use of carbon fiber laminates for strengthening reinforced concrete beams in bending. ACI structural Journal 2, 67–84.

Meier, U., 1995. Strengthening of structures using carbon fibre/epoxy composites. Construction and Building Materials 9, 341–351.

Meisami, M.H., Mostofinejad, D., Nakamura, H., 2014. Strengthening of flat slabs with FRP fan for punching shear, Composite Structures. Elsevier Ltd.

Memon, M.S., Sheikh, S.A., 2005. Seismic Resistance of Square Concrete Columns Retrofitted with Glass Fiber-Reinforced Polymer. ACI structural Journal 102, 774–783.

Mofidi, A., Chaallal, O., 2011. Shear Strengthening of RC Beams with Externally Bonded FRP Composites: Effect of Strip-Width-to-Strip-Spacing Ratio. Journal of Composites for Construction 15, 732–742.

Nanni, A., de Luca, A., Zadeh, H., 2014. Reinforced Concrete with FRP Bars: Mechanics and Design. CRC Press: Taylor & Francis Group, Boca Raton.

Norris, T., Saadatmanesh, H., Ehsani, M.R., 1997. Shear and Flexural Strengthening of R/C Beams with Carbon Fiber Sheets. Journal of Structural Engineering 123.

Orton, S.L., Jirsa, J.O., Bayrak, O., 2008. Design Considerations of Carbon Fiber Anchors. Journal of Composites for Construction 12, 608–616.

Ozbakkaloglu, T., Fanggi, B.L., 2014. Axial Compressive Behavior of FRP-Concrete-Steel Double-Skin Tubular Columns Made of Normal- and High-Strength Concrete. Journal of Composites for Construction 18.

Paul, D., Datta, A.K., 2018. A Study on Flexural Strengthening of RC beam using FRP. In: International Conference on ADVANCES IN CONSTRUCTION MATERIALS AND STRUCTURES. Uttarakhand.

Pellegrino, C., Modena, C., 2002. Fiber Reinforced Polymer Shear Strengthening of Reinforced Concrete Beams with Transverse Steel Reinforcement. Journal of Composites for Construction 6, 104–111.

Pilkey, W.D., 2005. Formulae for stress, strain and structural matrices, John Wiley & Sons, Inc.

Polak, M.A., Lawler, N., 2011. Application of FRP for punching shear retrofit of concrete slab-column connections. Advances in FRP Composites in Civil Engineering - Proceedings of the 5th International Conference on FRP Composites in Civil Engineering, CICE 2010 854–857.

Priestley, M.J.N., Seible, F., 1995. Design of seismic retrofit measures for concrete and masonry structures. Construction and Building Materials 9, 365–377.

Richardson, A., Drew, P., 2011. Fibre reinforced polymer and steel rebar comparative performance. Structural Survey 29, 63–74.

Ritchie, P., Thomas, D., Lu, L., Conneley, G., 1991. External Reinforcement of Concrete Beams Using Fiber Reinforced Plastics. ACI Structural Journal 88, 490–500.

Ross, C.A., Muszynski, L.C., Jerome, D.M., Tedesco, J.W., Sierakowski, R.L., 1997. RC Beams and Slabs Externally Reinforced with Fiber Reinforced Plastic (FRP) Panels. In: Proceedings of the Twenty-Seventh DoD Explosives Safety Seminar.

Saribiyik, A., Abodan, B., Balci, M.T., 2020. Experimental study on shear strengthening of RC beams with basalt FRP strips using different wrapping methods. Engineering Science and Technology, an International Journal.

Sayed-Ahmed, E.Y., Bakay, R., Shrive, N.G., 2009. Bond strength of FRP laminates to concrete: State-of-the-art review. Electronic Journal of Structural Engineering 45–61.

Shahawy, M.A., Beitelman, T., Arockiasamy, M., Sowrirajan, R., 1996. Experimental investigation on structural repair and strengthening of damaged prestressed concrete slabs utilizing externally bonded carbon laminates. Composites Part B: Engineering 27, 217–224.

Sharif, A., Al-Sulaimani, G., Basunbul, I., Baluch, M., Ghaleb, B., 1994. Strengthening of Initially Loaded Reinforced Concrete Beams Using FRP Plates. ACI Structural Journal 91, 160–168.

Sheikh, S.A., Yau, G., 2002. Seismic behavior of concrete columns confined with steel and fiber-reinforced polymers. ACI Structural Journal 99, 72–80.

Silva, M.A.L., Dedigamuwa, K. v., Gamage, J.C.P.H., 2021. Performance of severely damaged reinforced concrete flat slab-column connections strengthened with Carbon Fiber Reinforced Polymer. Composite Structures 255, 112963.

Sundarraja, M.C., Rajamohan, S., 2009. Strengthening of RC beams in shear using GFRP inclined strips - An experimental study. Construction and Building Materials 23, 856–864.

Tamura, T., Murata, H., 2010. Experimental study on the ultimate strength of R / C curved beam. Fracture Mechanics of Concrete and Concrete Structures - High Performance, Fiber Reinforced Concrete, Special Loadings and Structural Applications 1783–1788.

Teng, J.G., 2001. Failure modes of FRP-strengthened restructures. In: 26th Conference on Our World in Concrete & Structures. Singapore, pp. 627–634.

Teng, J.G., Chen, J.F., Smith, S.T., 2001. Debonding Failures in FRP-Strengthened RC Beams: Failure Modes, Existing Research and Future Challenges. In: Composites in Construction: A Reality. Italy, pp. 139–148.

Teng, J.G., Chen, J.F., Smith, S.T., Lam, L., 2002. FRP-Strengthened RC Structures. John Wiley and Sons, Inc., Chichester.

Teng, J.G., Chen, J.F., Smith, S.T., Lam, L., 2003. Behaviour and strength of FRP-strengthened RC structures: A state-of-the-art review. Proceedings of the Institution of Civil Engineers: Structures and Buildings 156, 51–62.

Teng, J.G., Lam, L., Chen, J.F., 2004. Shear strengthening of RC beams with FRP composites. Progress in Structural Engineering and Materials 6, 173–184.

Triantafillou, T.C., 1998. Shear strengthening of reinforced concrete beams using epoxy-bonded FRP composites. ACI Structural Journal 95, 107–115.

Triantafillou, T.C., Antonopoulos, C.P., 2000. Design of Concrete Flexural Members Strengthened in Shear with FRP. Journal of Composites for Construction 4, 198–205.

Triantafillou, T.C., Choutopoulou, E., Fotaki, E., Skorda, M., Stathopoulou, M., Karlos, K., 2016. FRP confinement of wall-like reinforced concrete columns. Materials and Structures 49, 651–664.

Wong, Y.-C., 1970. Horizontally curved beam analysis and design.

Yao, J., Teng, J.G., Chen, J.F., 2005. Experimental study on FRP-to-concrete bonded joints. Composites Part B: Engineering 99–113.

Yindeesuk, S., 2009. Overpass Bridge Crossing Intersection between Highway No.345 and Highway No. 3100 in THAILAND [WWW Document]. tonsukit.com. URL http://www.tonsukit.com/blog-and-article/personsnamesnewwebsitewinswobbyaward (accessed 5.18.20).

Zeng, J.J., Lin, G., Teng, J.G., Li, L.J., 2018. Behavior of large-scale FRP-confined rectangular RC columns under axial compression. Engineering Structures 174, 629–645.

Zhang, J., Chen, Z., Guo, X., 2016. Experimental Study on Fracture Behaviors of Concrete Beams Strengthened with FRP Sheet of Different Width. International Journal of Materials Science and Applications 5, 31.

Zhang, Z., Hsu, C.-T.T., 2005. Shear Strengthening of Reinforced Concrete Beams Using Carbon-Fiber-Reinforced Polymer Laminates. Journal of Composites for Construction 9, 158–169.

ANNEXES

ANNEX A

Horizontally curved beam fixed at both ends and subjected to concentrated load

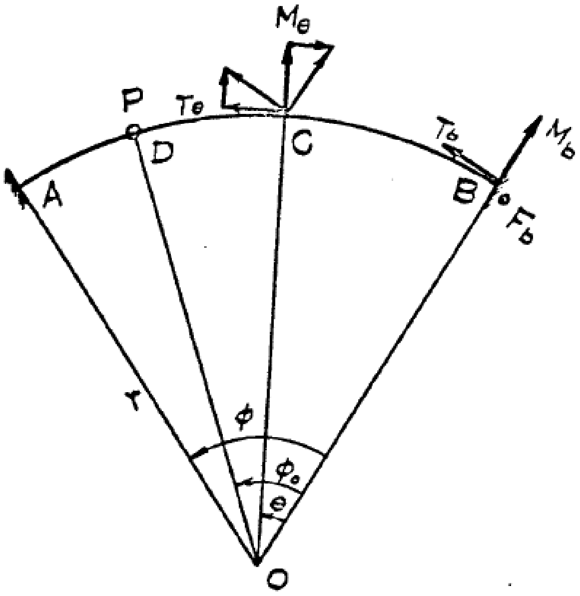

As shown in Figure, a concentrated load acts at point D with an angular distance Φ from support B. M_θ and T_θ represent the bending moment and torsional moment at any section C with an angular distance θ from B.

For portion BD ($0 \leq \theta \leq \Phi_0$)

$$M_\theta = M_b \cos\theta + T_b \sin\theta - F_b r \sin\theta \quad (1)$$

$$T_\theta = -M_b \sin\theta + T_b \cos\theta + F_b r(1 - \cos\theta) \quad (2)$$

For portion DA ($\Phi_0 \leq \theta \leq \Phi$)

$$M_\theta = M_b \cos\theta + T_b \sin\theta - F_b r \sin\theta + Pr\sin(\theta - \emptyset_0) \quad (3)$$

$$T_\theta = -M_b \sin\theta + T_b \cos\theta + F_b r(1 - \cos\theta) - Pr(1 - \cos(\theta - \emptyset_0)) \tag{4}$$

Applying Castigliano's theorem with U representing the strain energy

$$U = \int \frac{M_\theta^2}{2EI} r d\theta + \int \frac{T_\theta^2}{2GJ} r d\theta \tag{5}$$

At support B

$$Ш_b = \Upsilon_b = \mathit{\Delta}_b = 0$$

$$\frac{\partial U}{\partial M_b} = \frac{\partial U}{\partial T_b} = \frac{\partial U}{\partial F_b} = 0 \tag{6}$$

From (5) and (6)

$$\frac{\partial U}{\partial M_b} = \frac{1}{EI} \int \frac{M_\theta . M_\theta}{M_b} r d\theta + \frac{1}{GJ} \int \frac{T_\theta . T_\theta}{M_b} r d\theta = 0 \tag{7}$$

Partially differentiating (1) and (2) by M_b

$$\frac{\partial M_\theta}{\partial M_b} = \cos\theta, \frac{\partial T_\theta}{\partial M_b} = -\sin\theta$$

Let

$$m = \frac{EI}{GJ}$$

Applying the above results to (7)

$$\frac{1}{EI}\left[\int M_\theta r \cos\theta \, d\theta + m \int T_\theta \, r(-\sin\theta) d\theta\right] = 0 \tag{8}$$

Applying from (1), (2), (3) and (4)

$$\frac{r}{EI}\Big\{\int_0^{\emptyset_0}(M_b\cos\theta + T_b\sin\theta - F_b r\sin\theta)\cos\theta\, d\theta + \int_{\emptyset_0}^{\emptyset}[M_b\cos\theta + T_b\sin\theta - F_b r\sin\theta + Pr\sin(\theta-\emptyset_0)]\cos\theta\, d\theta + m\int_0^{\emptyset_0}[-M_b\sin\theta + T_b\cos\theta + F_b r(1-\cos\theta)](-\sin\theta)d\theta + m\int_{\emptyset_0}^{\emptyset}[-M_b\sin\theta + T_b\cos\theta + F_b r(1-\cos\theta) - Pr(1-\cos(\theta-\emptyset_0))](-\sin\theta)d\theta\Big\} = 0$$

$$\frac{r}{EI}\Big[M_b\int_0^{\emptyset}\cos^2\theta d\theta + mM_b\int_0^{\emptyset}\sin^2\theta\, d\theta + T_b\int_0^{\emptyset}\sin\theta\cos\theta\, d\theta + mT_b\int_0^{\emptyset}(-\sin\theta\cos\theta)\, d\theta - F_b r\int_0^{\emptyset}\sin\theta\cos\theta\, d\theta + mF_b r\int_0^{\emptyset}\sin\theta\cos\theta\, d\theta - mF_b r\int_0^{\emptyset}\sin\theta\, d\theta + Pr\int_0^{\emptyset}\sin(\theta-\emptyset_0)\cos\theta\, d\theta + mPr\int_0^{\emptyset}(1-\cos(\theta-\emptyset_0))\sin\theta\, d\theta\Big] = 0$$

$$\frac{r}{EI}\Big[M_b\Big(\frac{\emptyset}{2} + \frac{\sin 2\emptyset}{4} + m\frac{\emptyset}{2} - m\frac{\sin 2\emptyset}{4}\Big) + T_b\Big(-\frac{1}{4}(\cos(2\emptyset-1)) + \frac{m}{4}(\cos(2\emptyset-1))\Big) + F_b r\Big(\frac{(1-m)}{4}(\cos 2\emptyset - 1) + m(\cos\emptyset - 1)\Big)\Big] = \frac{Pr^2}{EI}\Big\{(m-1)\cos\emptyset_0\Big(-\frac{1}{4}(\cos 2\emptyset - \cos 2\emptyset_0)\Big) + \sin\emptyset_0\Big[(\emptyset-\emptyset_0) + (m-1)\frac{(\emptyset-\emptyset_0)}{2} - \frac{(\sin 2\emptyset - \sin 2\emptyset_0)}{4}\Big] + m(\cos\emptyset - \cos\emptyset_0)\Big\}$$

$$M_b[\emptyset(m+1) - \sin\emptyset\cos\emptyset(m-1)] - T_b\sin^2\emptyset(m-1) + F_b r[\sin^2\emptyset(m-1) + 2m(\cos\emptyset - 1)] = Pr\Big[(m-1)\cos\emptyset_0(\sin^2\emptyset - \sin^2\emptyset_0) + \sin\emptyset_0(\emptyset-\emptyset_0)(m+1) - \sin\emptyset_0\frac{(m-1)}{2}(\sin 2\emptyset - \sin 2\emptyset_0) + 2m(\cos\emptyset - \cos\emptyset_0)\Big] \quad (9)$$

Similarly, for $\frac{\partial U}{\partial T_b} = 0$ we can obtain

$$-M_b[\sin^2 \emptyset(m-1)] + T_b[\emptyset(m+1) + \sin\emptyset \cos\emptyset(m-1)] + F_b r[2m \sin\emptyset - \emptyset(m+1) - \sin\emptyset\cos\emptyset(m-1)] = Pr\left[-\cos\emptyset_0(\emptyset-\emptyset_0)(m+1) - \frac{1}{2}\cos\emptyset_0(m-1)(\sin 2\emptyset - \sin 2\emptyset_0) - (m-1)\sin\emptyset_0(\sin^2\emptyset - \sin^2\emptyset_0) + 2m(\sin\emptyset - \sin\emptyset_0)\right] \tag{10}$$

Similarly, for $\frac{\partial U}{\partial F_b} = 0$ we can obtain

$$M_b[\sin^2 \emptyset_0(m-1) + 2m(\cos\emptyset - 1)] + T_b[2m\sin\emptyset - \emptyset(m+1) - \sin\emptyset\cos\emptyset\,(m-1)] + F_b r[\emptyset(m+1) + \sin\emptyset\cos\emptyset(m-1) - 4m\sin\emptyset + 2m\emptyset] = Pr\left[\frac{(m-1)}{2}\cos\emptyset_0(\sin 2\emptyset - \sin 2\emptyset_0) - 2m(1+\cos\emptyset_0)(\sin\emptyset - \sin\emptyset_0) + 2m\sin\emptyset_0(\cos\emptyset - \cos\emptyset_0)\right] \tag{11}$$

Let

$$a_1 = \emptyset(m+1) - \sin\emptyset\cos\emptyset(m-1) \tag{12}$$

$$b_1 = \sin^2\emptyset\,(m-1) \tag{13}$$

$$c_1 = \sin^2\emptyset(m-1) + 2m(\cos\emptyset - 1) \tag{14}$$

$$d_1 = (m-1)\cos\emptyset_0(\sin^2\emptyset - \sin^2\emptyset_0) + \sin\emptyset_0(\emptyset-\emptyset_0)(m+1) - \sin\emptyset_0\frac{(m-1)}{2}(\sin 2\emptyset - \sin 2\emptyset_0) + 2m(\cos\emptyset - \cos\emptyset_0) \tag{15}$$

$$a_2 = b_1 \tag{16}$$

$$b_2 = \emptyset(m+1) + \sin\emptyset\cos\emptyset(m-1) \tag{17}$$

$$c_2 = 2m\sin\emptyset - \emptyset(m+1) - \sin\emptyset\cos\emptyset(m-1) \tag{18}$$

$$d_2 = -\cos\emptyset_0(\emptyset-\emptyset_0)(m+1) - \frac{1}{2}\cos\emptyset_0(m-1)(\sin 2\emptyset - \sin 2\emptyset_0) - (m-1)\sin\emptyset_0(\sin^2\emptyset - \sin^2\emptyset_0) + 2m(\sin\emptyset - \sin\emptyset_0) \tag{19}$$

$$a_3 = c_1 \tag{20}$$

$$b_3 = c_2 \tag{21}$$

$$c_3 = \emptyset(m+1) + \sin\emptyset\cos\emptyset(m-1) - 4m\sin\emptyset + 2m\emptyset \tag{22}$$

$$d_3 = \Big[\frac{(m-1)}{2}\cos\emptyset_0(\sin 2\emptyset - \sin 2\emptyset_0) + (\emptyset - \emptyset_0)(\cos\emptyset_0\,(m+1) + 2m) + (m-1)\sin\emptyset_0\,(\sin^2\emptyset - \sin^2\emptyset_0) - 2m(1 + \cos\emptyset_0)(\sin\emptyset - \sin\emptyset_0) + 2m\sin\emptyset_0(\cos\emptyset - \cos\emptyset_0)\Big] \tag{23}$$

Then the equations can be simplified into the following simultaneous equations

$$a_1 M_b - b_1 T_b + c_1 F_b r = d_1 Pr \tag{24}$$

$$-b_1 M_b + b_2 T_b + c_2 F_b r = d_2 Pr \tag{25}$$

$$c_1 M_b + c_2 T_b + c_3 F_b r = d_3 Pr \tag{26}$$

Placing the above equation system in matrix form and carrying out operations for matrices the following result can be obtained.

$$|A| = \begin{vmatrix} a_1 & -b_1 & c_1 \\ -b_1 & b_2 & c_2 \\ c_1 & c_2 & c_3 \end{vmatrix}$$

$$M_b = \frac{Pr}{|A|}\begin{vmatrix} d_1 & -b_1 & c_1 \\ d_2 & b_2 & c_2 \\ d_3 & c_2 & c_3 \end{vmatrix} \tag{27}$$

$$T_b = \frac{Pr}{|A|}\begin{vmatrix} a_1 & d_1 & c_1 \\ -b_1 & d_2 & c_2 \\ c_1 & d_3 & c_3 \end{vmatrix} \tag{28}$$

$$F_b = \frac{P}{|A|}\begin{vmatrix} a_1 & -b_1 & d_1 \\ -b_1 & b_2 & d_2 \\ c_1 & c_2 & d_3 \end{vmatrix} \tag{29}$$

These equations can be solved using computer programs such as Matlab or Excel.

The bending moment will be maximum at supports (hogging) and when $\theta = \Phi_0$ (sagging). M_b is the BM at support and since in this experiment a symmetrical loading is considered, M_b will be equal to BM at both supports.

Therefore,

$$M_{max} = M_b \cos \emptyset_0 + T_b \sin \emptyset_0 - F_b r \sin \emptyset_0 \tag{30}$$

To find maximum torsion (2) and (4) are differentiated by θ and equated to zero.

For $0 \leq \theta \leq \Phi_0$

$$\frac{dT_\theta}{d\theta} = -M_b \cos \theta - T_b \sin \theta + F_b r \sin \theta = 0$$

$$\theta_1 = \tan^{-1}\left[\frac{M_b}{F_b r - T_b}\right] \tag{31}$$

For $\Phi_0 \leq \theta \leq \Phi$

$$\frac{dT_\theta}{d\theta} = -M_b \cos \theta - T_b \sin \theta + F_b r \sin \theta - \cos \emptyset_0 \sin \theta \, Pr + \sin \emptyset_0 \cos \theta \, Pr$$

$$\theta_2 = \tan^{-1}\left[\frac{M_b - Pr \sin \emptyset_0}{F_b r - T_b - \cos \emptyset_0 Pr}\right] \tag{32}$$

Applying θ_1 and θ_1 to (2) and (3) maximum torsion values can be calculated.

Horizontally curved beam fixed at both ends and subjected to a UDL

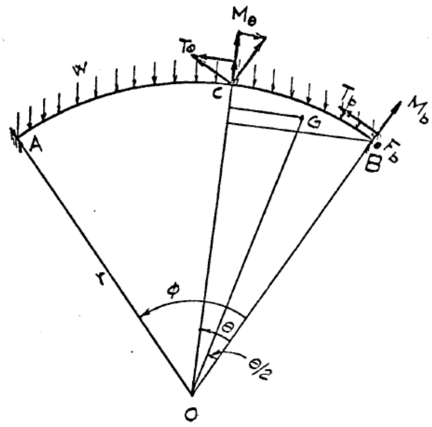

Since this study only concentrated loads will be considered only the final equations will be considered,

For BC section

$$M_\theta = M_b \cos\theta + T_b \sin\theta - \frac{(wr\theta)}{2} r \sin\theta + wr^2(1 - cos\theta) \tag{33}$$

$$T_\theta = -M_b \sin\theta + T_b \cos\theta + \frac{(wr\theta)}{2} r(1 - \cos\theta) - wr^2(\theta - \sin\theta) \tag{34}$$

Using Castigliano's theorem following results for M_b and T_b can be obtained

$$M_b = -wr^2\left[\frac{2(m+1)\sin\Phi - m\Phi(1+\cos\Phi)}{\Phi(m+1) - sin\Phi(m-1)} - 1\right] \tag{35}$$

$$T_b = -wr^2\left[\frac{2(m+1)\,(1-\cos\Phi) - m\Phi\sin\Phi}{\Phi(m+1) - sin\Phi(m-1)} - \frac{\Phi}{2}\right] \tag{36}$$

Maximum hogging BM can be calculated from the above Equation 35 and maximum sagging moment can be calculated by applying M_b and T_b values from Equations 35 and 36, by applying $\theta = \Phi/2$ since the sagging moment will be maximum at the mid-span.

To find maximum torsion (34) is differentiated by θ and $dT_\theta/d\theta$ equated to zero

$$\theta = \tan^{-1}\left[\frac{(M_b - wr^2) + \frac{wr^2}{\cos\theta}}{(\frac{wr^2\Phi}{2} - T_b)}\right] \quad (37)$$

By Applying the above θ value and M_b and T_b values to (34), maximum torsion can be obtained.